(2)

NAVAL POSTGRADUATE SCHOOL
Monterey, California

THESIS

DYNAMIC PERFORMANCE
OF SMALL DIAMETER
TUNNEL THRUSTERS

by

Michael B. McLean

March, 1991

Thesis Advisor: Anthony J. Healey

Approved for public release; distribution is unlimited.

REPORT DOCUMENTATION PAGE

1a. REPORT SECURITY CLASSIFICATION Unclassified	1b. RESTRICTIVE MARKINGS
2a. SECURITY CLASSIFICATION AUTHORITY	3. DISTRIBUTION/AVAILABILITY OF REPORT Approved for public release; distribution is unlimited.
2b. DECLASSIFICATION/DOWNGRADING SCHEDULE	
4. PERFORMING ORGANIZATION REPORT NUMBER(S)	5. MONITORING ORGANIZATION REPORT NUMBER(S)
6a. NAME OF PERFORMING ORGANIZATION Naval Postgraduate School 6b. OFFICE SYMBOL (*If applicable*) 55	7a. NAME OF MONITORING ORGANIZATION Naval Postgraduate School
6c. ADDRESS (*City, State, and ZIP Code*) Monterey, CA 93943-5000	7b. ADDRESS (*City, State, and ZIP Code*) Monterey, CA 93943-5000
8a. NAME OF FUNDING/SPONSORING ORGANIZATION 8b. OFFICE SYMBOL (*If applicable*)	9. PROCUREMENT INSTRUMENT IDENTIFICATION NUMBER
8c. ADDRESS (*City, State, and ZIP Code*) UNCLASSIFIED/UNLIMITED	10. SOURCE OF FUNDING NUMBERS Program Element No / Project No / Task No / Work Unit Accession Number

11 TITLE (*Include Security Classification*)
DYNAMIC PERFORMANCE OF SMALL DIAMETER TUNNEL THRUSTERS (U)

12 PERSONAL AUTHOR(S) Michael B. McLean

13a. TYPE OF REPORT	13b. TIME COVERED	14 DATE OF REPORT (*year, month, day*)	15. PAGE COUNT
Master's Thesis	From To	1991, March 22	149

16 SUPPLEMENTARY NOTATION
The views expressed in this thesis are those of the author and do not reflect the official policy or position of the Department of Defense or the U.S. Government.

17 COSATI CODES			18. SUBJECT TERMS (*continue on reverse if necessary and identify by block number*)
FIELD	GROUP	SUBGROUP	Autonomous Underwater Vehicle, AUV, Unmanned Untethered Underwater Vehicle, UUV, Small Tunnel Thrusters, Fluid Inertance

19 ABSTRACT (*continue on reverse if necessary and identify by block number*)

The transient response of a small tunnel thruster is studied for step changes in applied voltage to the thruster motor. Previous work on positioning Remotely Operated Vehicles with a ducted propeller had shown that lags in the thruster response caused limit cycling in the vehicle's behavior. These experiments have shown that the influence of the fluid inertia in the tunnel is significant and changes the lagging response to a leading response with a large transient peak following the step input. It is conjectured that such thrusters will enhance vehicle stability.

20 DISTRIBUTION/AVAILABILITY OF ABSTRACT	21. ABSTRACT SECURITY CLASSIFICATION	
☒ UNCLASSIFIED/UNLIMITED ☐ SAME AS REPORT ☐ DTIC USERS	Unclassified	
22a NAME OF RESPONSIBLE INDIVIDUAL Anthony J. Healey	22b TELEPHONE (*Include Area code*) (408) 646-2586	22c OFFICE SYMBOL 69HY

Approved for public release; distribution is unlimited.

Dynamic Performance of Small Diameter Tunnel Thrusters

by

Michael B. McLean
Lieutenant, United States Navy
B.C.E., Auburn University, 1982

Submitted in partial fulfillment
of the requirements for the degree of

MASTER OF SCIENCE IN MECHANICAL ENGINEERING

from the

NAVAL POSTGRADUATE SCHOOL
March 1991

Author: 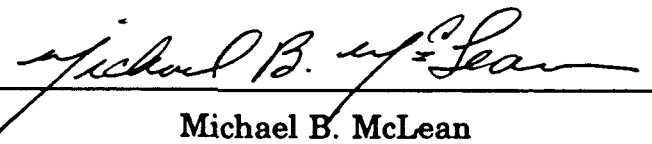

Michael B. McLean

Approved by: 

Anthony J. Healey, Thesis Advisor

Anthony J. Healey, Chairman
Department of Mechanical Engineering

ABSTRACT

The transient response of a small tunnel thruster is studied for step changes in applied voltage to the thruster motor. Previous work on positioning Remotely Operated Vehicles with a ducted propeller had shown that lags in the thruster response caused limit cycling in the vehicle's behavior. These experiments have shown that the influence of the fluid inertia in the tunnel is significant and changes the lagging response to a leading response with a large transient peak following the step input. It is conjectured that such thrusters will enhance vehicle stability.

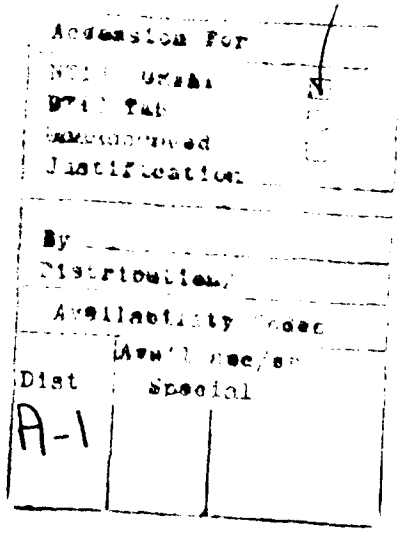

TABLE OF CONTENTS

LIST OF FIGURES

LIST OF TABLES

NOMENCLATURE

A	cross sectional area of the control volume
C	conversion factor used in continuous torque equation
C_M	motor shaft viscous friction coefficient
C_P	propeller shaft viscous friction coefficient
C_{PM}	combination of propeller and motor shaft viscous friction coefficients reflected to the motor side of the reduction gear
D	pole of motor transfer function in thruster computer model
e	motor back electromotive force (back EMF)
$\dot{E}_{CV}$	rate of energy buildup inside the control volume
$\dot{E}_{IN}$	rate of energy flow into the control volume
$\dot{E}_{OUT}$	rate of energy flow out of the control volume
f_s	sampling frequency
f_{max}	maximum expected frequency
$\boldsymbol{F}$	force vector
FRCTN	abbreviation for "friction" used in tables

gz	potential energy per unit mass due to elevation(z) above reference datum
h	specific enthalpy
i	armature current
INL	no load current
J_M	polar mass moment of inertia for the motor
J_P	polar mass moment of inertia for the propeller
J_{PM}	polar mass moment of inertia for the propeller and motor
K	constant pertaining to type of commutating used by DC motor
Ka	added mass coefficient
K_G	motor back EMF constant
K_T	motor torque constant
K_0	$1/K_G$
K_1	R/K_T; converts torque into volts
L	length of the thruster tunnel
Le	effective length of the tunnel when added inertance is considered
N	reduction gear ratio
n	outward normal vector to control volume surface

p	pitch; the axial distance projected by a propeller blade for one radian of rotation
p_{REV}	pitch using dimensions of length per revolution
Pe	effective pitch; product of propeller efficiency and pitch
Pe2	variable equal to the square of effective pitch
Pe3	variable equal to the cube of effective pitch
PKO	motor constant
$\dot{Q}$	rate of heat energy crossing the control volume boundary
Q(t)	time varying volumetric flowrate
R	terminal resistance
s	Laplace complex frequency
S	motor speed (RPM)
T	time vector in thruster computer model
TAMB	ambient temperature
TCONT	continuous load torque capability
TPR	motor thermal impedance
T_{APP}	torque applied to the propeller shaft
T_F	motor friction torque
T_M	motor torque

T_P	propeller torque
u	fluid velocity component in the z--direction
$\bar{u}$	average fluid velocity component in the z--direction
$\breve{u}$	specific internal energy
V	volume, velocity, or voltage, depending on context of usage
$\boldsymbol{V}$	fluid velocity vector in an inertial reference frame
V_A	speed of advance
VM	virtual mass coefficient, (1 + Ka)
$\dot{W}_{H2O}$	rate of work done on the water by the propeller
$\dot{W}_S$	rate of shaft work crossing the control volume boundary
$\dot{W}_V$	rate of shear work at the control surface
Z	gain of pole--zero block for motor in thruster computer model
α	kinetic energy correction factor
β	momentum flux correction factor; "BETA" is used in computer simulation executable file
η	propeller efficiency; W_{H2O}/W_S or $(1-\sigma)$; "ETA" is used in computer simulation executable file
ρ	fluid density

σ	slip; the difference between actual and theoretical advance through the water per revolution of the propeller ($\sigma=p\omega-V_A$)
σ_R	relative slip; the percentage difference between actual and theoretical advance through the water per revolution of the propeller
τ_M	collection of constants and variables in the motor transfer function with respect to motor inertia
τ_{PM}	collection of constants and variables in the motor transfer function with respect to motor and propeller inertia
ω_d	damped natural frequency
ω_M	motor angular velocity
ω_P	propeller angular velocity
ς	damping ratio
CS	control surface
CV	control volume
XS	cross sectional surface area normal to the flow direction

ACKNOWLEDGEMENTS

I would like to take the time now to thank several individuals who made the preparation of this thesis a worthwhile experience.

- Jo Ann, my wife, who has always been my biggest supporter
- Jim Selby, who spent many hours supporting my research and teaching me how to use a machine shop
- Dr. Fotis Papoulias, a professor who maintained a true "open door policy" and assisted immensely in my education here
- Dr. Morris Driels, a second professor, who was "always available" for my questions and brought a breath of fresh air to the Department
- And last but not least, to my advisor, teacher, and most importantly, my friend, Dr. Tony Healey; thanks for treating the graduate student as a professional, and making the master's thesis what it was meant to be

Without the assistance of the individuals above, the completion of this research would have been much more difficult. In addition those named above, there are many others who were very helpful during the past year, and to each one of them I want to say "THANKS".

I. INTRODUCTION

A. GENERAL

The United States Navy has a great interest in the development of underwater platforms that are capable of performing a predetermined mission, either for unclassified oceanic research or classified military support, without the requirement for an onboard crew. A platform of this type, with no external connections to a support system, is commonly referred to as an Autonomous Underwater Vehicle, or simply **AUV**.

The Mechanical Engineering (ME) Department at the Naval Postgraduate School (NPS) has been the major partner in a research and development program in Autonomous Underwater Vehicles since 1987. The first such development involved a small, tethered vehicle, known as AUV I, which was not autonomous. AUV I was designed to operate in a 4' by 4' by 40' tank located in the Fluid Mechanics Laboratory. Commands were transmitted to the vehicle via radio frequencies from a tank--side personal computer, and a tether relayed information from the vehicle to the computer. This vehicle was only capable of diving transients due to the restrictions of the test tank, but was an important step in the development of advanced depth changing autopilots using Sliding Modes [Ref. 1].

It was soon recognized that a larger vehicle would be required if true autonomy were to be realized. Obviously a larger vehicle would require a larger test tank. The NPS swimming pool was planned for use as a testing area for a new vehicle that would be designed to conduct horizontal plane maneuvers together with vertical plane diving, changes in speed, and ultimately obstacle avoidance. This second generation vehicle was denoted AUV II and construction began in early 1989. In June 1990, AUV II was officially launched in the NPS swimming pool by Rear Admiral West, the school's superintendent. Since the initial launch, the vehicle has been tested several times to change speeds, turn in a circle, and dive. All testing was performed with hollow tubes installed for the four tunnel thrusters. Figure 1 is a photograph of AUV II in the Controls Laboratory.

The need for thru rs to be installed into the vehicle is now an important next step in the evolution process. Up to this stage, the vehicle has been limited to simple steering and diving maneuvers. Additionally, the vehicle dynamic model used to simulate steering and diving maneuvers has yet to include an input from the four thrusters [Ref. 2]. The installation of the four thruster units into the tunnels will allow low speed operations, hovering, and greatly improved maneuverability. Thruster development, in general, and the understanding of dynamic response performance, in particular, is the subject here.

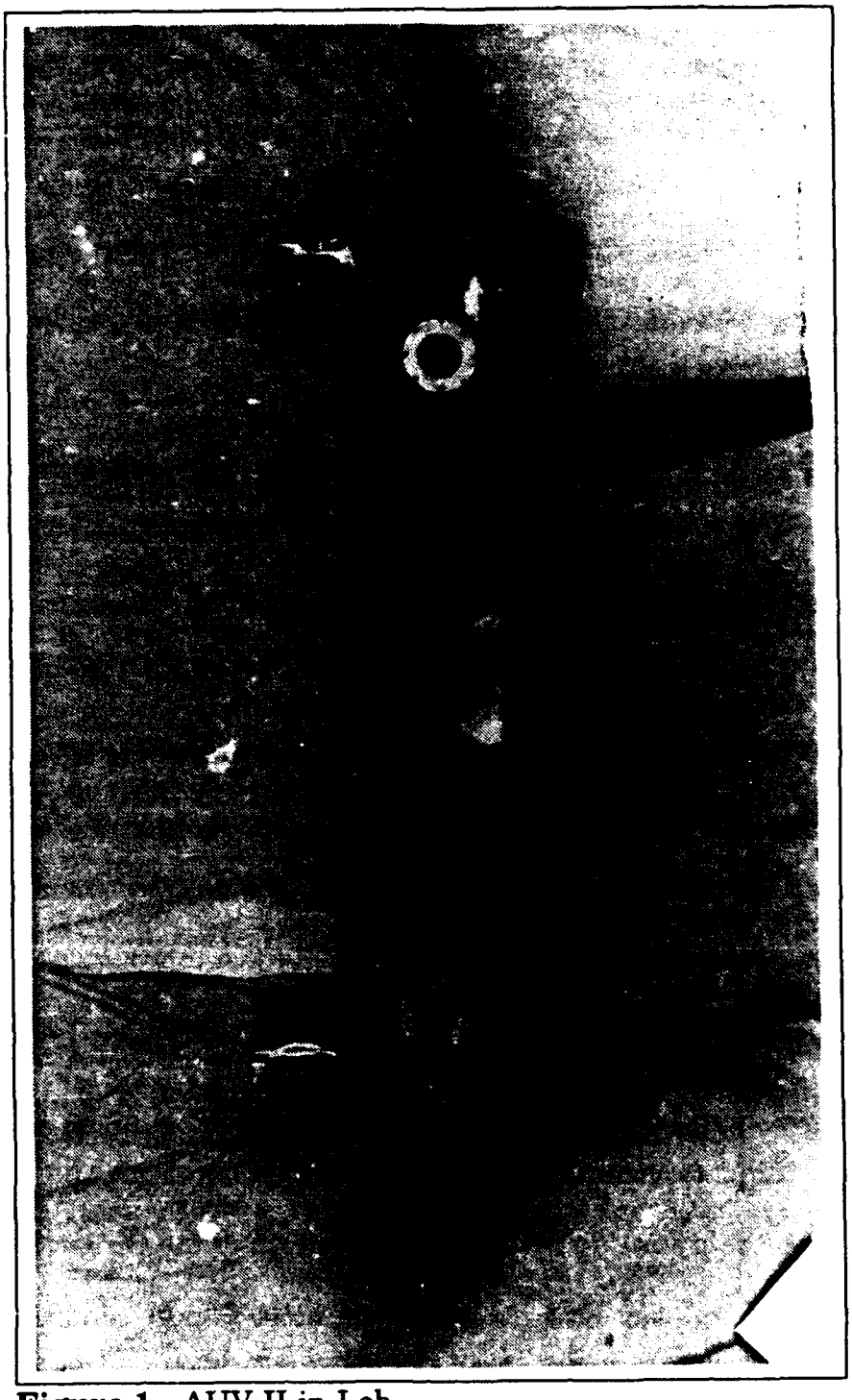

Figure 1 AUV II in Lab

B. BACKGROUND

The study of thrusters for the maneuvering of vehicles is well documented in the literature [Ref. 3]. One major use of the thruster in the bow of a surface vessel, thus the term "bow thruster", provides the needed yaw moment to maneuver the vessel when the speeds are too low for the rudder to maintain steerageway. The following paragraph will briefly mention several areas of research involving thruster performance.

The University of New Hampshire conducted research on AUV propulsion systems, testing 7.5 inch propellers with and without Kort nozzles, powered from a 24 volt--22 horsepower DC motor [Ref. 4]. A unique method of representing propeller thrust for ease of use in computer simulations of prime movers was developed by Baker and Patterson. The authors of this paper approached the propeller design problem from a purely mathematical standpoint in order to graphically display the torque, thrust, and speed equations obtained from propeller theory [Ref. 5]. A thorough paper describing the design and performance of bow thrusters was written in 1971 by Beveridge and is still regarded as an important reference [Ref. 6]. The above papers all have one thing in common; they all are concerned with the **steady state** rather than the **dynamic** response performance of the thruster, whether the vessel is making way or in a static, or bollard--pull condition. A library computer search of journals and research papers resulted in very few papers

that were published on the topic of this thesis as of the spring of 1990. Two that were found should be mentioned here. Thompson determined the "time--dependent thrust coefficient" of a propeller using experimental testing and simulations modeled by lift and airfoil theory [Ref. 7]. The four--quadrant propulsion dynamics of a deep submergence rescue vehicle (DSRV) were determined using a 17 horsepower DC motor from a 120 volt battery. The thrust and other parameters from a computer simulation were plotted against time, with the thrust exhibiting the characteristics of a first--order system [Ref. 8]. Since last spring, a research paper based on a thesis at the Massachusetts Institute of Technology has been published [Refs. 9,10]. This paper develops the thruster dynamics of a shrouded propeller and compares the results from a computer simulation to the actual test of a thruster in the laboratory.

The steady state performance alone cannot tell the whole story regarding a thruster's ability to maneuver a vehicle. In general, thrusters are not used as a source of constant thrust, but for variable amounts of thrust that are dependent upon the mission and/or the environmental conditions of the operating area. Examples of each of the above may be illustrated using the requirement to videotape or photograph an underwater object and:

- maintain a given distance in the presence of wave forces, or
- slowly pan the perimeter and allow the use of a robotic arm to collect samples.

The experimental and computer simulation time responses of the tunnel thruster from AUV II for a step input of motor voltage revealed an initial peak in thrust followed by an exponential decay to steady state. This type of response is indicative of a **leading** system. The shrouded propeller used in the Woods Hole vehicle, JASON, displayed a typical **lagging** time response [Ref.9]. This lagging response was shown to result in a classic **limit cycle**, a condition that is characteristic of nonlinearities in an unstable system. The differences in the response of the two types of thrusters is believed to be a result of the **added mass** associated with the water in and around the tunnel openings, as the development that follows will attempt to show.

C. SCOPE/AIM OF THIS THESIS

The purpose of this paper is to derive a mathematical model of the AUV II tunnel thruster using basic principles to show that the simulated response to a step input is legitimate based on an experimental test rig for an actual thruster unit. The model can then be used cautiously to predict the response of the actual thruster to a variety of inputs or changes in parameters. In addition, a section addressing the load matching of thruster propellers is included as an Appendix.

In Chapter I, the author has discussed the overall significance of the study of tunnel thrusters and their use to the Navy, presented a brief background into the past study of thrusters, and finally a discussion of what

is currently known about the dynamic performance of thrusters. Chapter II will cover in detail the theory necessary to develop a mathematical model of the thruster. This topic will be further divided into an electromechanical section and a fluid mechanics section. Chapter III describes building the block diagram using $MATRIX_X$[1] software. This section will include a block--by--block description of all equations, constants, and variables that make up the model. The results from the computer simulations will then be presented. Chapter IV details the set up of laboratory equipment required to obtain the time response of a tunnel thruster. Following the set up, the testing conducted is described along with the results from the tests. Chapter V is used to compare the results from the computer simulation and the laboratory tests. Conclusions are drawn from these results and recommendations for improvements and further research are addressed.

There are also two appendices to this thesis that are related to the study of thrusters. Appendix A will present a method for matching the propeller load in the tunnel to the DC motor that supplies the power. FORTRAN codes and computer graphics are used to solve and then display the results. For ease of reference, Appendix B contains two tables of DC motor characteristics that are used throughout the thesis.

[1] Registered Trademark, Integrated Systems, INC., Santa Clara, CA.

II. THEORY

A. GENERAL

The tunnel thrusters used on AUV II consist mainly of four components:

- a three inch diameter tunnel
- a three inch propeller
- a reduction gear set
- a DC servomotor

The above components will be described in detail below. A cross--sectional drawing of the thruster assembly is shown in Figure 2. In this chapter, a detailed description of the physical configuration of the thruster design is given, followed by an analysis of a mathematical model set in the context of unsteady energy and momentum conservation. These conditions are proposed as an explanation of the thruster's transient response performance.

1. Description of the Thruster Configuration

There are four thruster tunnels, or ducts, on the vehicle; one pair is located with the centerline axes horizontal and the other pair is located just inside the horizontal ones with the centerline axes vertical. The center distances for the horizontal and vertical tunnels are 46 and 34 inches respectively. The material used for construction was 3.0"--schedule 40,

polyvinyl chloride (PVC) piping. The length of the horizontal tunnels is 16.5 inches and the length of the vertical tunnels is 10.5 inches. The inside diameter and area of all tunnels is 0.2557 feet and 0.05134 square feet. The outer lips of the tunnels are slightly rounded to develop favorable flow conditions [Ref. 6].

2. Propeller

The propeller is a four--bladed Kaplan type with an outside diameter of three inches. The pitch angle of the blades is constant at approximately 30 degrees along their entire length, which results in a pitch (p) of 0.0721 feet per radian at the tip, and a pitch ratio ($\frac{p_{REV}}{D}$) of 1.77, where p_{REV} is the pitch in units of feet per revolution and the diameter is in feet. The blades have zero camber, which makes them equally effective in either direction of operation. The thrust is transmitted through a support strut located on either side of the propeller. The struts contain a dual thrust/journal bearing which serve not only to transfer the thrust but also to align the propeller shaft with the centerline of the tunnel. The bearing material is PVC with a very low coefficient of friction that requires no additional lubrication. The propeller is crude, being handmade in the machine shop, and should be improved to increase the performance of the thrusters.

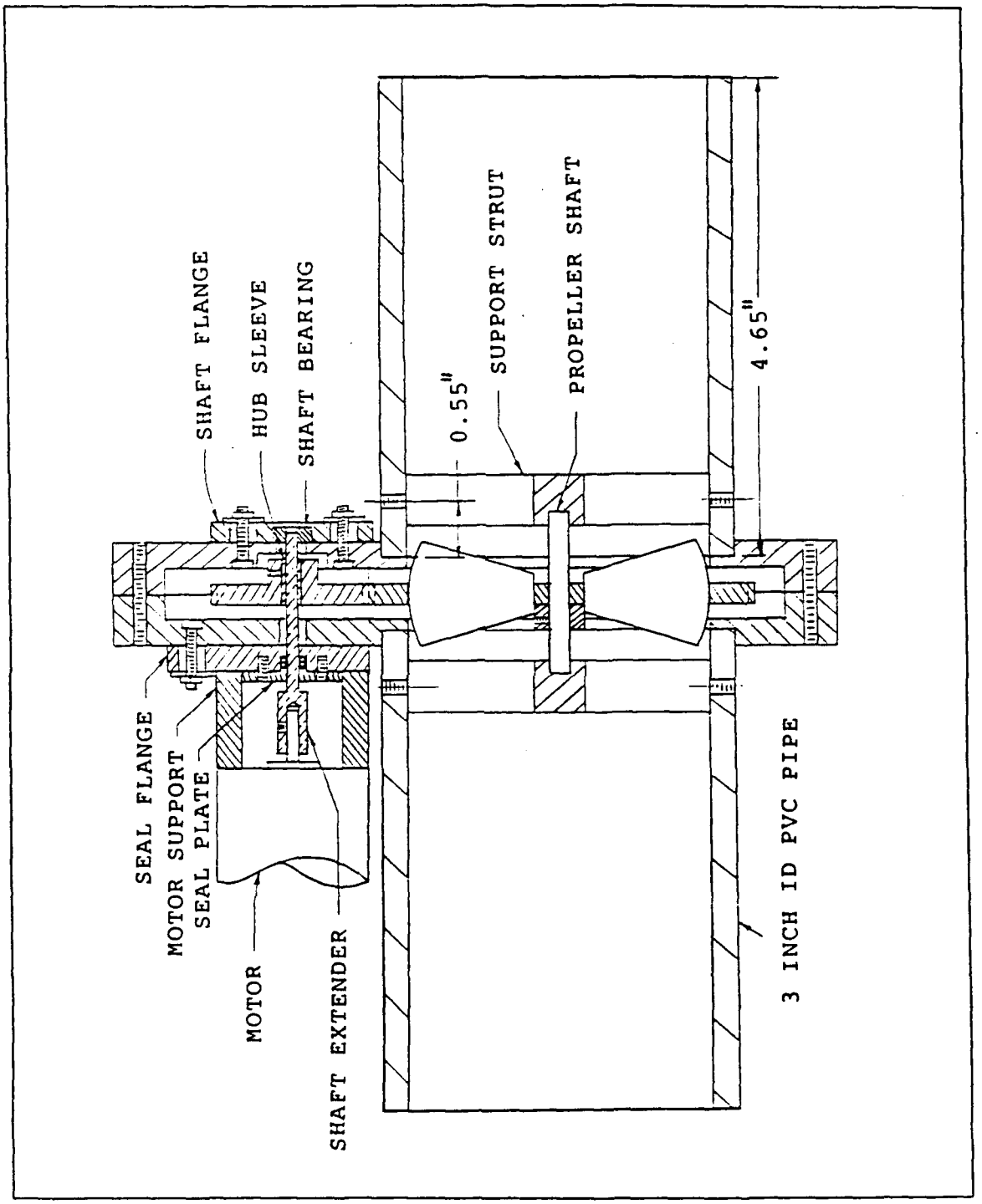

Figure 2 Cross--Sectional Drawing of Thruster Assembly

3. Reduction Gear

The pinion and gear that connect the propeller and motor shafts are both spur gears made of a polymer called Delrin[2]. The pinion has a 1.5 inch pitch diameter with 36 teeth. The gear has a 3.75 inch pitch diameter with 90 teeth. Both gears therefore have a pitch of 24 teeth per inch. The gear had the center portion of the face removed and the propeller was attached in the remaining opening. The result on shaft torque and speed, along with propeller thrust, of using different gear ratios can be observed in Appendix A.

4. Motor

The prime--mover is a DC servomotor, model number 9514[3], which has a stall torque of 24 ounce--inches and a no load speed of 7370 RPM. The winding selection (No. 3) allows operation at 24 volts with a no load current of 0.164 amps. The motor requires 143 watts of power at peak (stall) torque. The nominal outside diameter of the motor is 1.6 inches and the length is 2.25 inches, not including the shaft. The speed of the motor is controlled by varying the terminal voltage through a motor driver circuit card. The card uses two operational amplifiers and two sets of Darlington pair transistors to amplify a 0--10 volt control signal to 24 volts. This voltage can have either a positive or negative polarity for changing the direction of operation. See Figure 3 for

---

[2] Registered Trademark, Winfred M. Berg Company, East Rockaway, NY.

[3] Manufactured by Pittman Division of Penn Engineering and Manufacturing Corporation, Harleysville, PA.

a schematic of the control circuitry. For a listing of motor and winding parameters, see Appendix B.

B. MOTOR MODEL

1. General

The equations of motion, or state equations, were derived by considering a simplified electromechanical system shown in Figure 4. To facilitate the study of the time response due to the variation of key parameters, the motor transfer function was derived in a simple form, allowing additional components of the model to be represented by feedback gain loops. To comply with this format, but also present the general approach to this type of problem, the load torques applied to the motor will be the inertias of the motor and propeller and the viscous friction of the motor and propeller shafts, without the consideration of the hydrodynamic loading of the propeller.

The two basic laws that permit the electrical power supplied to be converted to mechanical horsepower and visa--versa are frequently called the motor and generator laws (attributed to Coulomb, Faraday, and Lenz):

- motor law..... $T_M = K_T i$ (2.1)
- generator law.....$e = K_G \omega_M$ (2.2)

The armature and the inertial load of a motor can be approximated as a pair of flywheels connected by a common shaft. In this thesis, the shaft compliance will be assumed negligible, so that a stiffness term will not appear in the state

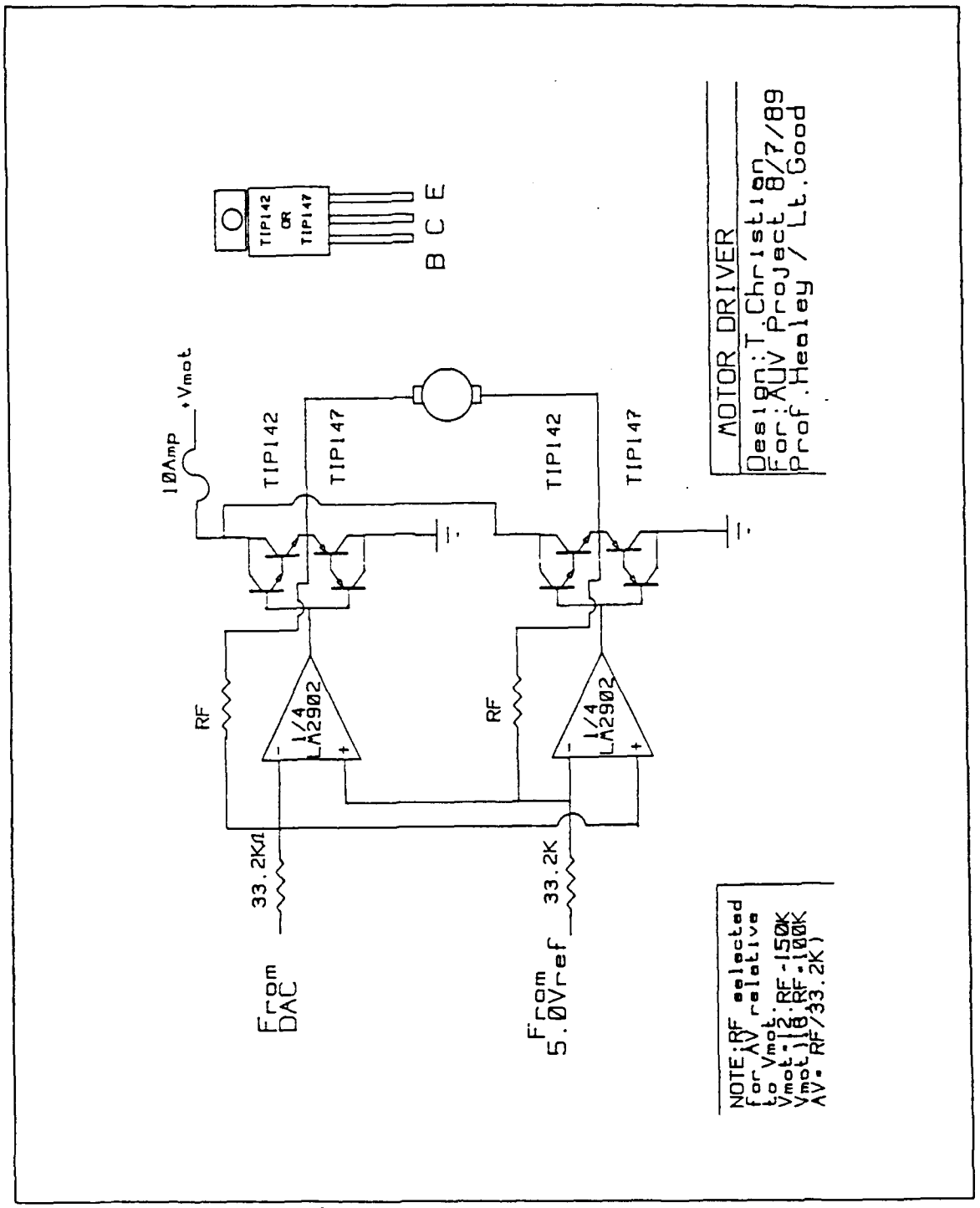

Figure 3 Motor Control Schematic

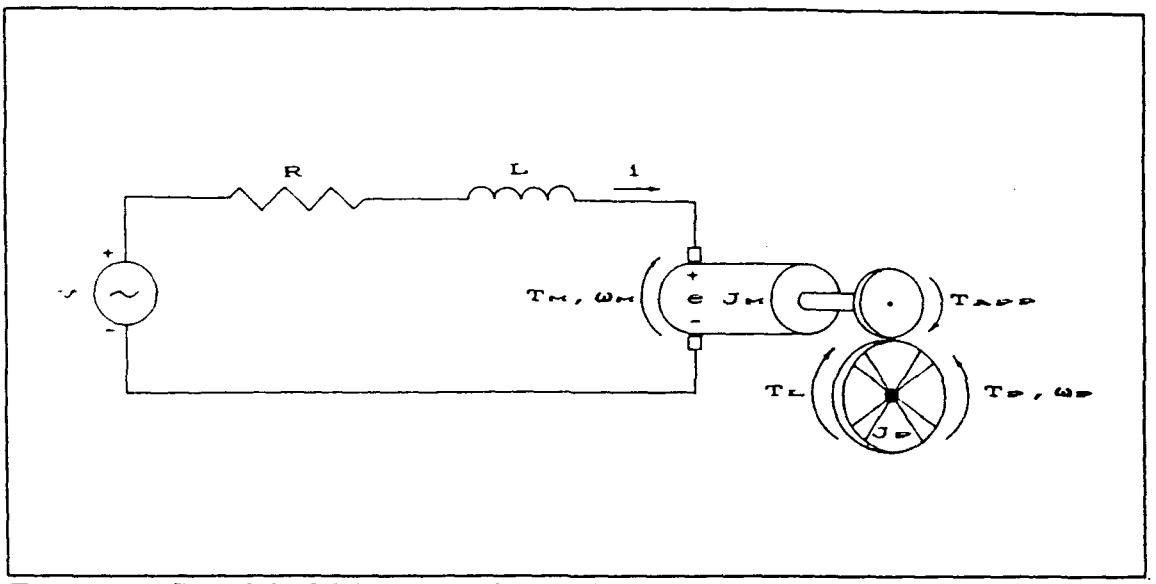

Figure 4 Simplified Electromechanical System Diagram

equations. The damping terms are due to the relative velocity between the motor or propeller shaft and the bearings, which both constitute a resistance to motion.

2. Derivation of Motor Transfer Function

Referring again to Figure 4, the state equation for the electrical circuit is first order in the motor angular velocity, ω_M, which we designate as the state variable. Using Kirchoff's voltage law around the loop, we get:

$$L(\frac{di}{dt}) + Ri = V - K_G \omega_M$$

We now assume that $L(\frac{di}{dt})$ is negligible since the electrical time constant is much smaller than the mechanical time constant (Refer to Appendix B).

Solving for the armature current:

$$i = \frac{V - K_G \omega_M}{R} \tag{2.3}$$

Now the mechanical relations will be addressed:

Motor: $J_M\dot{\omega}_M + C_M\omega_M + T_{APP} = T_M$

Propeller: $T_P = J_P\dot{\omega}_P + C_P\omega_P$

Gear Box: $\omega_M = N\omega_P$ and $T_P = NT_{APP}$ where N = 2.5

Combining the motor and propeller equations by using the gearbox relations, the mechanical state equation with all parameters reflected to motor quantities is:

$$T_M = (J_M + \frac{1}{N^2}J_P)\dot{\omega}_M + (C_M + \frac{1}{N^2}C_P)\omega_M \tag{2.4}$$

Note that the gear ratio shows up to the second power in the denominator of the terms on the propeller side of the reduction gear set, not to the first power as one might assume [Ref. 11]. Let the constants in the first parentheses be designated by "J_{PM}" and the constants in the second parentheses by "C_{PM}". Now from the motor law (EQ. 2.1) the motor torque can be related to the armature current. Using "i" from Equation 2.3 and Equation 2.1 and substituting the result into Equation 2.4 for "T_M", we get:

$$K_T(\frac{V - K_G \omega_M}{R}) = J_{PM}\dot{\omega}_M + C_{PM}\omega_M$$

Simplifying,

$$V - K_G \omega_M = \frac{J_{PM} R}{K_T} \dot{\omega}_M + \frac{C_{PM} R}{K_T} \omega_M$$

Taking the Laplace Transform of both sides:

$$V - K_G \omega_M = \frac{J_{PM} R}{K_T} s \omega_M + \frac{C_{PM} R}{K_T} \omega_M$$

Grouping like terms,

$$V = \left(\frac{J_{PM} R}{K_T} s + K_G + \frac{C_{PM} R}{K_T}\right) \omega_M$$

Rearranging the equation into transfer function form:

$$\frac{\omega_M}{V} = \frac{1}{\frac{J_{PM} R}{K_T} s + K_G + \frac{C_{PM} R}{K_T}}$$

Defining:

$$\tau_{P(M)} = \frac{J_{P(M)} R}{K_T K_G}$$

$$K_1 = \frac{R}{K_T}$$

$$K_0 = \frac{1}{K_G}$$

and substituting into the previous transfer function, we get:

$$\frac{\omega_M}{V} = \frac{1}{\frac{\tau_{PM} s}{K_0} + \frac{1}{K_0} + K_1 C_{PM}}$$

or:

$$\frac{\omega_M}{V} = \frac{K_0}{\tau_{PM} s + (K_0 K_1 C_{PM} + 1)} \qquad (2.5)$$

As mentioned earlier in this section, the model was derived using motor/propeller inertias and shaft viscous friction terms as a simplified and illustrative example of the general procedure for obtaining a transfer function for a DC motor driving an inertial load with only minor losses. Now we will further simplify the motor transfer function by removing the propeller inertia and viscous friction terms to allow them to be added back as separate feedback loop gains and then show that the two are equivalent. This uncoupling of inertia terms becomes important later when the inertial contributions from hydrodynamic effects need to be added. Therefore, from Equation 2.4, with "C_{PM}" and "J_P" = 0:

$$T_M = J_M \dot{\omega}_M \tag{2.6}$$

Following the same procedure as before, we get:

$$\frac{\omega_M}{V} = \frac{\frac{1}{K_G}}{\frac{J_M R}{K_T K_G} s + 1}$$

and using the same definitions:

$$\frac{\omega_M}{V} = \frac{K_0}{\tau_M s + 1} \tag{2.7}$$

Next we will show how these portions can be added back to the model as feedback loop gains to obtain the identical system. Starting with the propeller inertia term and recalling the gear box relations, the feedback gain will be:

- propeller inertia gain = $\frac{J_P K_1}{N^2}$

This loop must originate from the motor acceleration path which is not accessible in the present form. To get into the required form, the transfer function must be multiplied by a complex frequency term, "s", and then downstream an integrator is added in the path to compensate for this differentiation (Fig. 5).

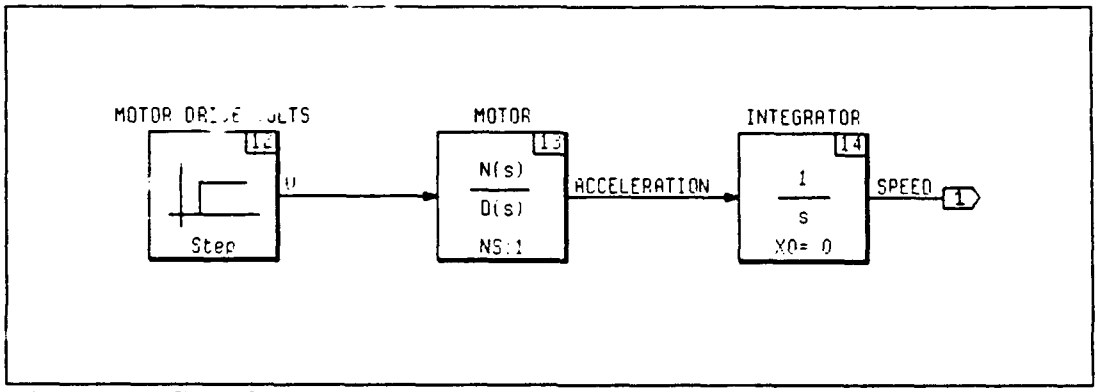

Figure 5 Simplified Motor Model

The propeller inertia gain will be given a negative sign at the voltage summer located upstream of the motor transfer function (Fig. 6).

Now we will add two more feedback loops for the motor and propeller viscous terms:

- motor shaft viscous friction = $K_1 C_M$
- propeller shaft viscous friction = $\frac{K_1 C_P}{N^2}$

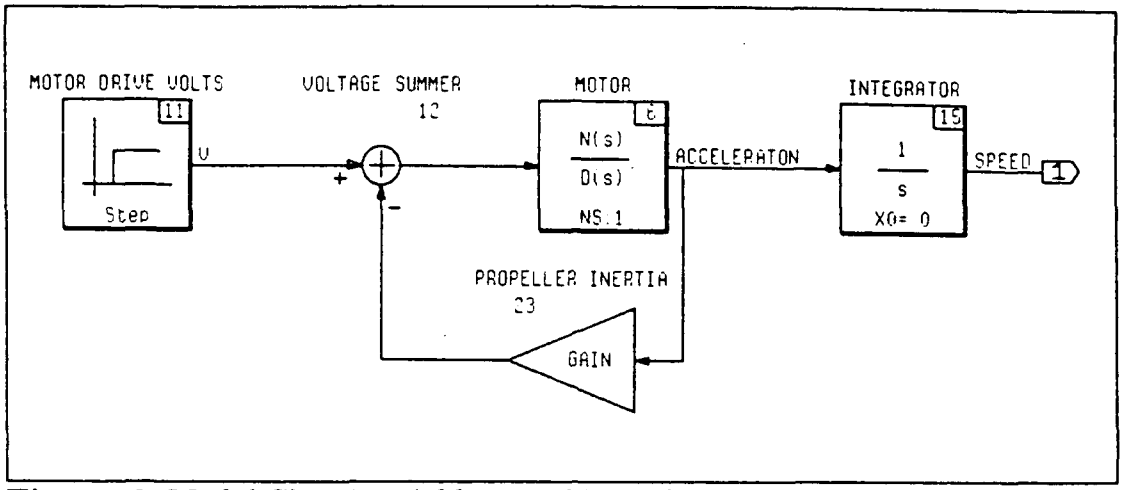

Figure 6 Model Showing Addition of Propeller Inertia

where we have divided the propeller term by the gear ratio squared (Fig. 7).

To show that the two models are identical, the loops will be closed on the model in Figure 7 using block diagram algebra:

$$\frac{\dfrac{K_0\, s}{\tau_M\, s + 1}}{1 + \left(\dfrac{K_0\, s}{\tau_M\, s + 1}\right)\left(\dfrac{K_1\, J_P}{N^2}\, s + \dfrac{K_1\, C_M}{s} + \dfrac{K_1\, C_P}{sN^2}\right)}$$

After several steps of algebra to find a common denominator, which will be omitted for brevity, we obtain:

$$\frac{K_0\, s}{\left(K_0\, K_1\, \dfrac{J_P}{N^2} + \tau_M\right)s + K_1\, K_0\, C_M + \dfrac{K_0\, K_1\, C_P}{N^2} + 1}$$

which, when reduced further by expanding the constant "τ_M" and grouping terms, results in:

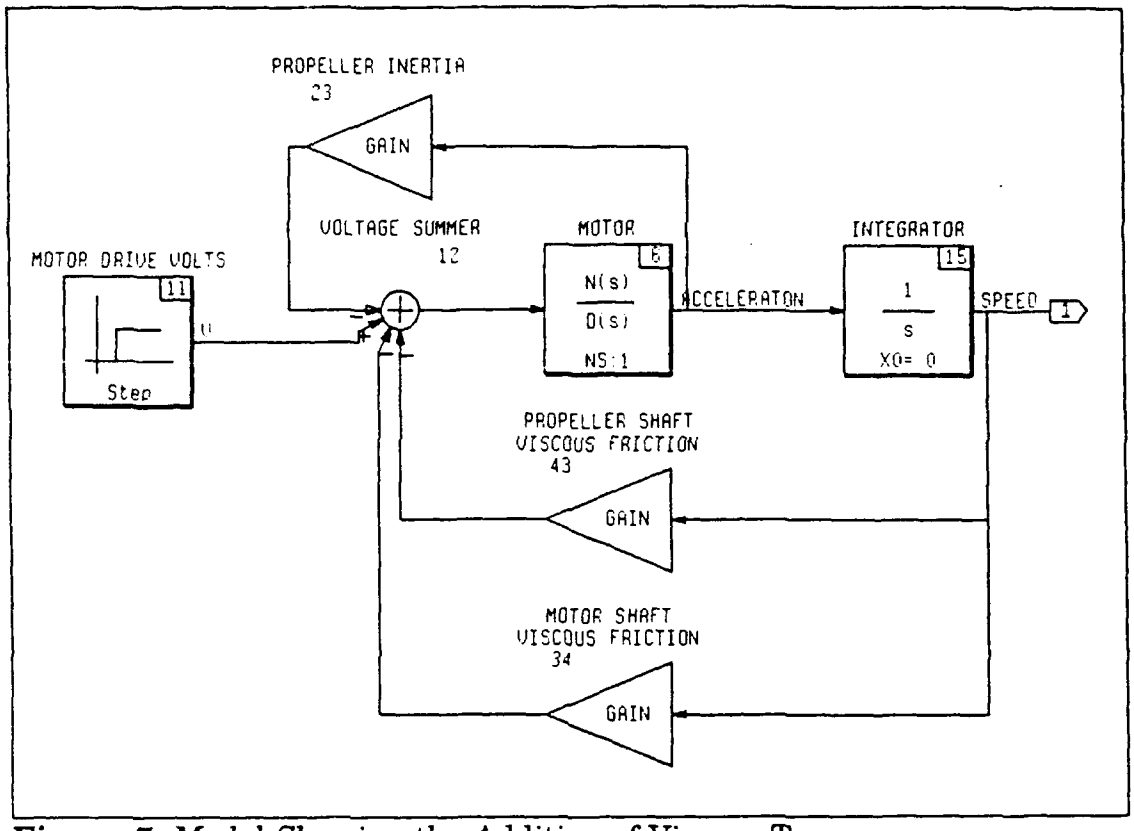

Figure 7 Model Showing the Addition of Viscous Terms

$$\frac{K_0 s}{\frac{RK_0}{K_T}\left(\frac{J_P}{N^2} + J_M\right)s + K_1 K_0\left(C_M + \frac{C_P}{N^2}\right) + 1}$$

and using the compound variables "τ_{PM}" and "C_{PM}" and removing the "s" term,

$$\frac{K_0}{\tau_{PM} s + (K_0 K_1 C_{PM} + 1)} \tag{2.8}$$

which agrees with Equation 2.5. This method of expressing each portion of the block diagram as a separate element will be continued in building the entire tunnel thruster model. Each element of the computer model is described in the following chapter. This method of constructing block diagrams is very "user--

friendly"; due to its ability to allow individual parameters to be changed independently, the effect on the output can be observed as they are varied, forming a one--to--one relationship between parameter values and output.

C. THRUSTER HYDRAULIC MODEL

Once the motor model had been developed and refined so as to agree favorably with the vendor's specifications, the hydraulic model could be developed and added to the motor to obtain the desired result: a thruster model. Since the output of the motor model was angular velocity, and the parameter that was desired as output was thrust, an approach was required that would include these quantities and at the same time satisfy the fluid mechanics involved in the physical system. This approach also had to marry the mechanical horsepower of the propeller with the various hydraulic sources of energy. The physical laws at the basis of this model are the conservation of linear momentum and the conservation of energy.

In both cases, the unsteady, nonuniform equations were required to obtain the proper conditions. The general approach was then to reduce the equation to its most simple form, using simplifications and approximations where appropriate. In the following three subsections, first a listing of assumptions used in the equations will be presented, followed by the application of conservation of momentum, and lastly the application of conservation of energy.

1. Assumptions for Hydraulic Model

The assumptions that were made regarding the conservation of energy and momentum laws are given below.

1. Adiabatic control volume
2. Inviscid fluid flow
3. Incompressible fluid flow
4. Potential energy is negligible
5. Internal energy is negligible
6. Enthalpy is negligible
7. W_V is negligible
8. Inlet and outlet of control volume are at constant pressure
9. E_{CV} is due solely to the change in kinetic energy
10. Change in kinetic energy is a function of W_S only
11. Control volume is nondeformable and can be simplified to a cross--sectional area (A) multiplied by the effective length (Le) that takes into account the influence of the added mass [Ref. 12]

2. Conservation of Momentum

In Newton's second law of motion, the quantity being differentiated is momentum, and the result of this operation is equal to the summation of all external forces acting on the mass. In the case of the thruster, the only external force that acts to accelerate the fluid inside the tunnel is the thrust from the propeller blades. To derive the thrust equation, the Reynolds

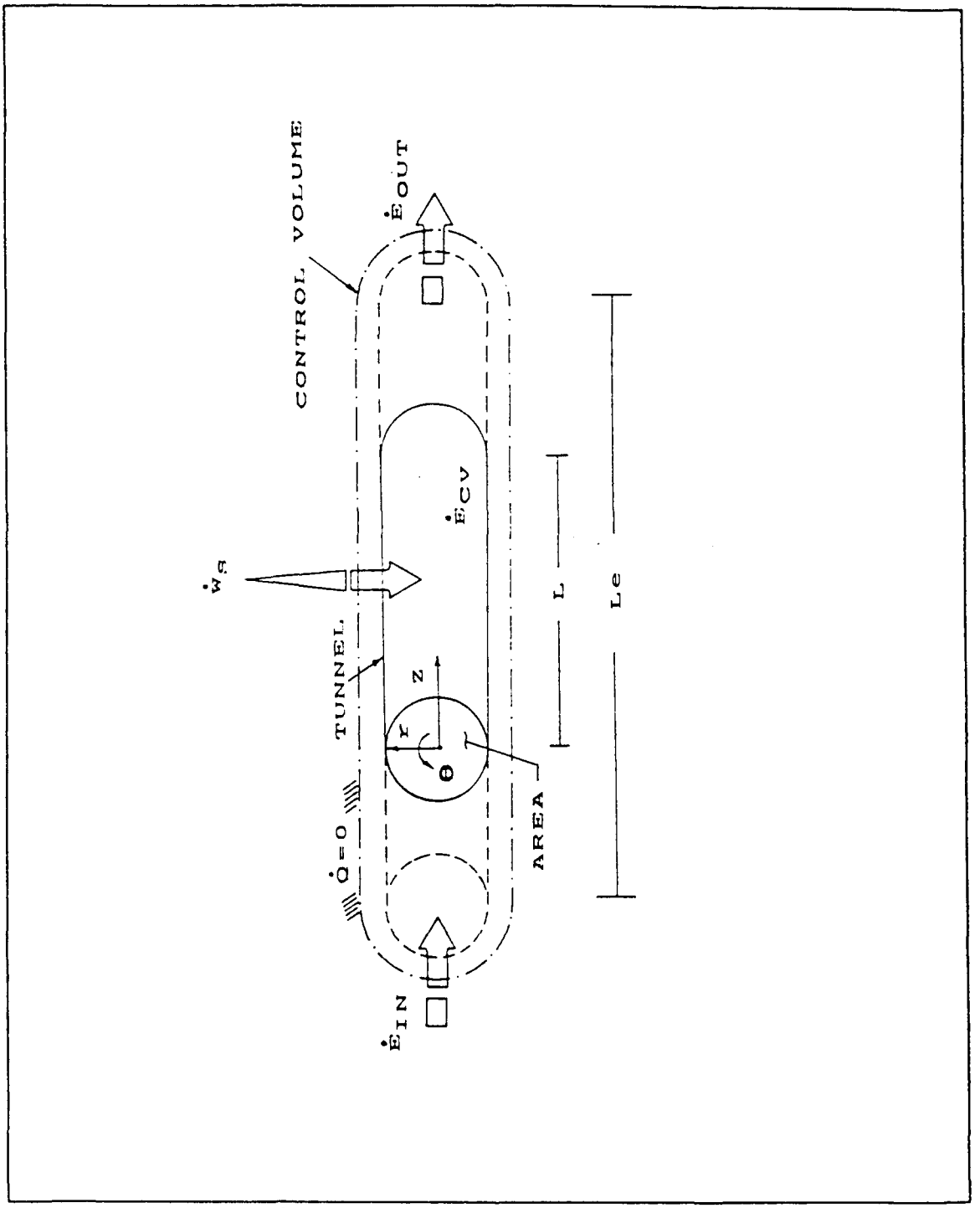

Figure 8 Control Volume Schematic Used in Analysis

transport theorem is applied to the linear momentum of the fluid:

$$\sum \boldsymbol{F} = \frac{\partial}{\partial t}\left[\iiint_{cv} V\rho dV\right] + \iint_{cs} V\rho(\boldsymbol{V}\cdot\boldsymbol{n})dA \qquad (2.9)$$

Substituting "*THRUST*" for the left side of the above equation and realizing that only the horizontal component of $\boldsymbol{V}$ is important, we get:

$$THRUST = \frac{\partial}{\partial t}\left[\iiint_{cv} u\rho\, dV\right] + \iint_{cs} u\rho(u\boldsymbol{k}\cdot\boldsymbol{n})dA$$

and for incompressible flow the density can be removed from the integrand:

$$THRUST = \rho\frac{\partial}{\partial t}\left[\iiint_{cv} u(r,t)dV\right] + \rho\iint_{cs} u(r,t)[u(r,t)\boldsymbol{k}\cdot\boldsymbol{n}]dA$$

where "u" has been set to "u(r,t)" to emphasize the velocity's dependence on radial position and time within the control volume. Here we will separate the equation into two parts and analyze them separately. The unsteady term will be denoted as "A" and the steady term will become "B".

$$\underline{A}: \quad \rho\frac{\partial}{\partial t}\left[\iiint_{cv} u(r,t)dV\right]$$

Since Q(t) can be defined as:

$$Q(t) = \iint_{cs} u(r,t)\cdot dA$$

and u = u(r,t) only, making the velocity independent of θ and z, a simplification can be made that was presented in the assumptions. This allows the triple integral over the control volume to be represented by a double integral over the cross--sectional area of the tunnel openings, multiplied by the effective length:

$$\rho \frac{\partial}{\partial t}\left[\int_{cv}\iiint u(r,t)dV\right] = \rho Le \frac{\partial}{\partial t}\left[\int_{xs}\iint u(r,t)\cdot dA\right]$$

$$= \rho Le \dot{Q}(t)$$

Replacing "Le" with L(1 + Ka) [Ref. 12], we get:

$$\underline{A} = \rho L(1+Ka)\dot{Q}(t) \qquad (2.10)$$

$$\underline{B}: \quad \rho \int_{cs}\iint u(r,t)[u(r,t)\boldsymbol{k}\cdot\boldsymbol{n}]dA$$

Since the scalar product flux term has two components:

$$\boldsymbol{V}\cdot\boldsymbol{n} = [+\beta_o u] \text{ for outflow and } [-\beta_i u] \text{ for inflow}$$

where the momentum correction factor is defined as:

$$\beta_o = \frac{\int_{\text{outlet xs}}\int u(r,t)^2 dA}{A\bar{u}^2} \quad ; \quad \beta_i = \frac{\int_{\text{inlet xs}}\int u(r,t)^2 dA}{A\bar{u}^2}$$

with:

$$\bar{u} = \frac{Q(t)}{A}$$

and, again:

$$Q(t) = \int_{xs}\iint u(r,t)\cdot dA$$

we get:

$$\underline{B} = \frac{\rho}{A}(\beta_o - \beta_i)Q(t)|Q(t)| \qquad (2.11)$$

and adding "A" and "B" together:

$$\text{THRUST} = \rho L(1 + Ka)\dot{Q}(t) + \frac{\rho}{A}(\beta_o - \beta_i)Q(t)|Q(t)|$$

Making the substitution, $Q(t) = \eta p A \omega_p$ {from the definition of relative slip (σ_R)} [Refs. 9,13]:

$$\text{THRUST} = \eta\, pA\rho L(1 + Ka)\dot{\omega}_p + (\eta p)^2 A\rho(\beta_o - \beta_i)\omega_p|\omega_p| \qquad (2.12)$$

Note that Equation 2.12 differs from the explanation in the Yoerger paper [Ref. 9]; the ω_p term has been recognized here due to the influence of the fluid mass in the tunnel and its associated hydrodynamic added mass which is important in tunnel thruster dynamics.

3. Conservation of Energy

To solve the unsteady energy equation for a control volume, again the Reynolds transport theorem was applied, in this case to the first law of thermodynamics [Ref. 14]:

$$\dot{Q} - \dot{W}_S - \dot{W}_V = \dot{E}_{CV} + \dot{E}_{OUT} - \dot{E}_{IN}$$

or:

$$\dot{Q} - \dot{W}_S - \dot{W}_V = \frac{\partial}{\partial t}\left[\iiint_{cv}\left(u + \frac{1}{2}|V|^2 + gz\right)\rho\, dV\right] + \iint_{cs}\left(h + \frac{1}{2}|V|^2 + gz\right)\rho(\boldsymbol{V}\cdot\boldsymbol{n})dA \qquad (2.13)$$

Assuming that $\dot{W}_V = z = \ddot{u} = h = Q = 0$ and letting $\dot{W}_S = -T_p\,\omega_p$, we get:

$$T_p \omega_p = \frac{\partial}{\partial t}[\iiint_{cv}(\frac{1}{2}|V|^2)\rho\, dV] + \iint_{cs}(\frac{1}{2}|V|^2)\rho(\boldsymbol{V}\cdot\boldsymbol{n})dA$$

Again, separating the equation into two parts, the unsteady term will be denoted as "A" and the steady term will become "B".

$$\underline{A}: \quad \frac{\partial}{\partial t}[\iiint_{cv}(\frac{1}{2}|V|^2)\rho\, dV]$$

From the previous discussion regarding the control volume:

$$\underline{A} = \frac{\rho}{2}\frac{\partial}{\partial t}[\iiint_{cv}u(r,t)^2 dV\ ] = \rho\frac{Le}{2}[\frac{\partial}{\partial t}\iint_{xs}u(r,t)^2 dA\ ]$$

and recalling that:

$$Q(t) = \iint_{xs}u(r,t)\cdot dA$$

the result is:

$$\underline{A} = \frac{\rho Le\beta}{A}Q(t)\dot{Q}(t)$$

but with, $Q(t) = \eta pA\omega_p$:

$$\underline{A} = \beta(\eta p)^2(\rho ALe)\dot{\omega}_p\omega_p$$

and finally, replacing "Le" with L(1 + Ka), the result is:

$$\underline{A} = \beta(\eta p)^2\rho AL(1 + Ka)\dot{\omega}_p\omega_p \qquad (2.14)$$

$$\underline{B} = \iint_{cs}(\frac{1}{2}|V|^2)\rho(\boldsymbol{V}\cdot\boldsymbol{n})dA$$

$$= (\frac{\rho}{2}\int_{outlet\,xs}\int u(r,t)^3dA - \frac{\rho}{2}\int_{inlet\,xs}\int u(r,t)^3dA)$$

This time, the energy correction factor is defined as:

$$\alpha_o = \frac{\int_{outlet\,xs}\int u(r,t)^3dA}{A\bar{u}^3} \quad ; \quad \alpha_i = \frac{\int_{inlet\,xs}\int u(r,t)^3dA}{A\bar{u}^3}$$

and recalling the definition of Q(t) from before,

$$\underline{B} = \frac{\rho}{2A^2}(\alpha_o - \alpha_i)Q(t)^3$$

Again making the substitution, $Q(t) = \eta pA\omega_p$:

$$\underline{B} = \frac{(\eta p)^3 \rho A}{2}(\alpha_o - \alpha_i)\omega_p^3 \qquad (2.15)$$

Combining parts "A" and "B" back together:

$$T_p = (\eta p)^2(\rho A)L(1 + Ka)\beta\dot{\omega}_p + \frac{(\eta p)\rho A}{2}(\alpha_o - \alpha_i)\omega_p|\omega_p| \qquad (2.16)$$

These equations will be used in the following chapter to develop the complete thruster computer model using $Matrix_X$ software, on the ME Department's CAD/CAE Laboratory VAX--2000 workstation. Each equation will be expanded as necessary to allow the important parameters to be easily accessible and values for each quantity will be addressed block--by--block. In

addition to building the block diagram, the results from the computer simulations of thruster transient response performance will be presented and discussed. Of interest is the response of propeller speed and net thrust versus time, as well as the influence of key parameters such as tunnel length, added mass coefficient, and the product of propeller efficiency and pitch.

III. COMPUTER SIMULATION

A. GENERAL

The computer simulation of the AUV II tunnel thruster was used to obtain the time response of thrust for three levels of step input voltages for comparison with experimental results, and to study the response sensitivity of the model to variations in several key parameters. Using the block diagram of the motor and the hydrodynamic equations of torque and thrust derived in Chapter II, the complete thruster computer model will be built and described, block--by--block, in Section B of this chapter. Section C will then present and interpret the results obtained from the computer simulations.

B. BUILDING THE BLOCK DIAGRAM

The complete tunnel thruster block diagram was built, element--by--element, as described in Chapter II. As a preliminary phase before the entire thruster model was constructed, a model of the motor and propeller alone without hydrodynamic load was built to ensure that the motor itself had been modeled properly. In this model the propeller was a simple inertial load, as if it were a disk spinning in air (Fig. 9). The motor speed response was simulated using a 24 volt input signal and compared to the vendor's specifications. From Figure 10 it is clear that the motor model closely

approached these values, especially mechanical time constant (18 milliseconds) and no load speed (7370 RPM).

After the motor model had been built and simulated with favorable results, the elements representing the hydrodynamic effects were added. The two equations from the conservation of momentum and energy were naturally divided into two distinct parts, one that was a function of propeller angular acceleration and one that was a function of the propeller absolute--squared angular velocity. These blocks were then further divided into groups of terms that could be easily changed without recalculating the gain for the entire loop. This complete model is shown in Figure 11, and Figures 12 and 13 present a blowup of the model, where the numbered arrows connect the paths between the two figures. The following section will describe each block, where the number before each name is shown on the block diagram (Fig. 11 or 12/13).

1. Block Description

2: PROPELLER INERTIA

The polar mass moment of inertia of the propeller was calculated by considering the blades and gear ring separately. The blades were divided into 12 rectangular elements and the inertia from each was calculated, then these elements were summed to get the total inertia for all four blades. The gear ring was calculated by assuming it to be a solid disk and then subtracting out an inner disk. The sum of these two inertias became the propeller inertia.

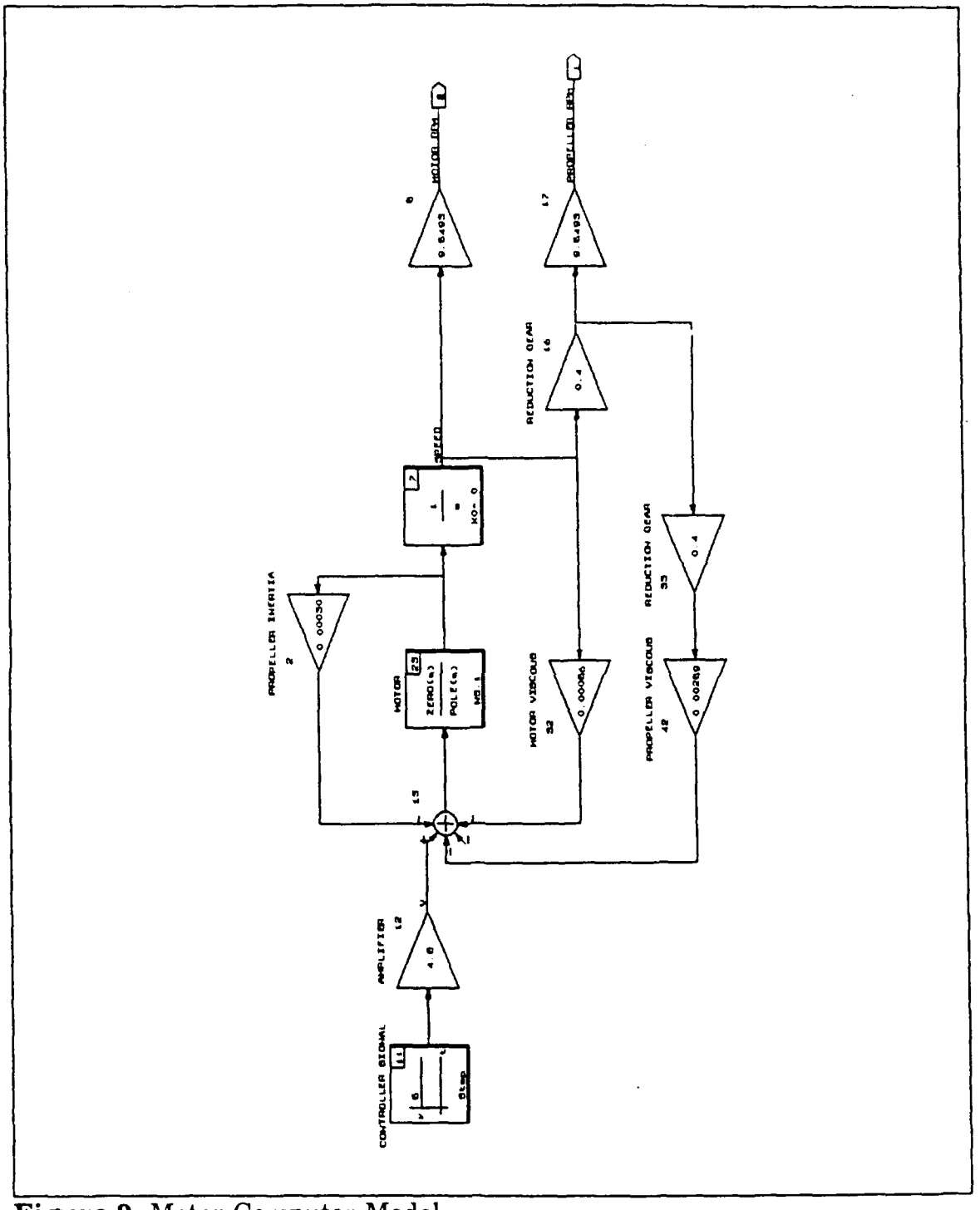

Figure 9 Motor Computer Model

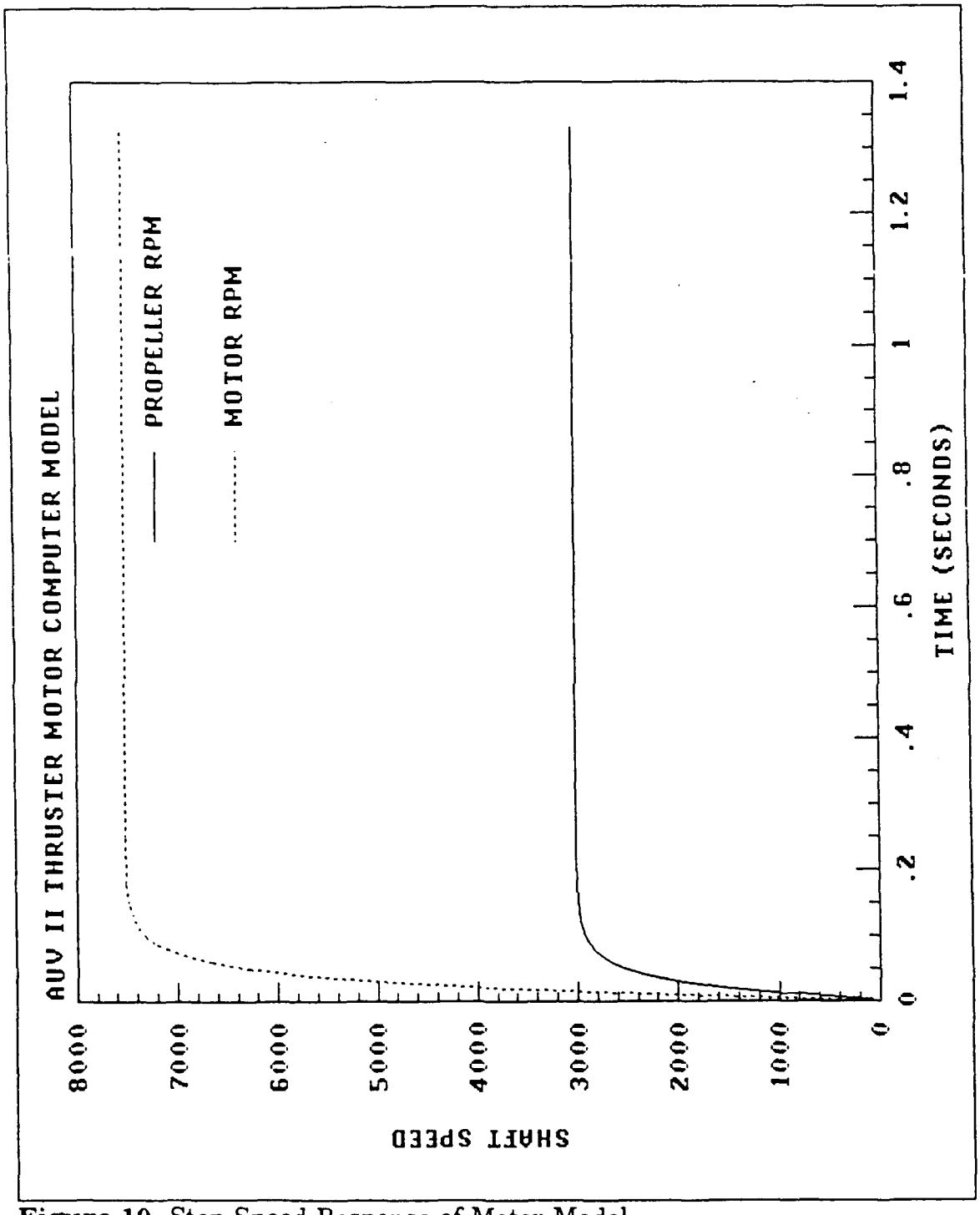

Figure 10 Step Speed Response of Motor Model

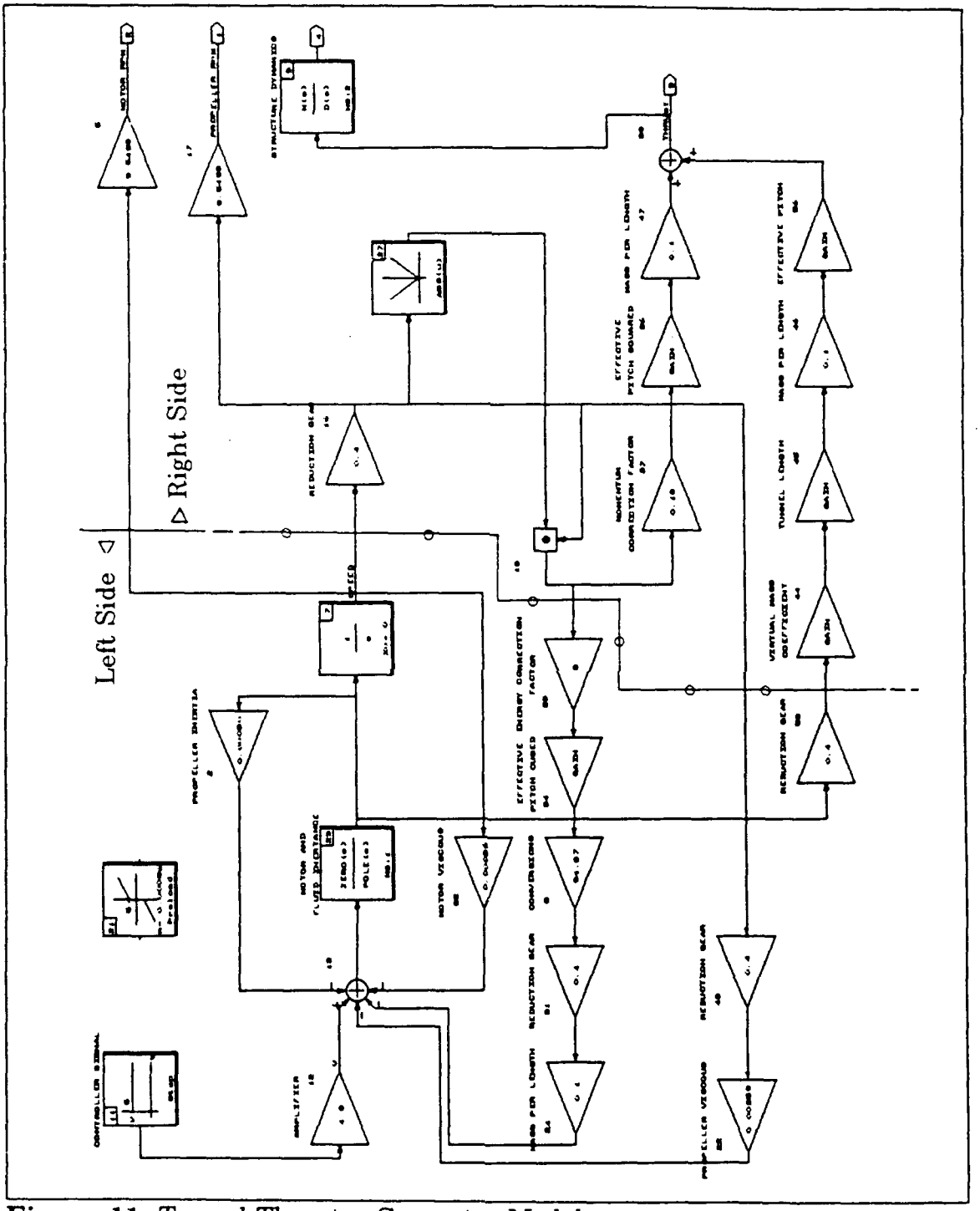

Figure 11 Tunnel Thruster Computer Model

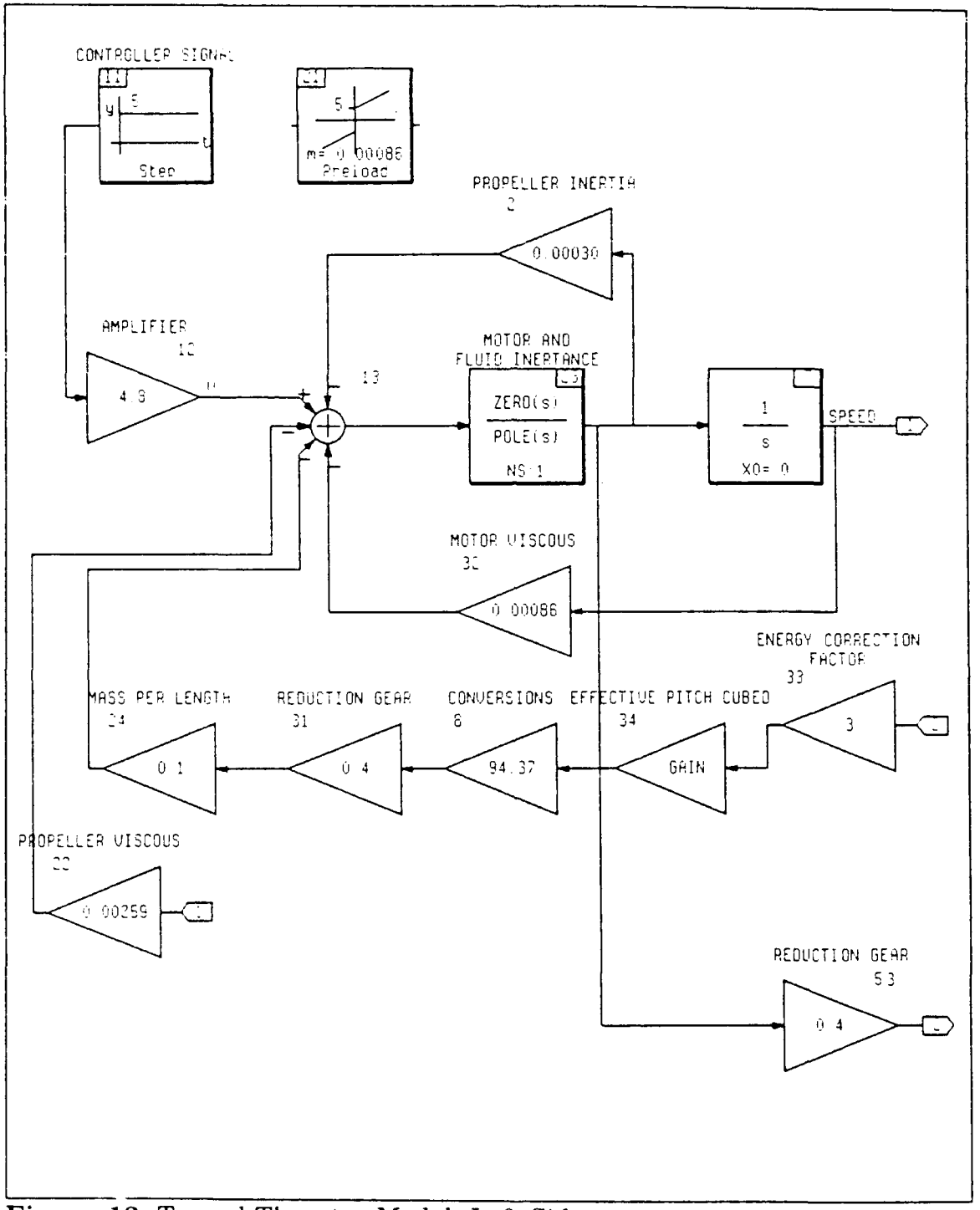

Figure 12 Tunnel Thruster Model--Left Side

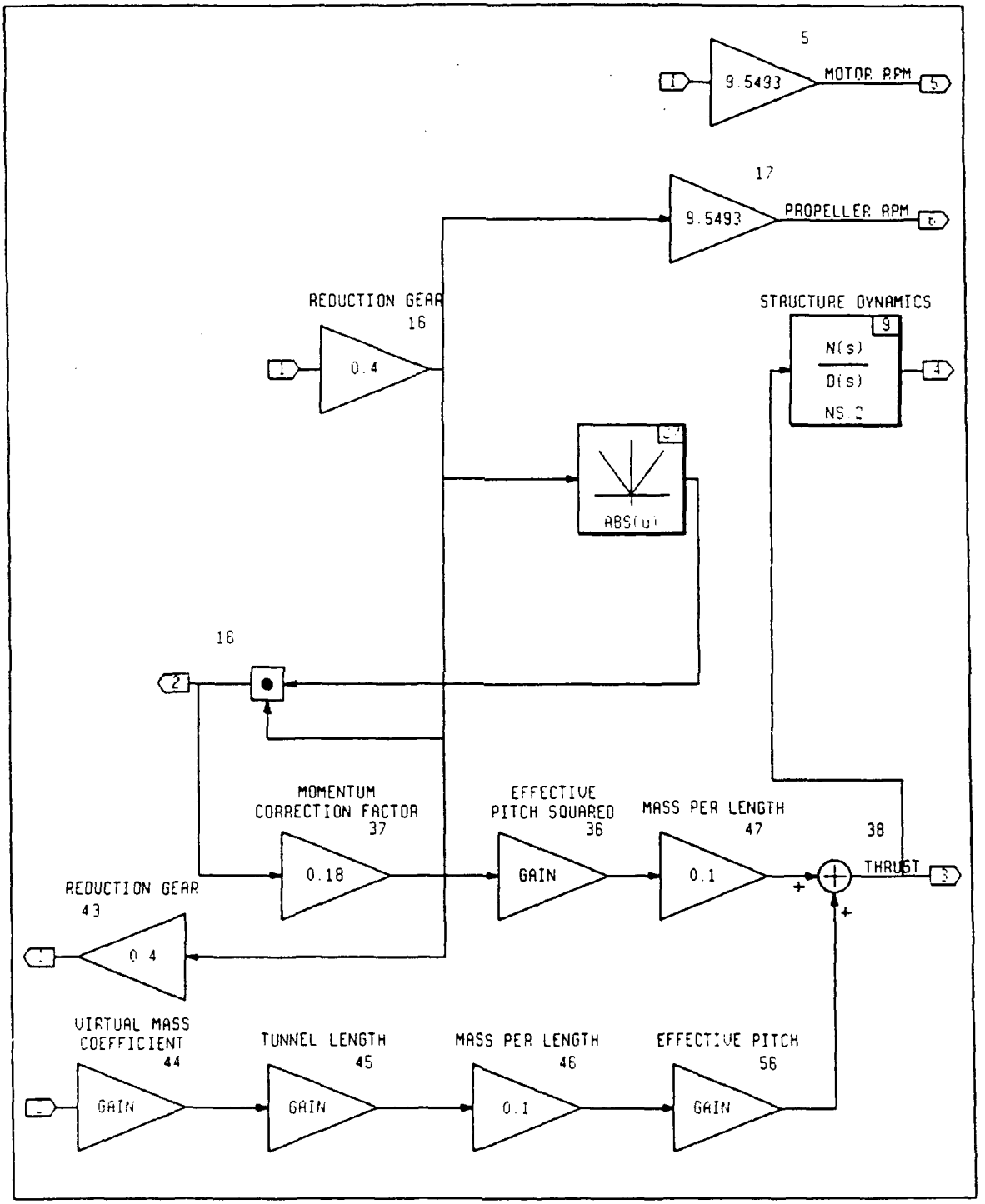

Figure 13 Tunnel Thruster Model--Right Side

Since this value was reflected to the motor side of the reduction gear, a N^2 term was required in the denominator. The value was then converted from torque units into volts by multiplying with K_1.

5: RPM CONVERSION

This constant converts radians per second for output in revolutions per minute.

7: INTEGRATOR

This element performs an integration with respect to time to the entering value, assuming that all initial conditions are zero.

8: CONVERSIONS

This constant is the product of K_0, K_1, and 0.5. These constants are defined under Nomenclature at the front of the thesis.

9: STRUCTURE DYNAMICS

This element models the response of the test box to the thrust transient with a "mass--spring--damper" second order transfer function. The damped natural frequency (ω_d) of the structural system was identified from separate experimental data as 7 Hz and the damping ratio (ς) was estimated to be 0.16. This data will be discussed further in Chapter IV under Experimental Results. The actual transfer function is:

$$\frac{1935}{s^2 + 14.1\,s + 1935} \tag{3.1}$$

11: CONTROLLER SIGNAL

This signal can be zero to five volts, positive or negative. As shown in Figure 3 of Chapter II, the signal from the digital to analog converter (DAC) is positive zero to ten volts, but the reference voltage is five volts. This signal is then sent to an amplifier before reaching the motor.

12: AMPLIFIER

This element amplifies the controller signal from the DAC using a gain of 4.8 (5.0 x 4.8 = 24.0).

13: VOLTAGE SUMMER

This element sums the four voltage inputs from the various feedback loops (-) with the input signal from the amplifier (+). The output voltage is sent to the motor terminals to be converted to mechanical energy.

16: REDUCTION GEAR

The 2.5:1 gear ratio between the motor shaft and the propeller shaft. The larger gear is on the propeller side.

17: RPM CONVERSION

See Block **5**.

18: SCALAR PRODUCT

Simple multiplication of propeller angular velocity with itself, although due to the absolute value block upstream, this results in a "signed"-- or absolute--square result. Using this form the result is not positive definite, but retains the original direction of the rotation.

21: COULOMB FRICTION

This block was used in one of the simulations in place of the MOTOR VISCOUS element. This element may better model the static and dynamic friction of the thruster. The zero offset used was five volts, which was observed in the laboratory during steady state testing. The slope was the same as that used for the block that it replaced (0.000862).

22: PROPELLER VISCOUS

Assumed to be a factor of three times greater than the motor viscous friction (3 x Block **32**).

23: MOTOR AND FLUID INERTANCE

This block contains the motor/hydrodynamic load transfer function developed in Chapter II. The energy term, which manifests the inertance of the fluid in the control volume, was required due to the large amount of feedback it represented. The makeup of the block is as follows:

$$\frac{\dfrac{34.25}{(103 * BETA * Pe2 * L * VM + 0.01808)}}{(s + \dfrac{1}{(103 * BETA * Pe2 * L * VM + 0.01808)})} \qquad (3.2)$$

The values of the variables in the transfer function are entered from an executable file in VMS named "THRUST.X".

24: MASS PER LENGTH

The product of cross--sectional area of the tunnel and the density of the fluid inside ($A\rho$).

27: ABSOLUTE VALUE

Taking the absolute value of one of the propeller angular velocities before multiplying it by itself allows the sign of the term to be conserved. See Block **18**.

31: REDUCTION GEAR

See Block **16**.

32: MOTOR VISCOUS

This friction torque term was estimated as friction torque divided by no load speed. Friction torque can be defined as no load current times the torque constant (INL x K_T). This value was then multiplied by K_1 to convert torque into volts.

33: ENERGY CORRECTION FACTOR

This block is the difference between the outlet and inlet energy correction factors. This factor accounts for the nonuniformity of the inlet and outlet flow profiles. If these factors are equal ($\alpha = 1.0$ for uniform flow), then the steady state energy term is zero.

34: EFFECTIVE PITCH CUBED

The cube of the product of propeller efficiency and pitch ($[\eta p]^3$).

36: EFFECTIVE PITCH SQUARED

The square of the product of propeller efficiency and pitch ($[\eta p]^2$).

37: MOMENTUM CORRECTION FACTOR

This block is the difference between the outlet and inlet momentum correction factors. This factor accounts for the nonuniformity of the inlet and outlet flow profiles in the momentum equation.

38: THRUST SUMMER

The addition of transient and steady state thrust.

43: REDUCTION GEAR

See Block **16**.

44: VIRTUAL MASS COEFFICIENT

The factor multiplying the actual mass of an object or closed volume to give the effective total mass under influence of the driving force. VM = (1 + Ka).

45: TUNNEL LENGTH

The actual length of the tunnel or duct under consideration.

46,47: MASS PER LENGTH

See Block **24**.

56: EFFECTIVE PITCH

The product of propeller efficiency and pitch (ηp).

2. Simulations Using MATRIX$_x$ Software

The simulation was controlled from the executable VMS file, THRUST.X. The steps necessary to run a simulation were as follows: The model chosen to be "analyzed" was selected among several versions from a SystemBuild[4] directory. This action would show all the parameters that were being used and in what blocks they appear, along with other internal software commands and then return the "prompt <>" to the screen. Here the command "execute" would be typed in, along with the name of the executable file. At this point a second "window" would be opened by the programmer allowing the contents of the executable file to be edited. Here the values of all parameters would be checked to ensure they were correct for the case to be simulated. Figure 14 shows the file THRUST.X as it would look for simulating the baseline model. The Matrix$_x$ software will only allow single parameters to be placed in the blocks of the diagram, so for an equation with several variables in it like Block **23** (motor and fluid inertance), a single parameter such as Z (for the gain) or D (for the pole) was equated to the product of several variables. The other statements in the file pertain to vector definitions and graphics. After the executable file had been verified, the model was then run by striking the <ENTER> key in the SystemBuild window. After execution, the output was printed from a laser printer by using the "hardcopy"

[4] A dynamic modeling and simulation package within Matrix$_x$ that designs and manipulates block diagrams.

```
L=5.0/12.0
Ka=0.25
VM=1+Ka
BETA=1.5
ETA=0.75
P=0.0721
Pe=ETA*P
Pe2=Pe**2
Pe3=Pe**3
V=VM
Z=34.25/(103*BETA*Pe2*L*VM+0.01808)
N=Z
D=-1/(103*BETA*Pe2*L*VM+0.01808)
T=[0:0.01:1.333]';
Y=SIM(T);
y1=Y(:,1);
y3=Y(:,3);
y4=Y(:,4);
yy=[Y3 Y1 Y4 Y1];
PLOT('XLABEL\TIME (SECONDS)\ COLOR 0\ CHART...
 5 80 5 80')
MYSTY='NAME\AUV II TUNNEL THRUSTER COMPUTER...
 MODEL\ REPO4';
PLOT([MYSTY])
PLOT(T,YY,'STYLE 3 1 1 1\YMIN=0\STRIP2 YLAB\...
THRUST (POUNDS)|PROPELLER SPEED (RPM)')
```

Figure 14 Executable File THRUST.X

command. The procedure was then repeated for each case that was to be analyzed.

C. SIMULATION RESULTS

The **baseline** data for the model consisted of the following values or conditions:

- efficiency = 75%
- added mass coefficient = 0.25
- pitch = 0.0721 feet per radian (corresponding to a 30° pitch angle)

- length = 10.5 inches
- momentum correction factor = 1.5
- step input
- viscous friction terms for motor and propeller (vice coulomb friction)

All other values remain constant throughout the runs. After each case, the values were reset to baseline before altering the file for the next run.

Just how the baseline data came about will now be discussed. During the conduct of building the thruster model, a point was reached where parameters could no longer be obtained from theory or specifications, and therefore experimental results were required before continuing. These parameters were the energy and momentum correction factors, added mass coefficient, propeller efficiency, and the damping ratio and natural frequency of the structure dynamics block. At this time, the emphasis was shifted to the laboratory and the thruster test rig, all of which had been constructed to obtain the transient response of an actual tunnel thruster from AUV II. The experimental phase of the research was then conducted, which will be covered in detail in Chapter IV, and the results from the 8, 16, and 24 volt step responses were then available to guide the shaping of the computer model. With estimates of the first four unknown parameters described above being 1.0, 1.0, 1.0, and 0.70 respectively, the computer model was simulated and compared to the experimental results. These four parameters were then varied until the model

results closely resembled the experimental results. The matching was made much easier by adding the structure dynamics term onto the end of the output thrust. This element was previously described as Block **9**, a simple "mass--spring--damper" system modeling the dynamics resulting from the load cell compliance. The values for ς and ω_d were obtained from the impulse response of the test box. The 7 Hz frequency matched up well, but the damping ratio required some variation before the best match was settled on (ς=0.16).

The following cases were simulated and are included as output:

- 24 volt baseline
- 16 volt baseline
- 8 volt baseline
- 24 volt - length = 20 inches
- 24 volt - length = 5 inches
- 24 volt - added mass coefficient = 1.0
- 24 volt - added mass coefficient = 0.5
- 24 volt - effective pitch = 0.0270 feet per radian; this value represents a decrease from baseline in efficiency to 37.5% or in pitch angle to 16°.
- 24 volt - effective pitch = 0.0721 feet per radian; this value represents a increase from baseline in efficiency to 100% or in pitch angle to 37.5°.
- 24 volt - effective pitch = 0.0; this value represents a decrease from baseline in efficiency and/or pitch to zero.
- 24 volt - coulomb friction used in place of motor viscous friction; zero offset = 5 volts with a slope equal to previous viscous value (0.000862 volts per radian).

Following the output described above, each individual graph will be summarized, with any salient points breifly discussed. In Chapter V, the results will be tabulated and again the significant aspects of the findings will be addressed separately.

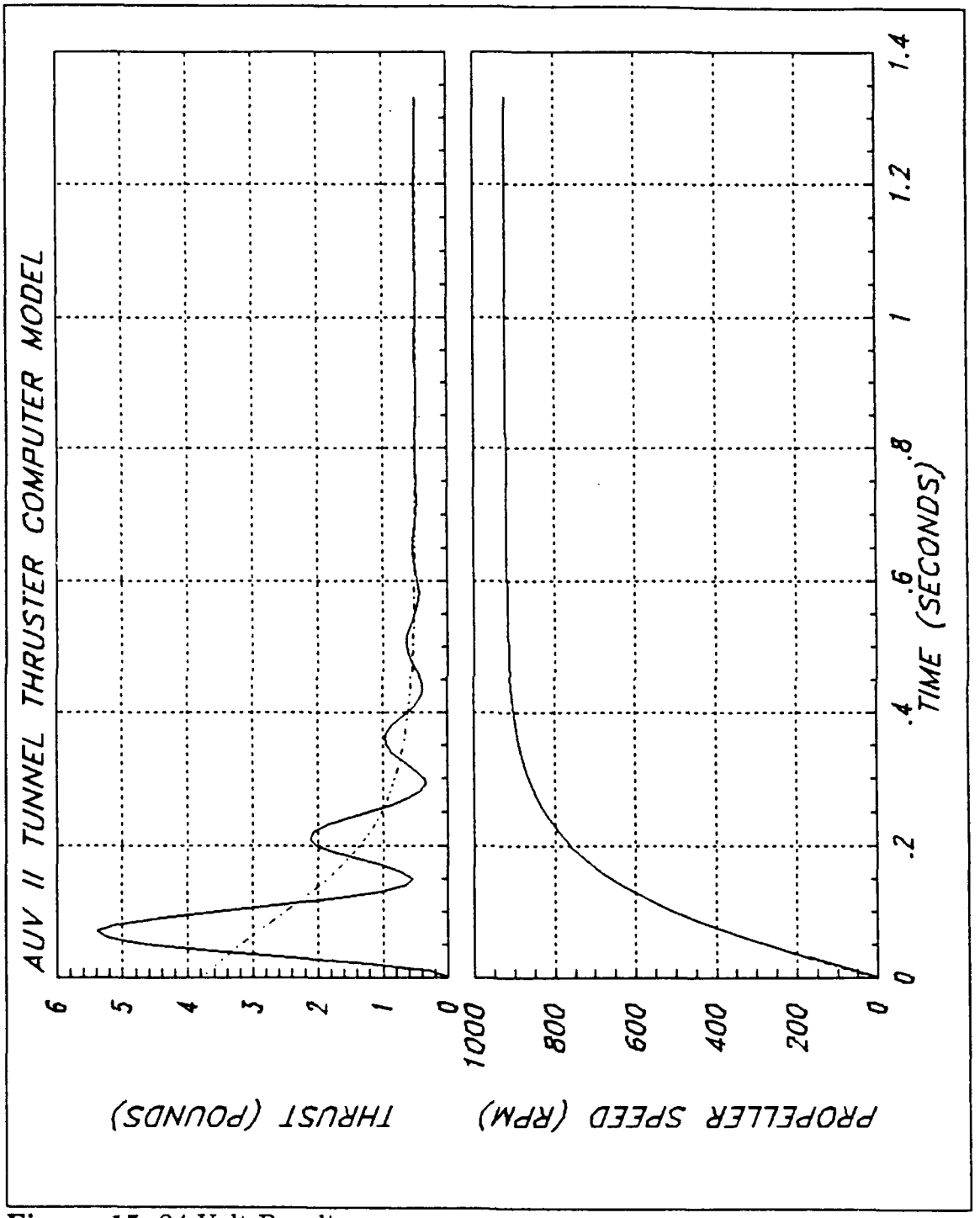

Figure 15 24 Volt Baseline

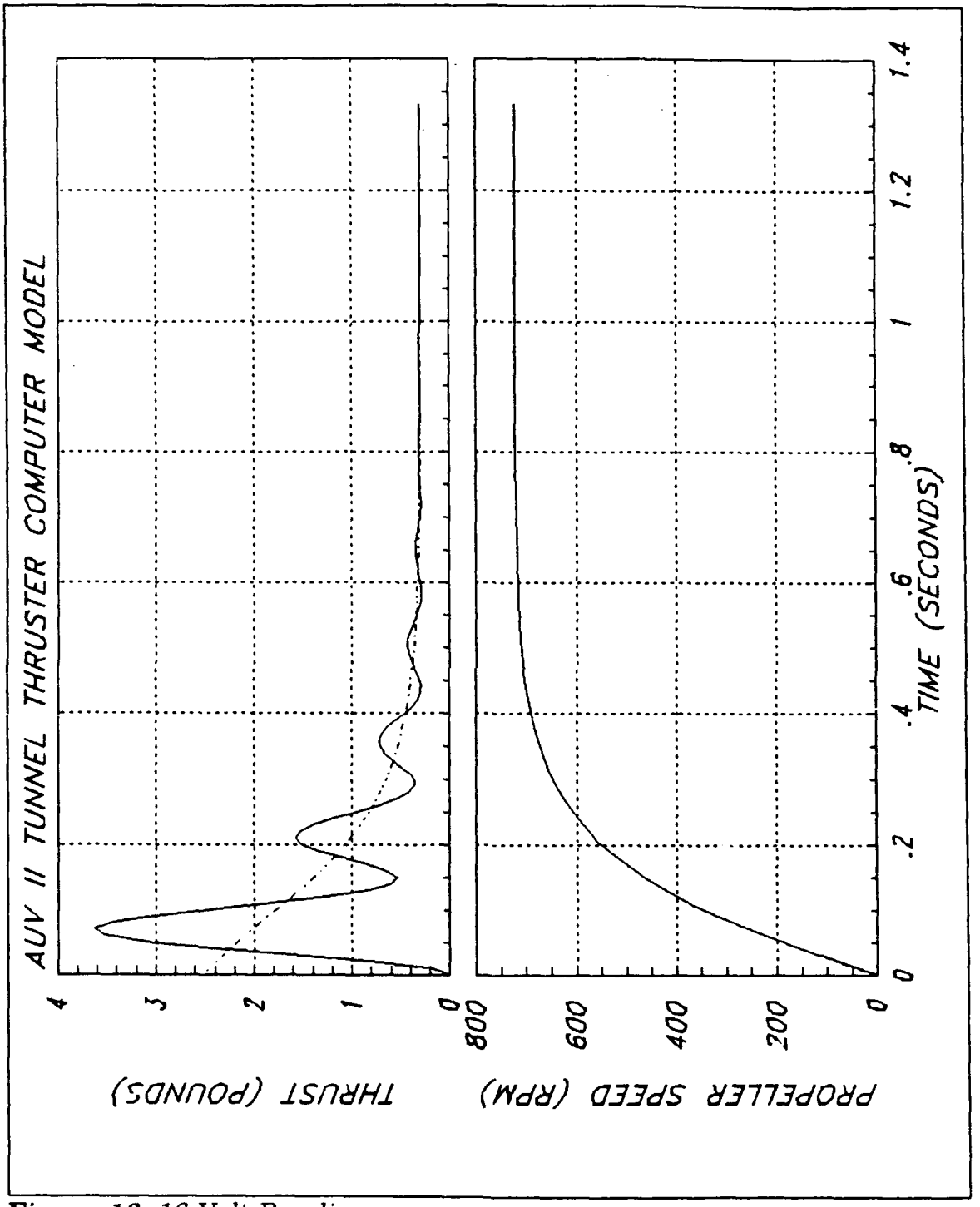

Figure 16 16 Volt Baseline

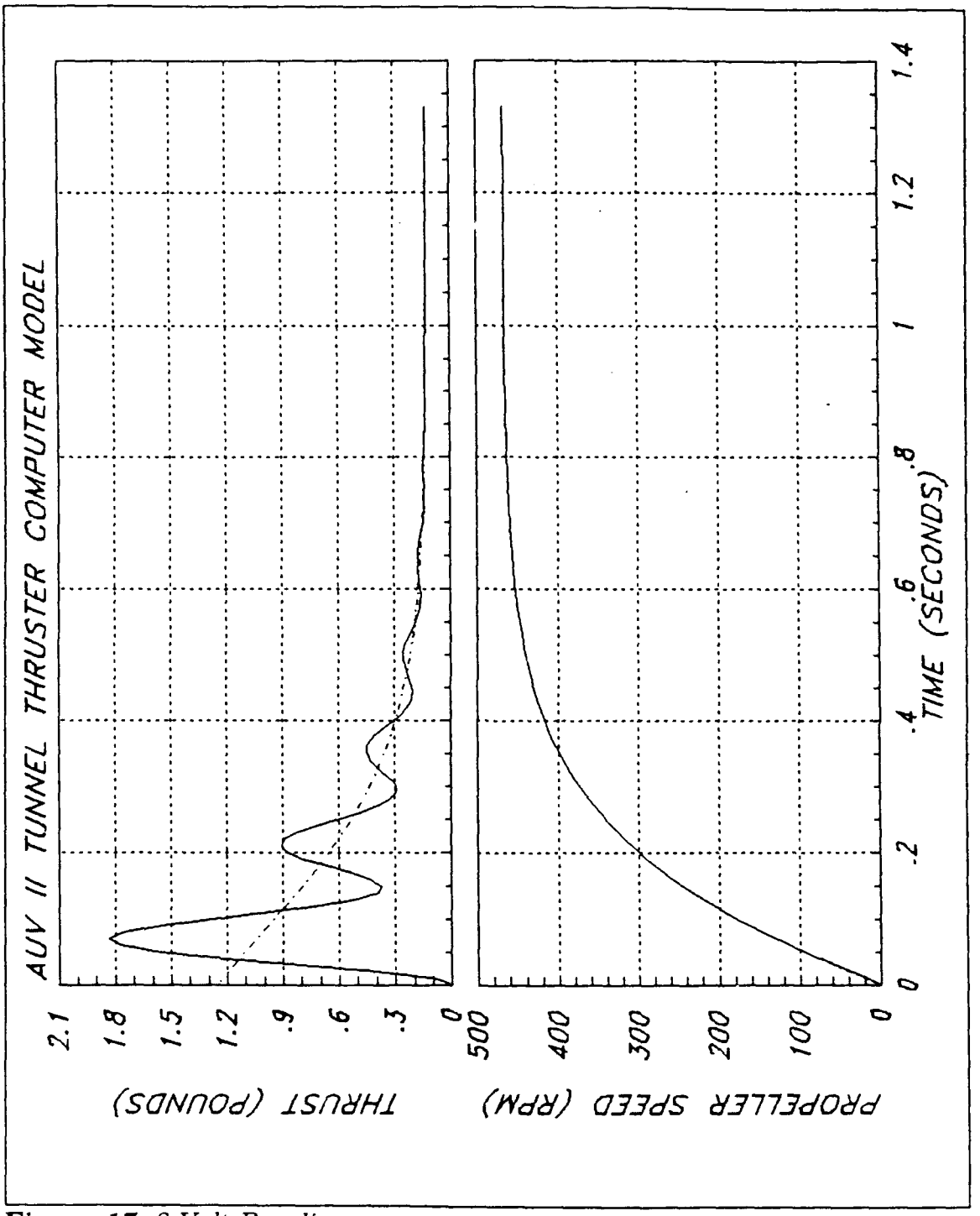

Figure 17 8 Volt Baseline

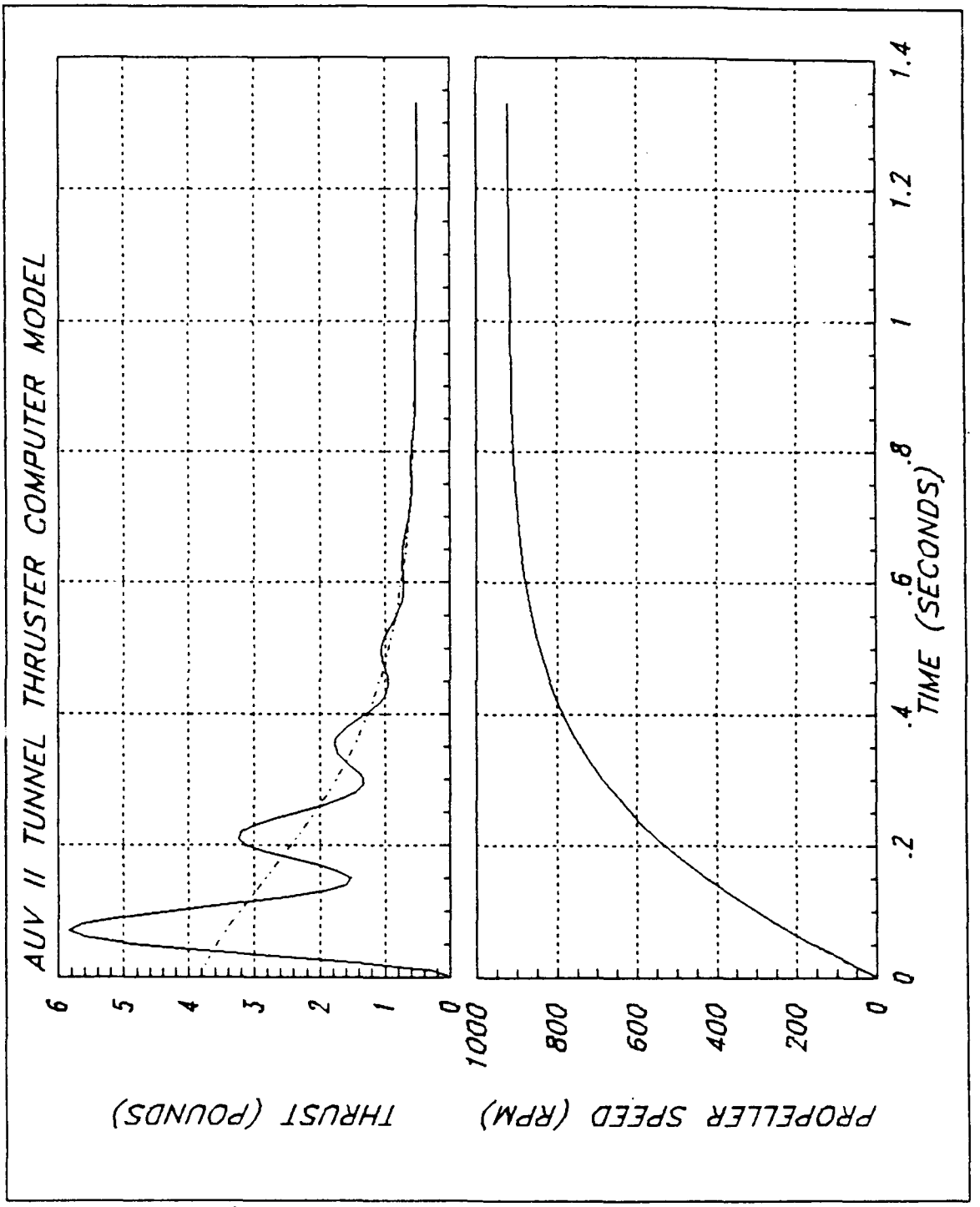

Figure 18 Length = 20 Inches

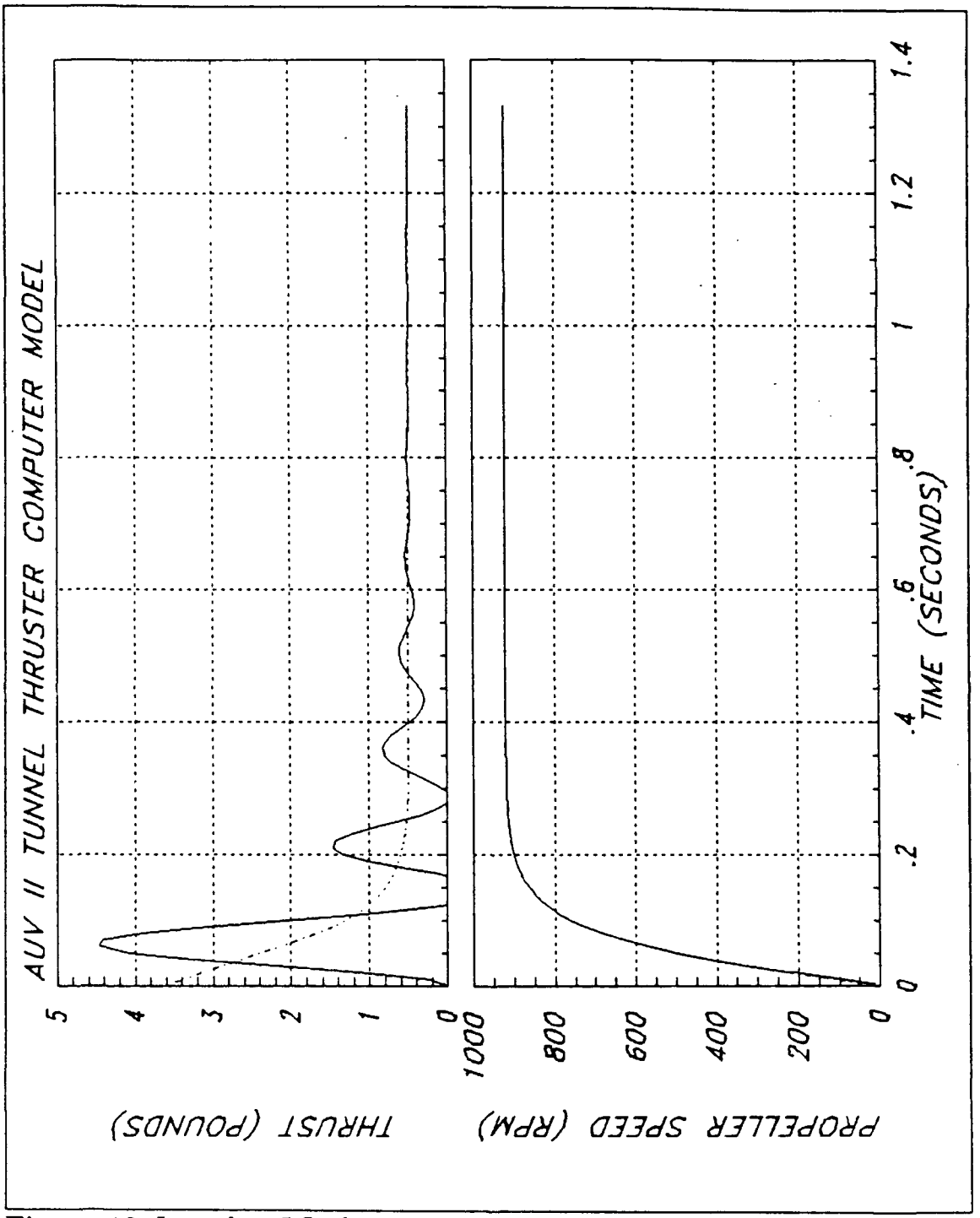

Figure 19 Length = 5 Inches

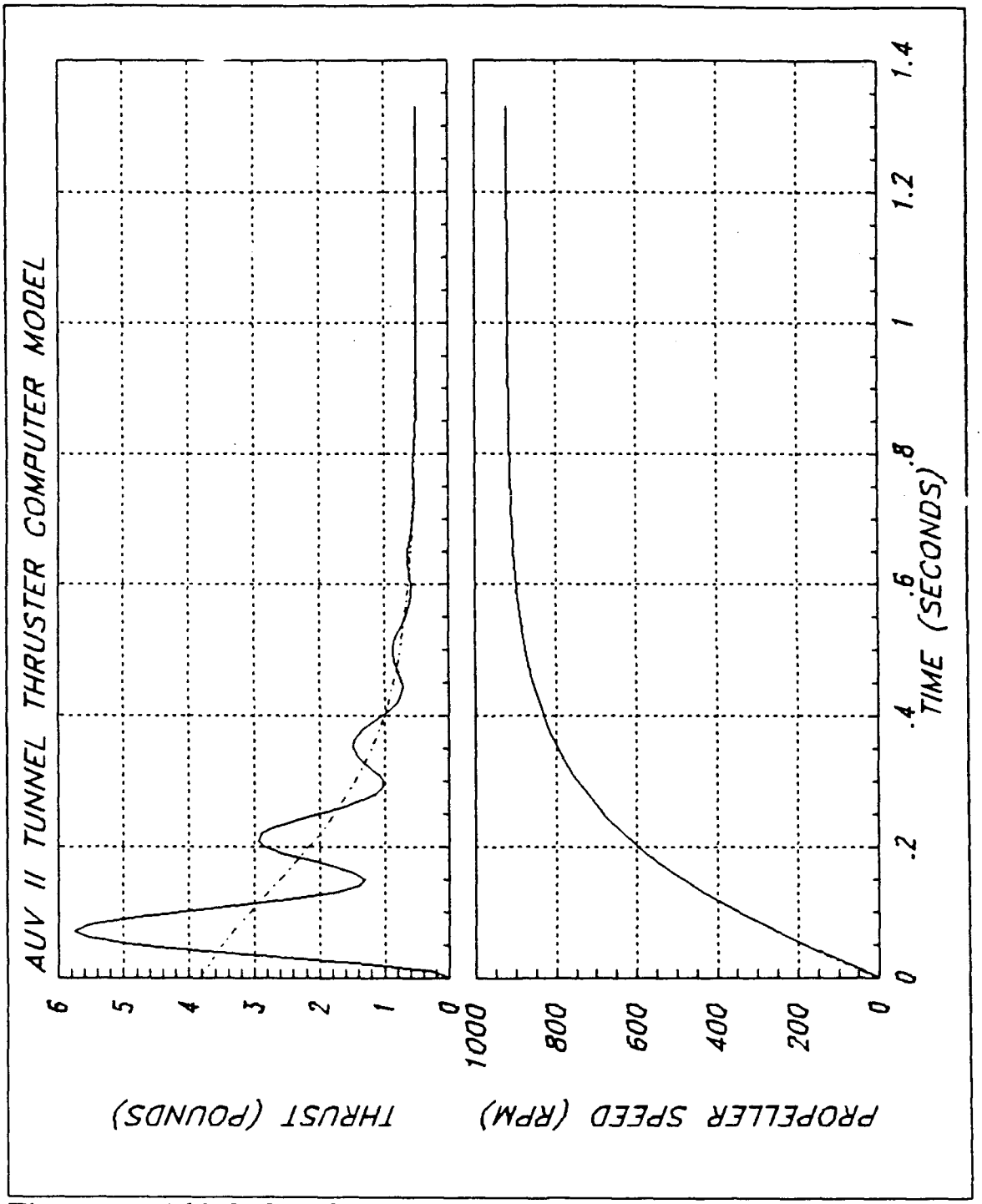

Figure 20 Added Mass Coefficient = 1.0

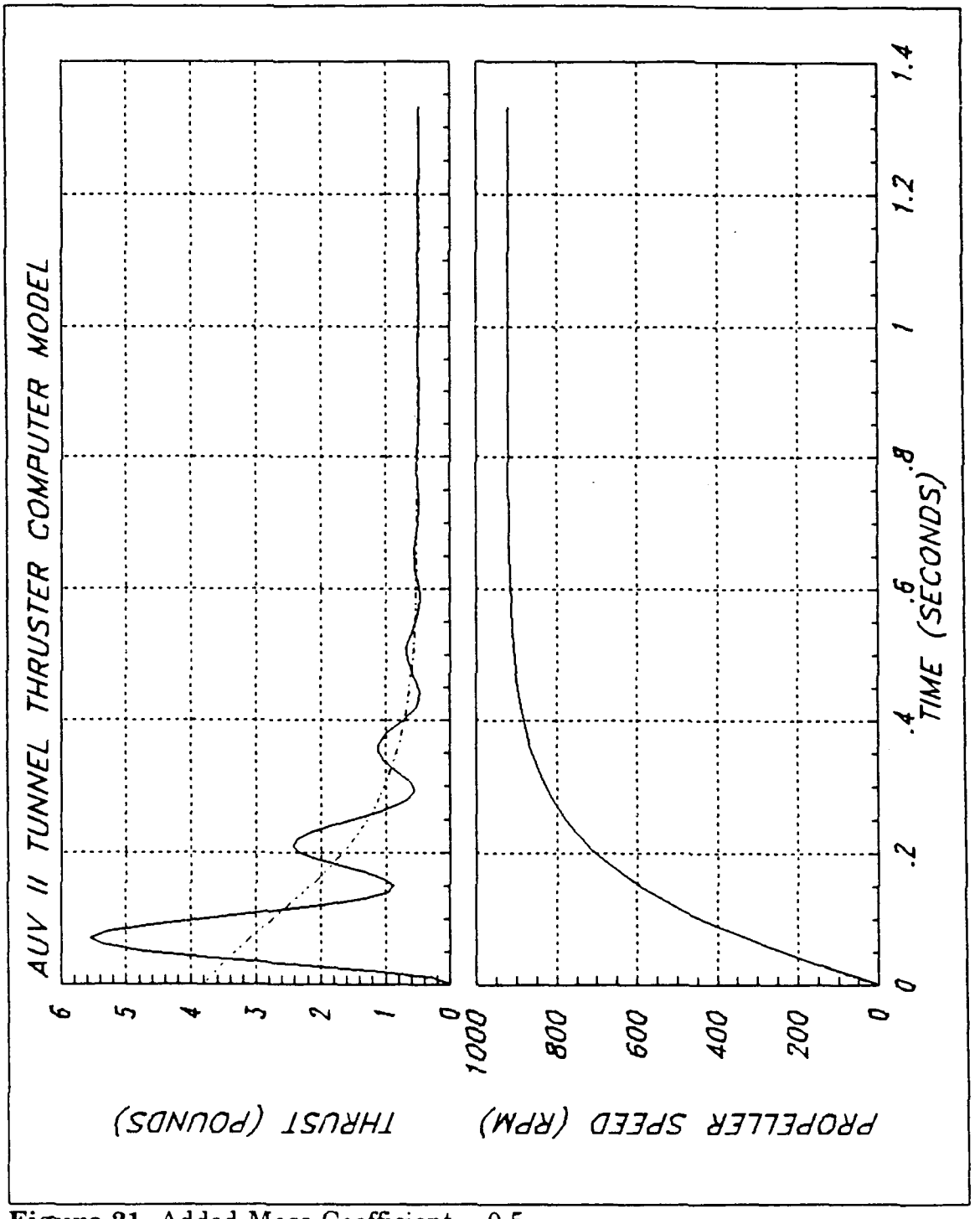

Figure 21 Added Mass Coefficient = 0.5

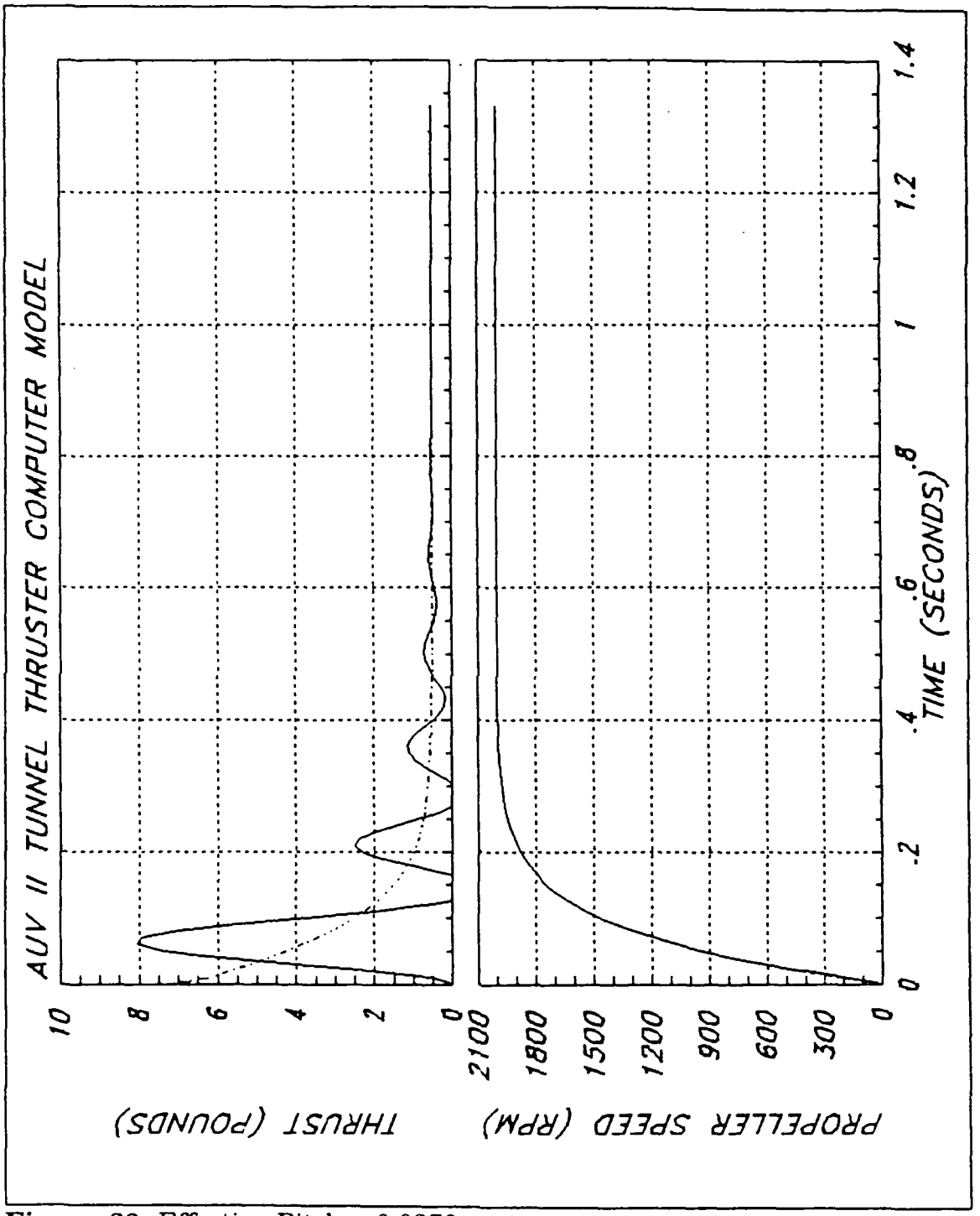

Figure 22 Effective Pitch = 0.0270

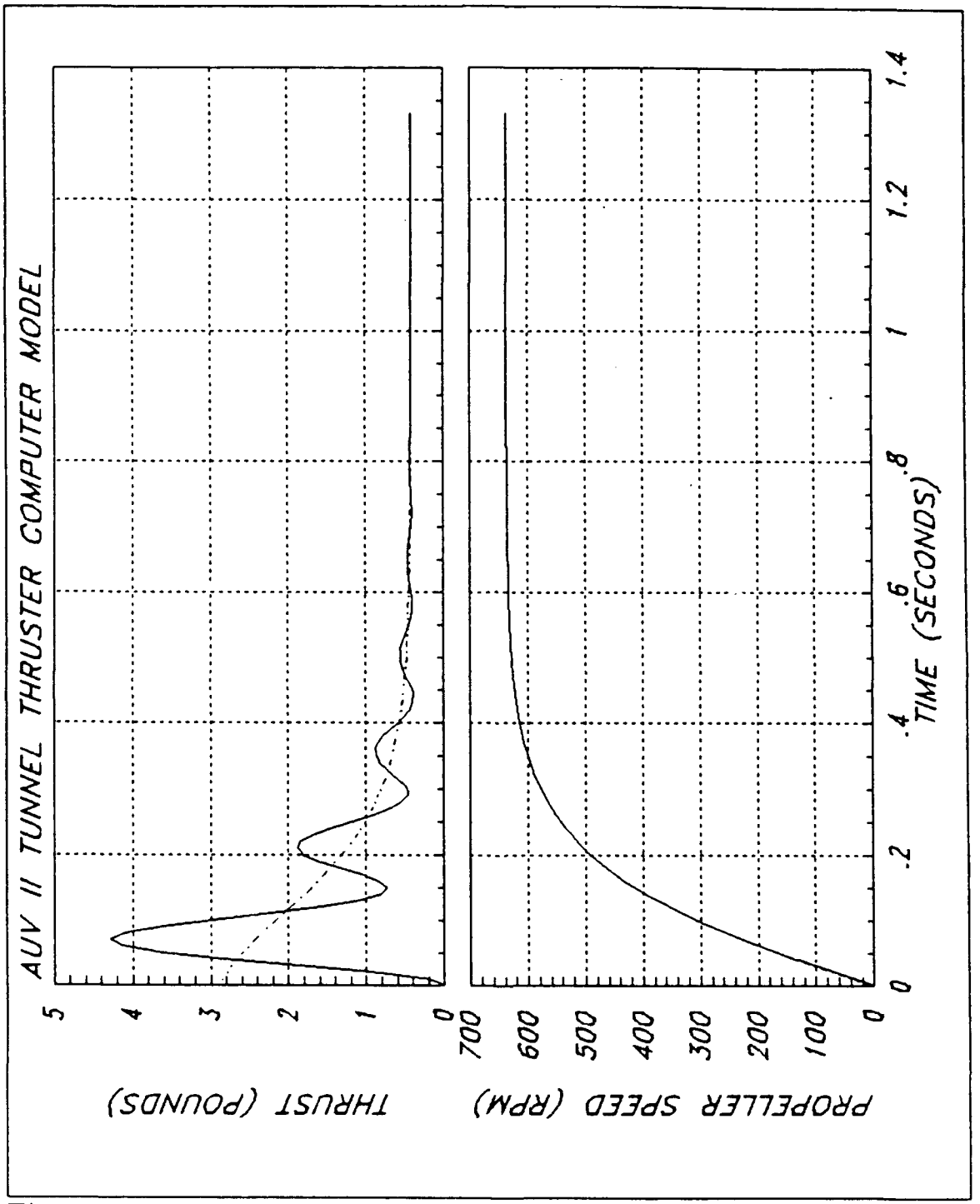

Figure 23 Effective Pitch = 0.0721

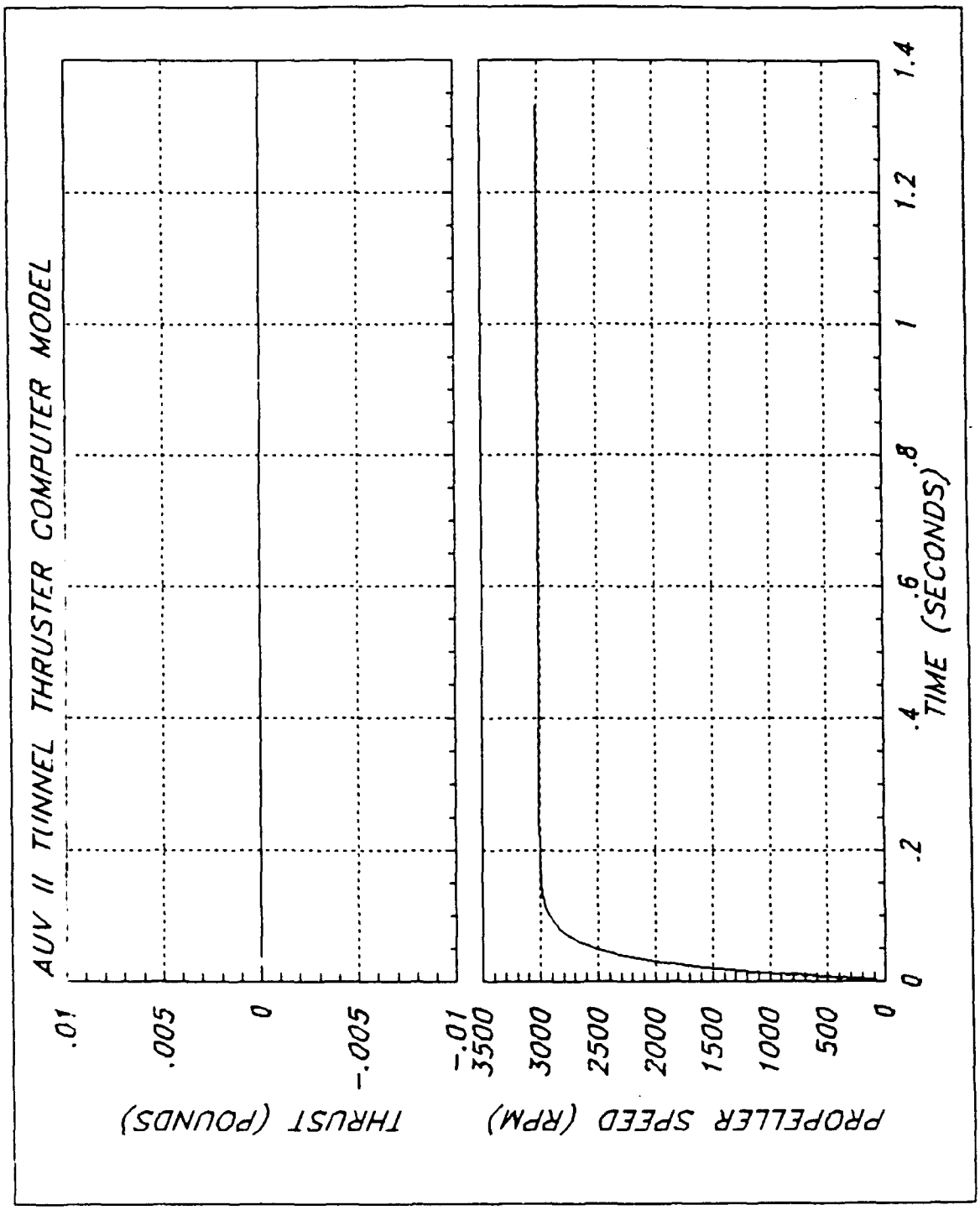

Figure 24 Effective Pitch = 0.0

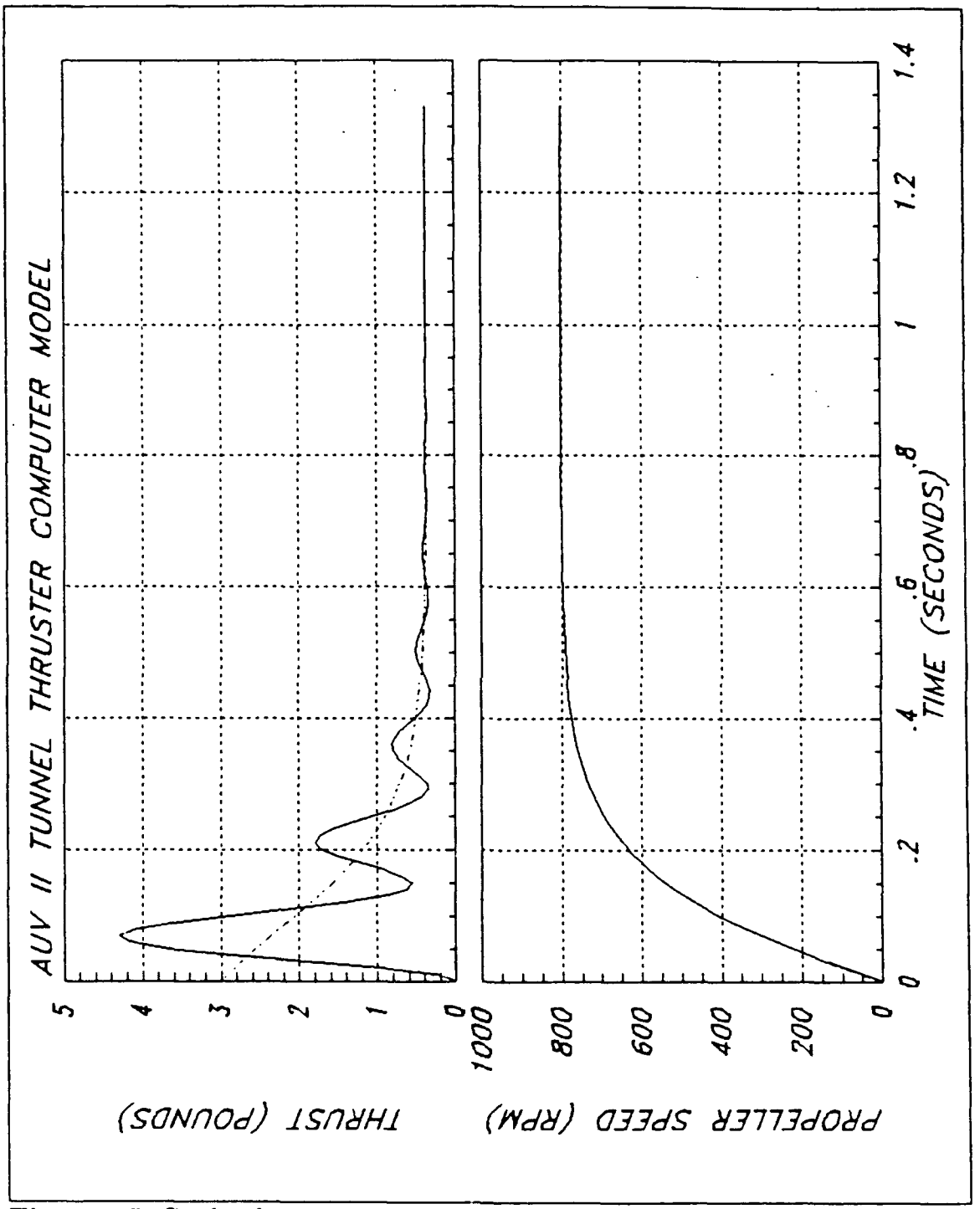

Figure 25 Coulomb Friction

1. Baseline Analysis

In the following analysis, the **true** thrust refers to the thrust developed by the propeller as predicted by the conservation of momentum equations. The **output** thrust represents the thrust as displayed from the test rig instrumentation, which includes the dynamics of the load cell. The **steady state** thrust was the level of thrust remaining after the transients no longer existed.

a. 24 Volt

This plot shows the general nature of the thrust response to have a sharp rise followed by an almost exponential decay (response shown as the dotted line), while the total output as viewed from the load cell (solid line) includes a structural resonant component superimposed. The true thrust begins at a value of 3.8 pounds and decays exponentially to a steady state thrust of 0.5 pounds, reaching this value in 0.5 seconds. The peak output thrust was 5.4 pounds as measured by the load cell. The structural transient has decayed away by 0.7 seconds. The time constant of the propeller speed was 0.125 seconds, reaching a steady state speed of 925 RPM. This time constant also happens to be the time constant for the thrust transient. A hand--held tachometer recorded the actual propeller speed at 900 RPM in the laboratory. The purpose of superimposing the structural resonant component on top of the simulated true thrust was to aid in later comparison with experimental data where the component separation was not possible.

b. 16 Volt

This plot was very similar to the previous results. The peak output thrust was 3.6 pounds and the steady state thrust was 0.33 pounds, reaching this value in 0.6 seconds. The structural transient has again decayed away by 0.7 seconds. The true thrust begins at a value of 2.5 pounds and decays to the steady state level given above. The time constant was 0.15 seconds. The steady state speed was 725 RPM.

c. 8 Volt

In this case the peak output thrust from the model was 1.85 pounds and the steady state thrust was 0.15 pounds. The true thrust begins at a value of 1.25 pounds and reaches steady state after 0.7 seconds. This time the structural transient remained until 0.8 seconds; this display of lower damping was expected. The steady state speed of the propeller was 480 RPM and the time constant 0.2 seconds.

2. Effect of Tunnel Length

a. 20 Inch

The influence of tunnel length, as expected, increased the peak output thrust and the decay time but had little effect on steady state thrust. The true thrust began at the same value as the baseline case. The time constant though was nearly double that of the baseline. The steady state speed was 925 RPM; in fact, all four cases regarding tunnel length and added

mass coefficient reached a constant speed of 925 RPM and steady state thrust of 0.5 pounds, showing that the effect of these parameters are transient in nature alone.

b. 5 Inch

Opposed to the above 20 inch case, the peak output thrust and decay time here was reduced from the baseline level. The thrust reached steady state in only 0.3 seconds, and the time constant was 0.06 seconds. The first two cycles of the structural transient dipped below the zero thrust level due to the short time constant. Note that the thrust was negative in this region even though the plot clips the response at zero.

3. Effect of Added Mass Coefficient

a. Ka = 1.0

This case was very similar to the 20 inch length case, the major difference being the shorter time constant. Therefore, we see that increasing the added mass coefficient increases the time constant for the same true thrust, resulting in a larger peak output thrust. The propeller time constant for this case was 0.195 seconds.

b. Ka = 0.5

This case was very similar to the previous one, as expected; the exception to this being a shorter time constant of 0.14 seconds, although still longer than the time constant for the baseline case.

4. Effect of Pitch Angle/Efficiency

a. 16 Degrees

The peak output thrust for this case is the largest of all the runs, reaching 8.0 pounds, while the steady state thrust is still 0.5 pounds. Only 0.35 seconds elapsed before steady state was obtained. The true thrust, also the largest of any run, begins at a value of 7.0 pounds. Like in the 5 inch length case, several of the thrust transients dipped below the zero thrust level, also due to a short time constant. The large peak thrust also played a part in the negative thrust in this case. The time constant for the propeller is 0.075 seconds and the steady state speed is 2000 RPM, more than double the baseline value of 925 RPM.

b. 37.5 Degrees

The peak output and steady state thrust this time is only 4.3 pounds and 0.4 pounds, respectively, taking 0.6 seconds to settle out. The true thrust begins at a value of only 2.9 pounds. The time constant for the propeller is 0.145 seconds and steady state speed is 67% of baseline at 640 RPM. Cases **a** and **b** will be discussed further in Chapter V; these findings were not expected before running the simulation.

c. 0.0 Degrees

As expected in this case, no thrust is developed for a zero pitch. This case is identical to the motor model shown in Figures 9,10.

5. Effect of Coulomb Friction

This case is very similar in appearance to **4.b.** above (effective pitch angle=37.5 degrees) except that steady state speeds are substantially different. The true thrust here decays to steady state from an initial value of 3.0 pounds. Note that all values of thrust and speed for this model are lower than baseline.

In the following chapter the experimental setup, testing, and results will be presented. There the plots of the actual tests can be compared to the simulations from this chapter. Then Chapter V, Summary and Recommendations, will compare and contrast the experimental and simulation results and draw conclusions from them.

IV. PROTOTYPE EVALUATION

The previous chapters of this thesis dealt with the theory, modeling, and simulation of the AUV tunnel thrusters. In the following chapter, the experimental research that corroborates the mathematical model will be presented.

A. LABORATORY EQUIPMENT SETUP

The collection of hardware and instrumentation, which will be designated as the **test rig**, that was required to support the collection of test data from the thruster unit is shown in Figures 26, 27, and 28. The goal of the design and fabrication of the thruster test box was to allow an actual thruster unit to be used for the performance testing; this objective was met using a plexiglass rectangular box, open at the top, with holes on either side to allow the mounting flanges to be affixed. The tunnel thruster was then able to fit between the flanges and obtain a watertight seal with the use of multiple o-rings (Fig. 29). The following two subsections will describe the mechanical hardware and instrumentation that embody the test rig.

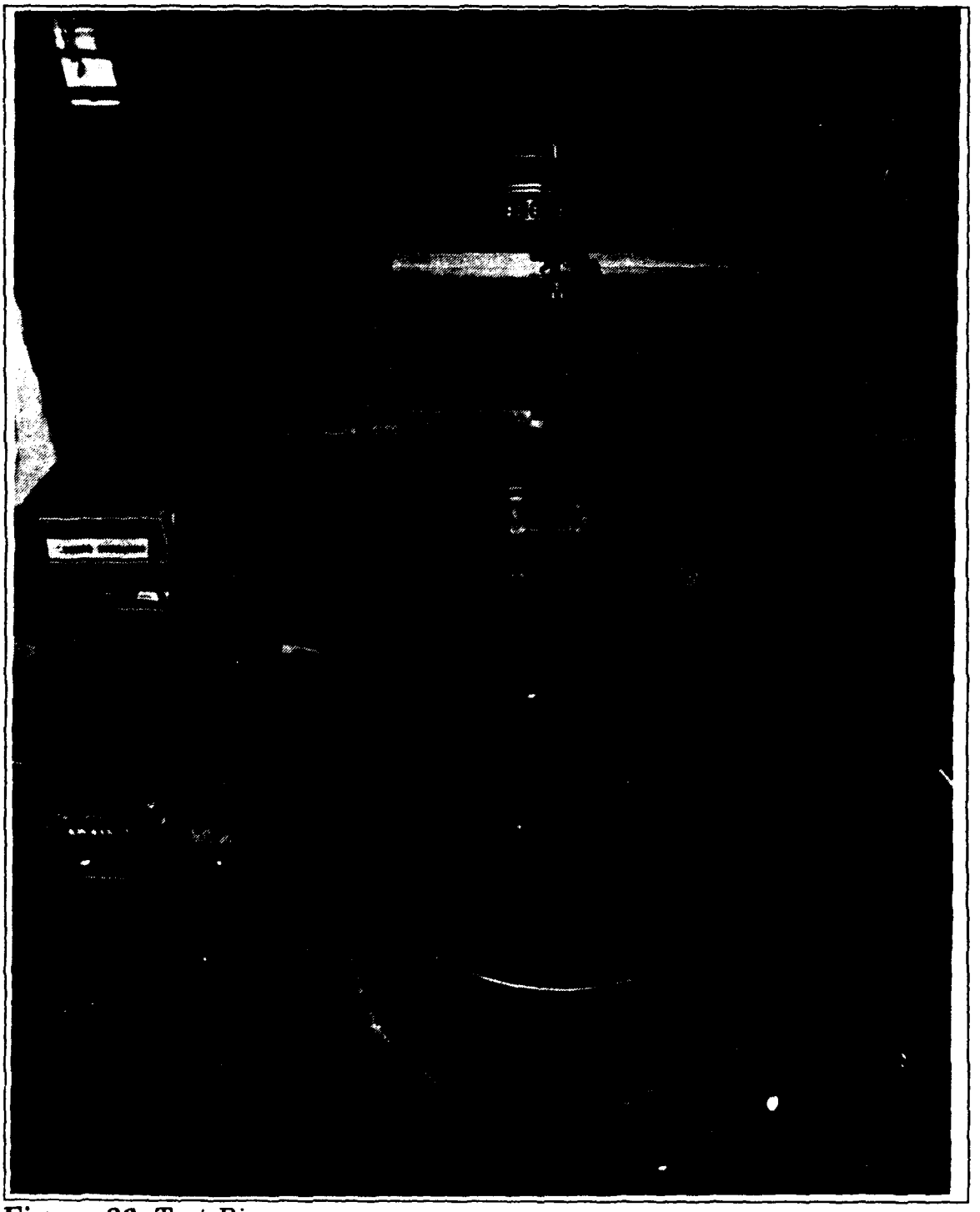

Figure 26 Test Rig

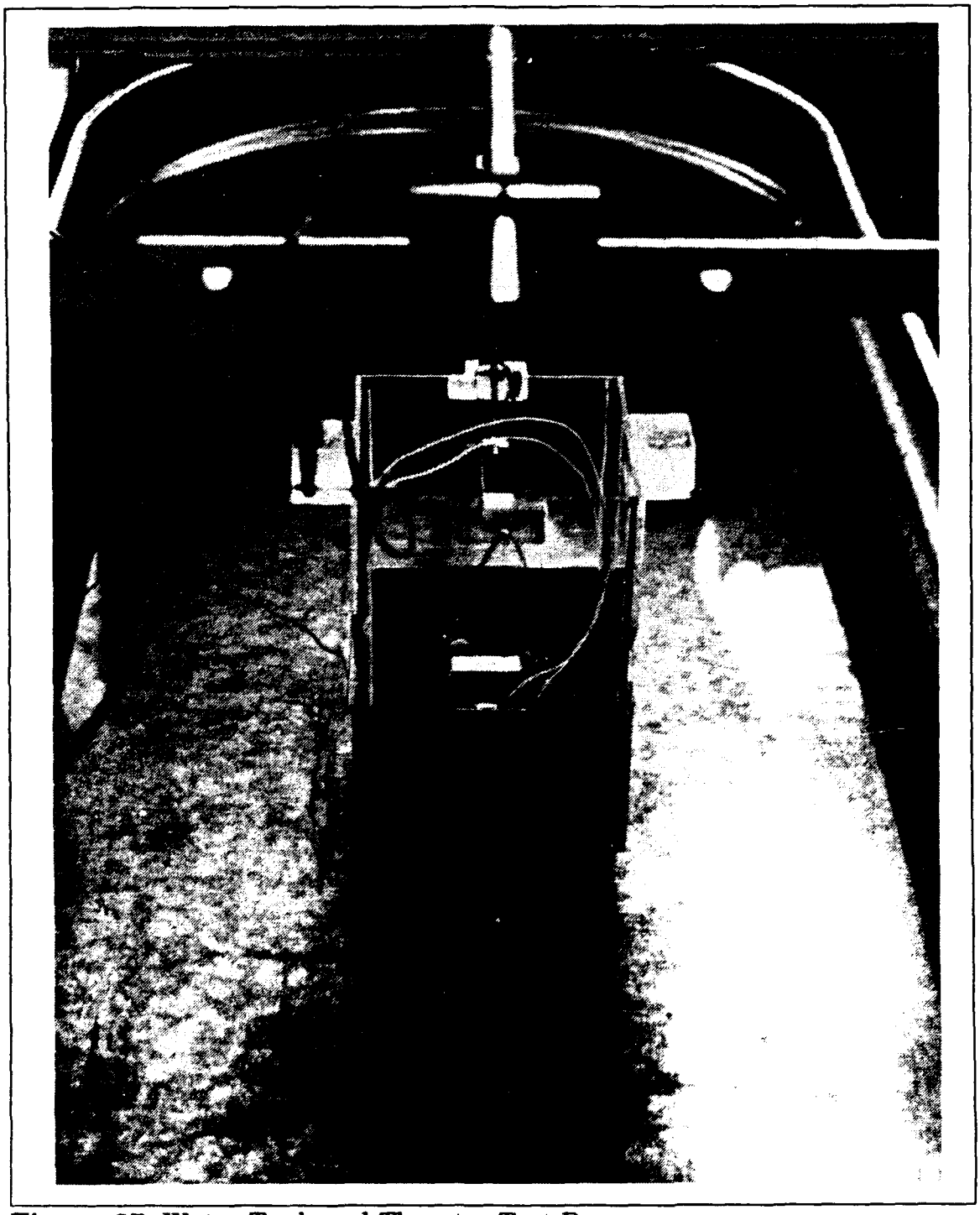

Figure 27 Water Tank and Thruster Test Box

Figure 28 Test Rig Instrumentation

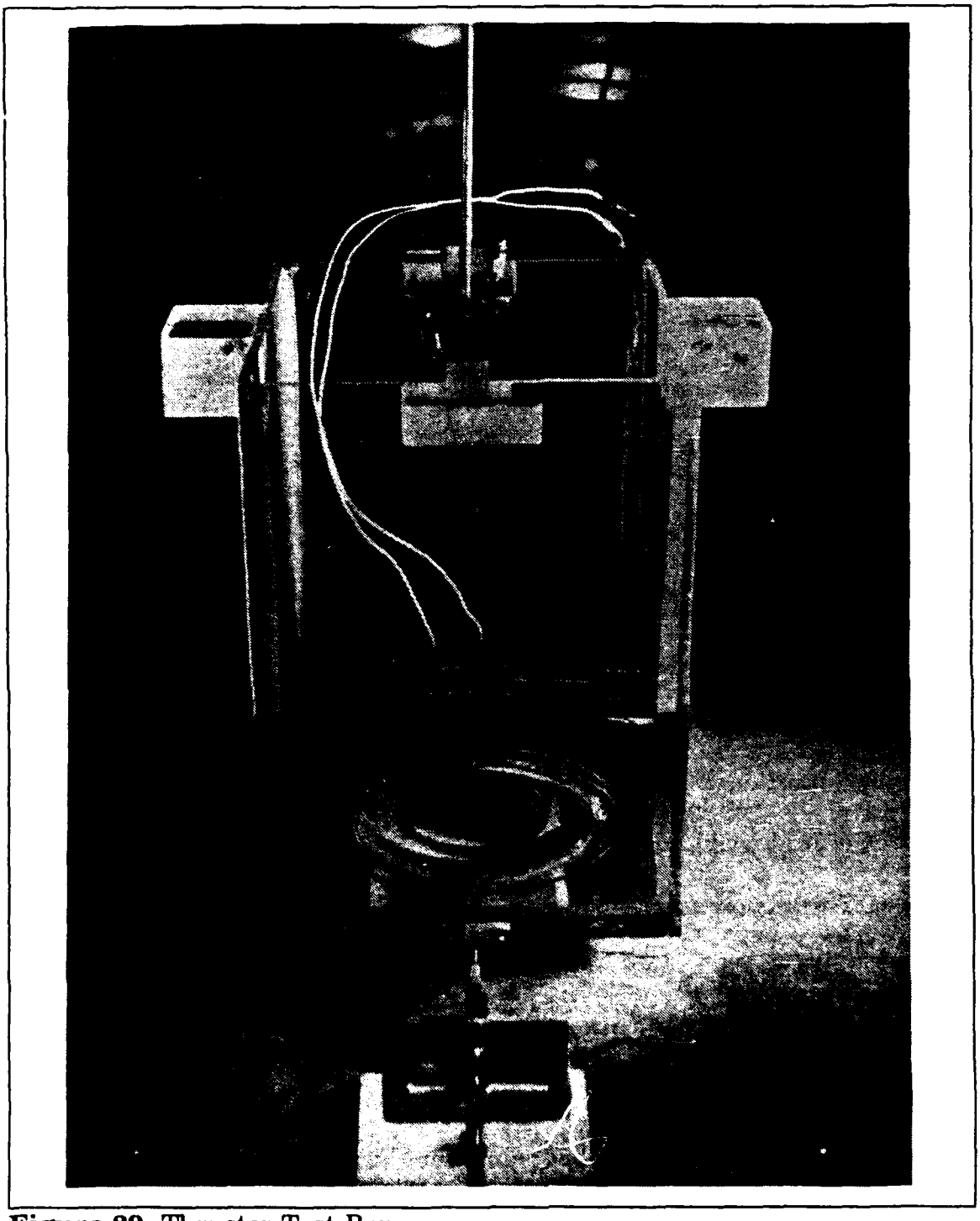

Figure 29 Thruster Test Box

1. Mechanical Hardware

The major components of the mechanical hardware that served to house, support, calibrate, measure thrust, and hold the water for the thruster unit are described below.

a. Test Box

As described briefly above, the test box was made of plexiglass, approximately 10" wide by 10.5" long by 20" high (Figs. 30,31). One flange was made of plexiglass and permanently fixed to the box, while the opposite flange was made of aluminum and identical to the ones used on the AUV. A sufficient amount of lead was glued to the bottom of the box to adjust the buoyancy as needed. This action assured that a level attitude and approximately two inch bottom clearance was maintained when the water level was at one tunnel diameter above the top of the intake.

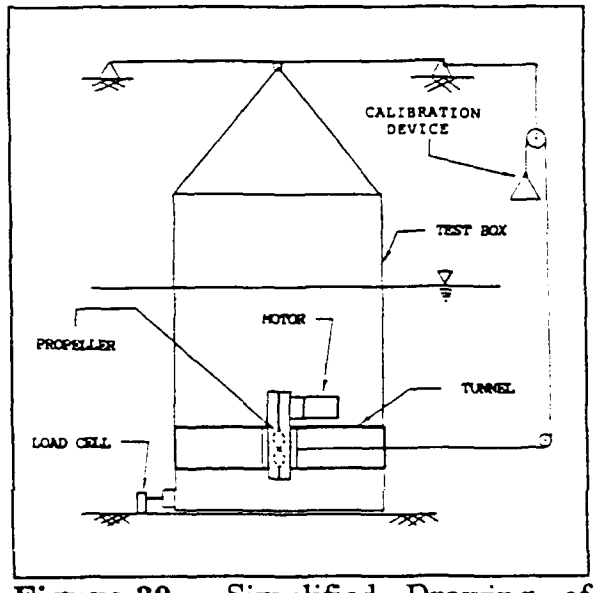

Figure 30 Simplified Drawing of Thruster Test Box

Connected to the top of the box are a pair of metal rods that form a simple truss; this setup supplied additional support and prevention of wave action from twisting the box. The truss was supported on a knife--edge cut

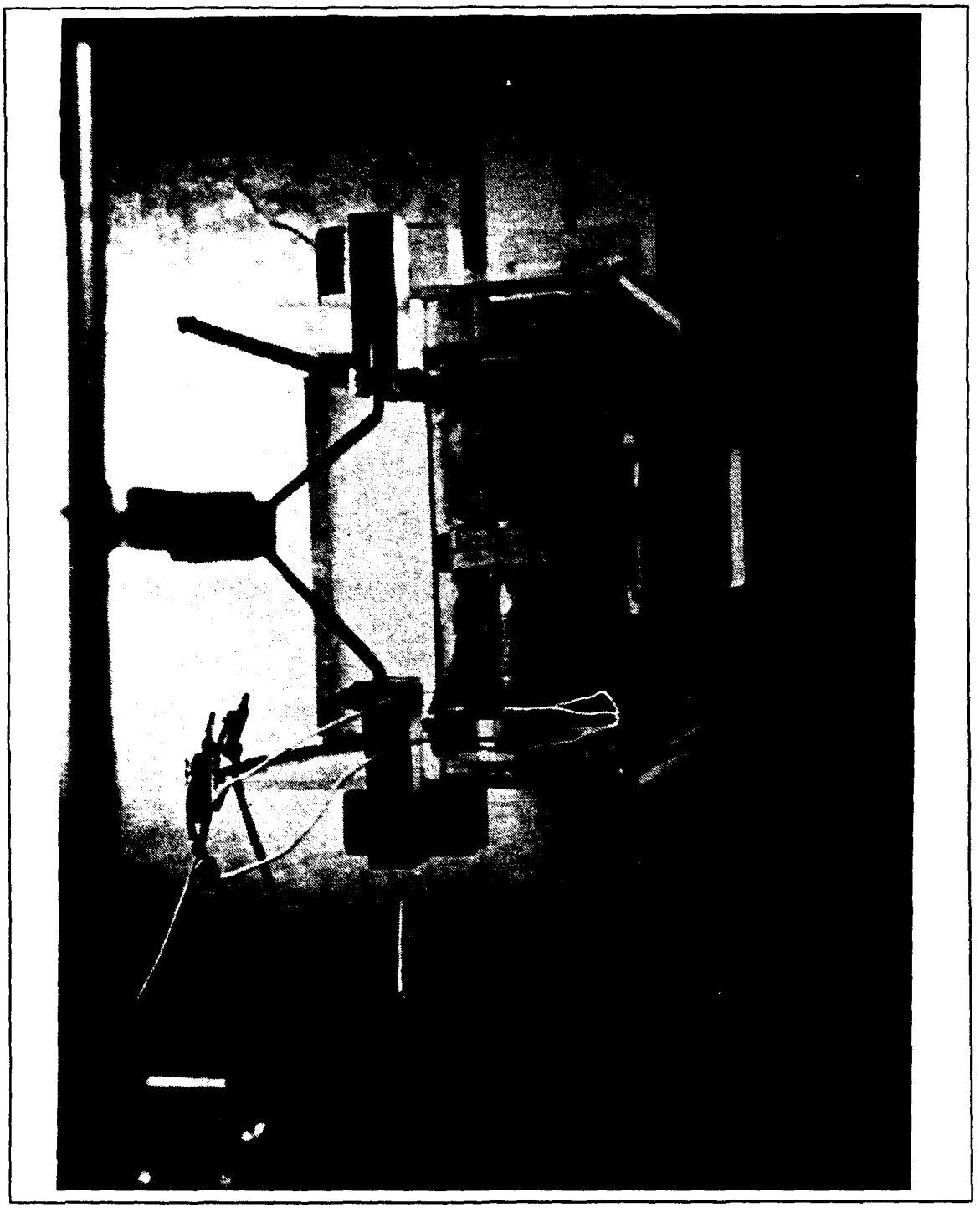

Figure 31 Test Box and Calibration Mechanism

into a stainless steel bar which in turn was supported by a pair of aluminum angles that span the tank between laboratory cabinets. On the bottom of the box was a fixture to hold the bolt that mated with the load cell. The fixture was constructed of PVC and designed to allow the bolt to move freely up to approximately 30 degrees in any direction to prevent binding.

b. Thrust Sensor

The thrust sensor was a beam--type load cell, with an input resistance of 350 ohms and a load range of 0 to 50 pounds[5]. The cell was waterproofed using a high quality electrical sealant. The high load range was used because of its availability; a lower range cell would have been more appropriate.

The load cell was connected to a support mechanism with several degrees of freedom to allow the underwater connection to the test box possible even if a slight misalignment was present. This mechanism was then held securely to the tank bottom using a 30 pound lead brick. The connection between the test box fixture and the load cell was a small diameter bolt (Fig. 32).

c. Calibration Mechanism

The calibration of the load cell was obtained by the most realistic conditions possible (Figs. 30,31). This resulted in a set of pulleys that directed

---

[5] Manufactured by Interface INC., Scottsdale, AZ.

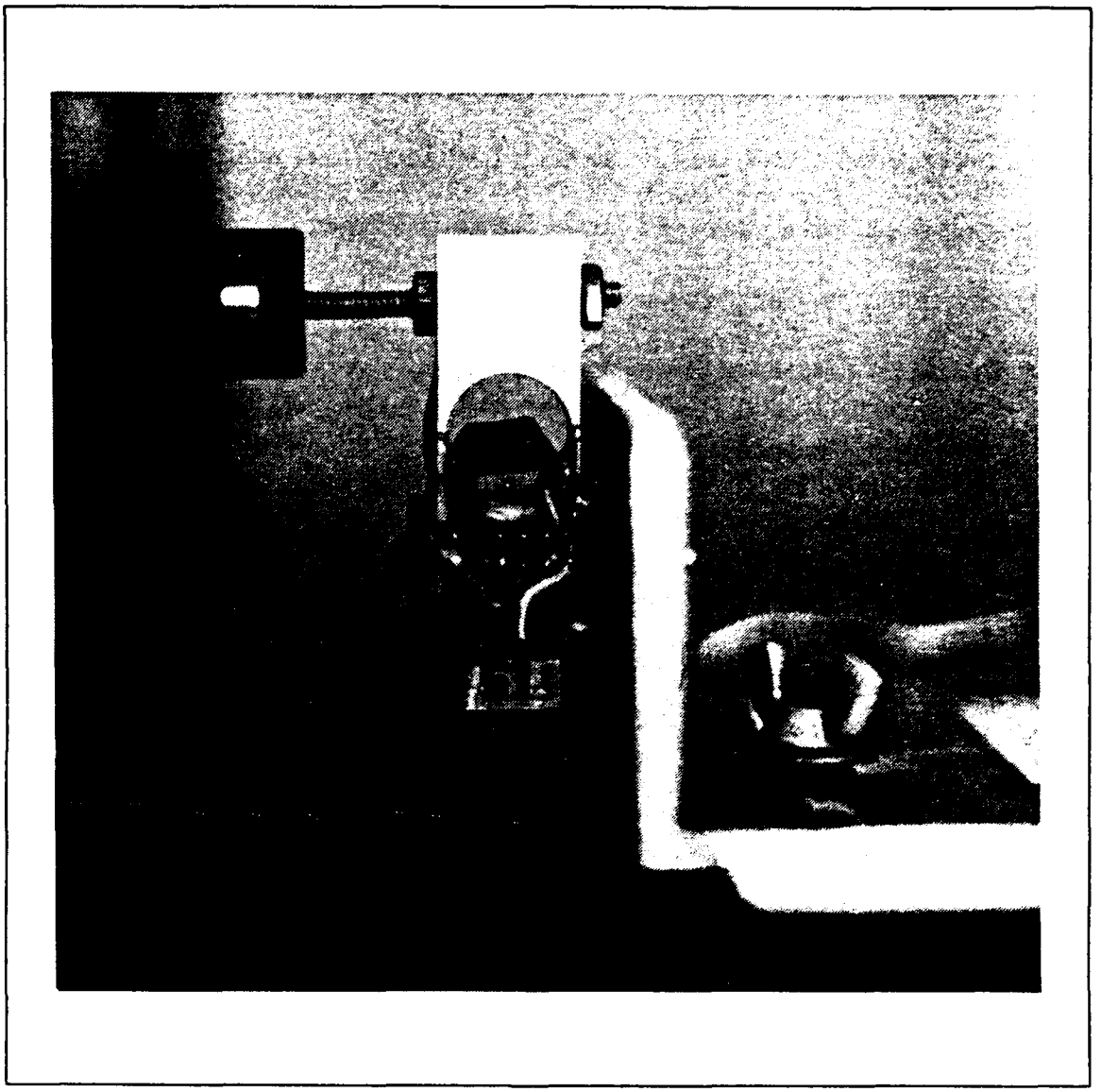

Figure 32 Thrust Sensing Device

a 10 pound test monofilament line from the support strut of the thruster to a platform for weights located above and in front of the test box. The upper pulley was hung from a cantilever beam attached to the forward cross support. Small weights were placed on the platform to incrementally raise the force on the load cell and the output was recorded.

d. Water Tank

The water tank that was used as a test pool was made of galvanized sheet metal, and it measured 10' long by 3' wide by 2' deep. The large volume of water afforded by this tank shortened the wait time between runs and increased the accuracy when obtaining a steady state thrust reading, due to a lower frequency "slosh mode"[6].

2. Instrumentation

The instrumentation used to produce, amplify, filter, display, and process the voltage output signal from the load cell will now be described, component--by--component. The electronics required to receive the raw signal and present the output in a manner that could best be analyzed consists of the following:

- BAM--1 bridge/amplifier: Ellis Associates; supplied 12 volt bridge excitation and amplified output voltage
- Filter: Krohn--Hite Model 3343; 25 Hz low pass filter allowed the transient to be observed while removing unwanted noise, and also increased the signal amplification
- Oscilloscope: Jiwatsu; two--channel scope for the observation of analog signals and also system calibration
- Function Generator: Hewlett--Packard (HP): supplied the trigger and sampling frequency to the ADC (80 HZ, 6.5 volts); the overall sampling frequency of system was 75 Hz

---

[6] The wave motion produced by the propeller.

- Analog to Digital Converter (ADC): Data Translation DT 2801; an external circuit card that connected to the personal computer for conversion of a continuous signal to discrete voltages; it received inputs from the function generator, a conditioned signal from the filter, a motor drive voltage signal from the DC power supply, and finally was connected to a common ground

- Personal Computer (PC): Zenith AT microcomputer running PASCAL for sampling of analog data on a MS--DOS operating system

- DC Power Supply: Lambda variable DC power supply capable of delivering up to 60 volts and 10 amps

- HP Digital Voltmeter: used as a meter for the power supply to allow accurate voltage inputs

B. OPERATION OF THE TEST RIG

This section deals with calibration and the collection of data. Prior to conducting the "production" runs to be described below, preliminary tests were run to verify the accuracy and repeatability of the output.

1. Calibration

The calibration of the test rig involved the determination of thrust per output voltage from the load cell, after amplification. The output signal was routed from the filter to the oscilloscope instead of the normal path to the ADC. The filter was set for 1 Hz--low pass, to allow the steady state value of the thrust to be read more easily. Known weight standards were placed on the platform and the corresponding output voltage was recorded after a sufficient time was allowed for the oscillations to diminish. This procedure was repeated

five times for increasing and decreasing weights with approximately linear results.

Some hysteresis in the calibration was observed when proceeding from the highest test weight in the decreasing weight direction. This effect was most probably caused by the friction between the pulleys and line, and many attempts were made to alleviate the problem with only slight success. The hysteresis could be eliminated entirely if the platform was lifted after each weight was removed to "release" the friction force. For this reason, namely that the problem only existed for slow transients, the hysteresis was not considered to effect the dynamic response of the thruster since the impulse and structural dynamics supplied the needed "release" of the friction force. This observation was witnessed many times using a slight tap on the water tank and/or calibration mechanism during subsequent calibrations. The calibration curve is presented as the first graph in the results section (Fig. 34).

2. Collection of Test Data

Eight runs were recorded from each of three separate drive motor step inputs: 24 volts, 16 volts, and 8 volts. After each individual 24 volt run, a wait period of approximately three minutes was required before the next was made to allow time for the slosh mode to dampen out; this wait period was somewhat less for the 16 and 8 volt runs.

For a typical test run, the ADC was controlled by a PASCAL code in the Zenith computer; this code was modified for this testing to incorporate a wait

command that allowed the ADC to be triggered at the same time that the on--off switch for the motor power supply was thrown. The power supply was set to the required voltage as read from the digital voltmeter, and then the power switch was turned to "off". Once the previous transient had significantly decayed away, as monitored on the oscilloscope, the data collection software was placed into the "wait" mode from the keyboard. While watching the oscilloscope to ensure that each run was commenced at the same point, the power switch was thrown, the test box would surge forward, and after two seconds the software would signal on the monitor that the data collection and translation was complete; the power supply was then turned off to minimize the disturbance for the subsequent run. Even though the trigger frequency from the function generator was set to 80 Hz, the PC/ADC could only sample at 75 Hz; this sampling frequency was still well above the recommended Nyquist criteria[7]. The results of these runs can be seen in the following section.

C. EXPERIMENTAL RESULTS

1. General

The results of the laboratory work will be presented in this section; the following section will provide the analysis. The calibration curve for the test

---

[7] Low pass filter set at 25 Hz (f_{max}); sampling rate of 75 Hz (f_s): a factor of three greater than highest expected frequency. Nyquist criteria requires $f_s \geq 2f_{max}$.

rig is presented as the first graph and a steady state thrust curve is second. The subsequent graphs were obtained from converting the output volts from the instrumentation to thrust in pounds using this calibration curve. Output in terms of thrust versus time was obtained for the following conditions:

- 24 volt step input signal
- 16 volt step input signal
- 8 volt step input signal
- eight runs for a 24 volt step input
- eight runs for a 16 volt step input
- eight runs for an 8 volt step input
- average thrust for 24 volt runs
- average thrust for 16 volt runs
- average thrust for 8 volt runs

In addition to the output associated with the step response of the thruster, two graphs were obtained that determined the structural natural frequency of the test rig. The time response of the test box to an impulsive input (tap) was recorded and then this data was converted to the frequency domain using a fourier transform available in Matrix$_x$. This natural frequency was then used in the computer model to simulate the structural dynamics of the test rig. These two graphs will follow the step response output listed above. Notice that the output from the test rig was a **convolution** of the

impulse response of the mechanical hardware with the step response of the tunnel thruster. This observation is presented schematically in Figure 33.

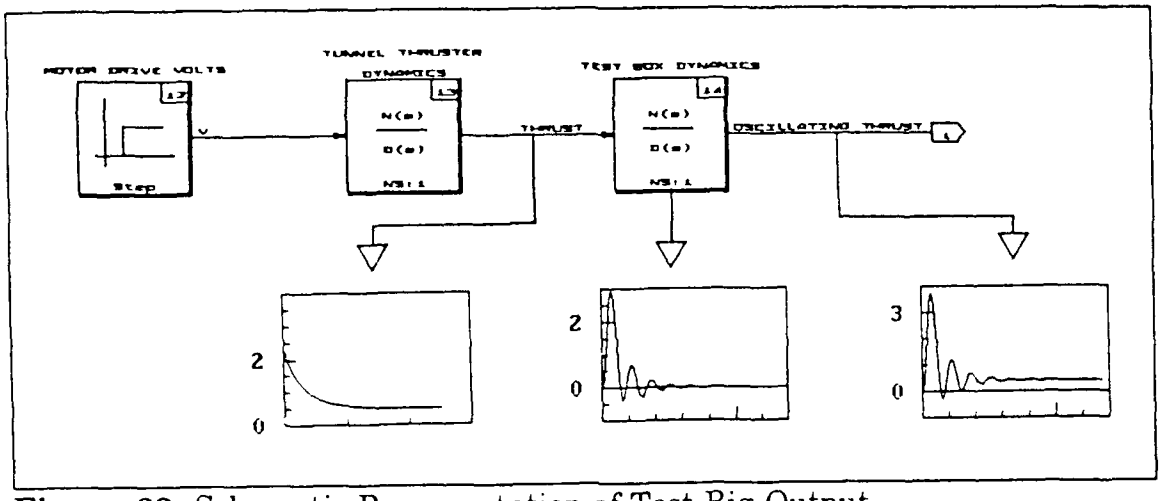

Figure 33 Schematic Representation of Test Rig Output

As seen in Chapter III, the separation of the **true** thrust from the structural dynamics[8] can make the analysis of the thruster's performance much easier and also more accurate.

[8] In Laplace transform terms, the "inverse transform".

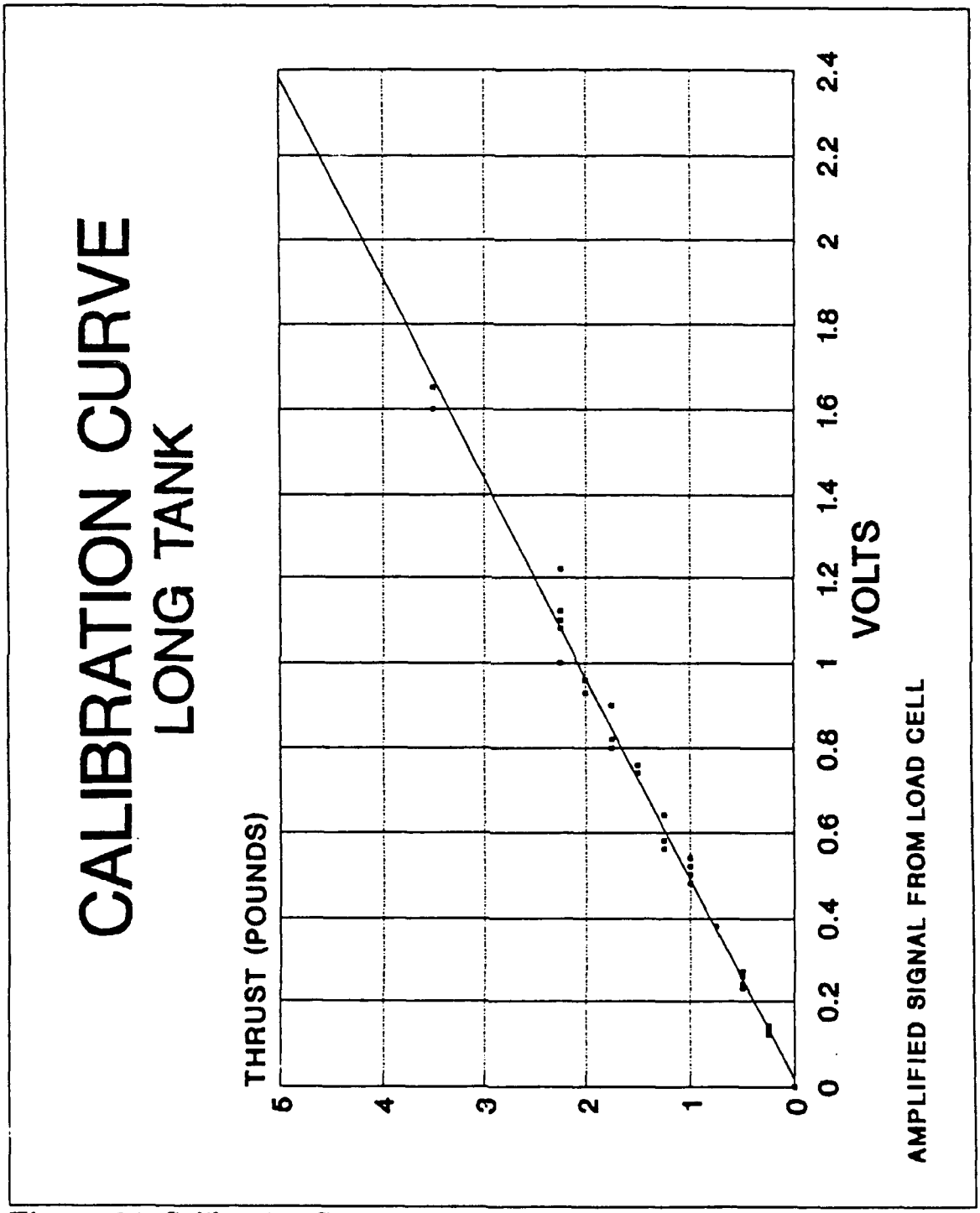

Figure 34 Calibration Curve

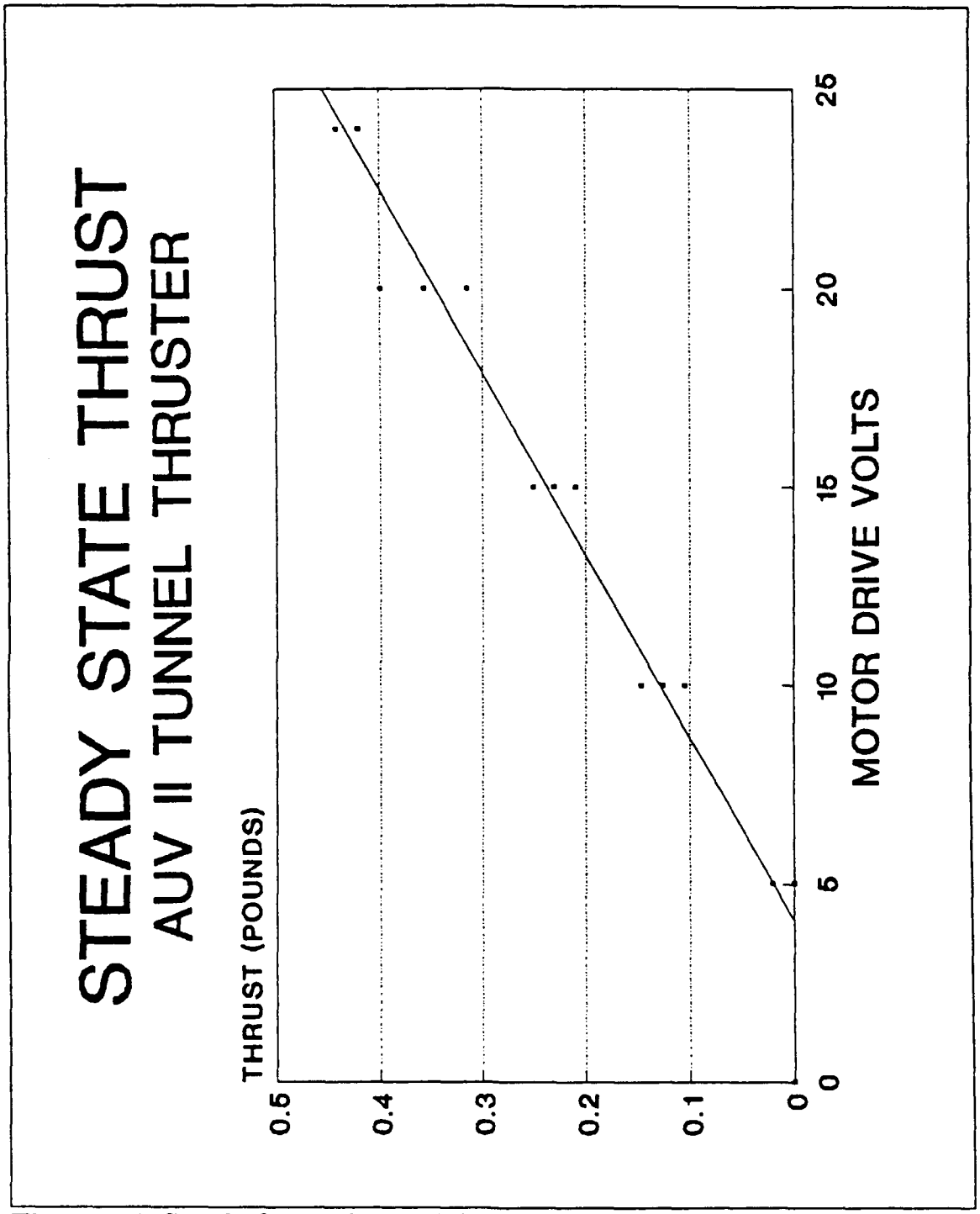

Figure 35 Steady State Thrust Values

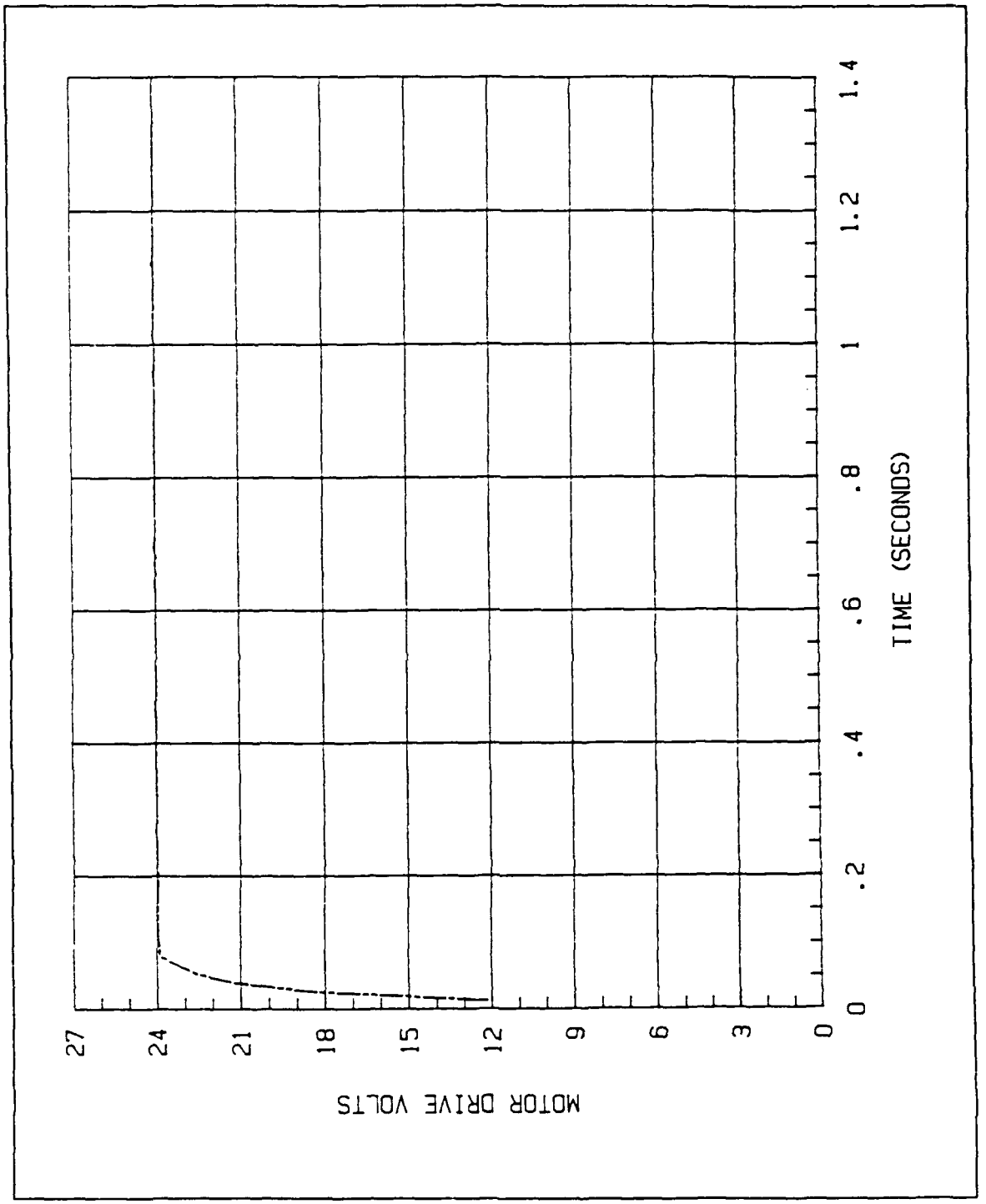

Figure 36 24 Volt Input Signal

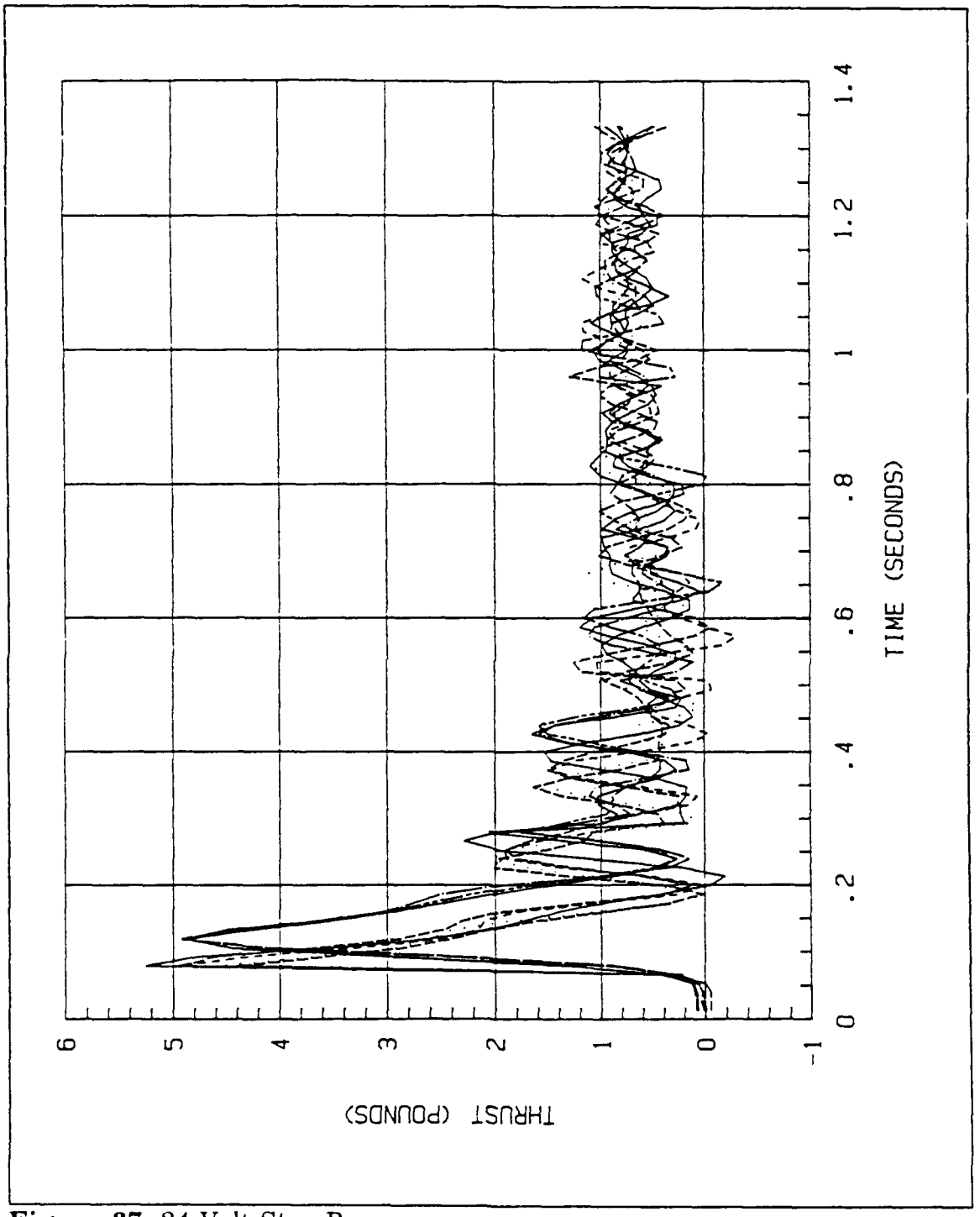

Figure 37 24 Volt Step Response

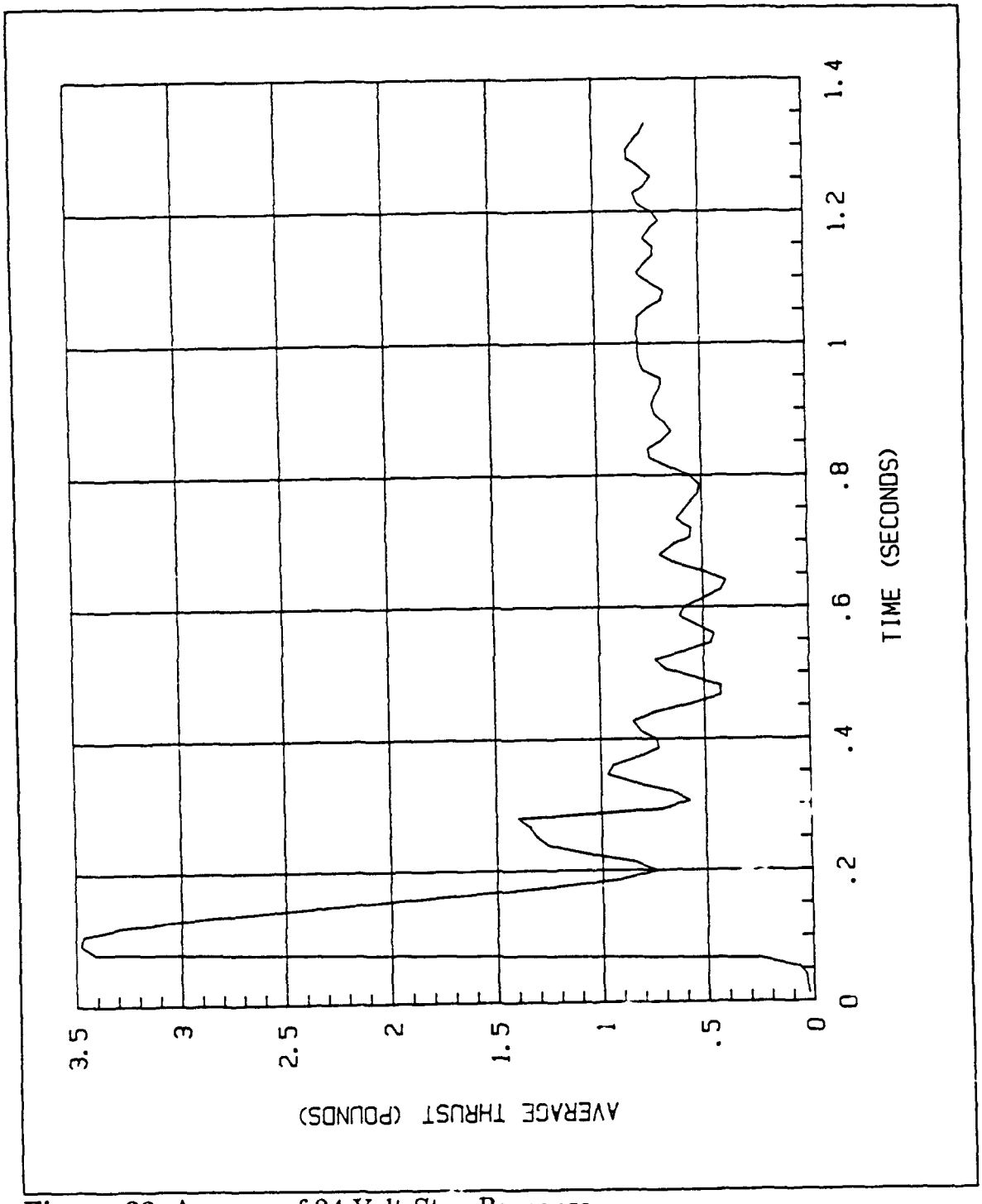

Figure 38 Average of 24 Volt Step Response

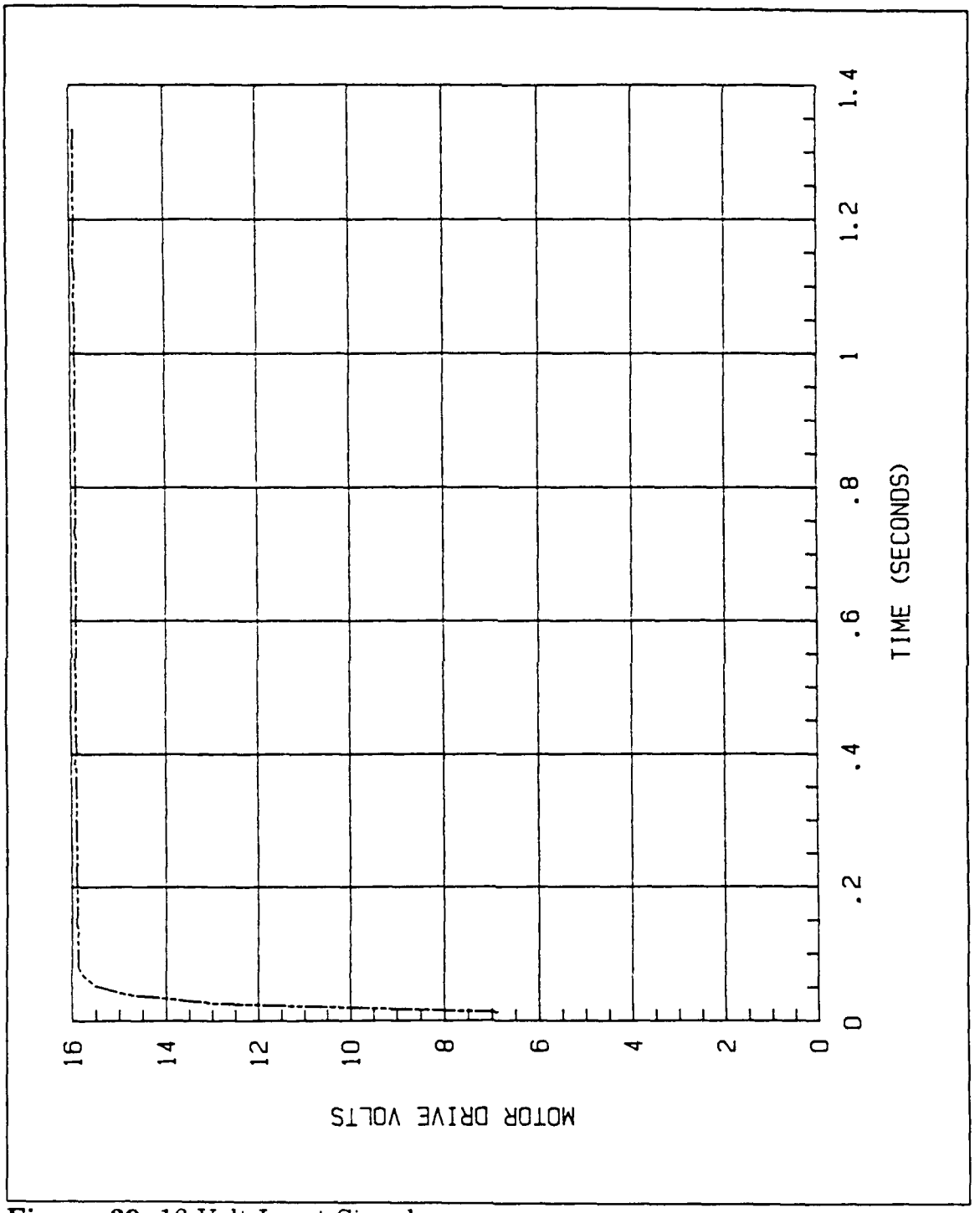

Figure 39 16 Volt Input Signal

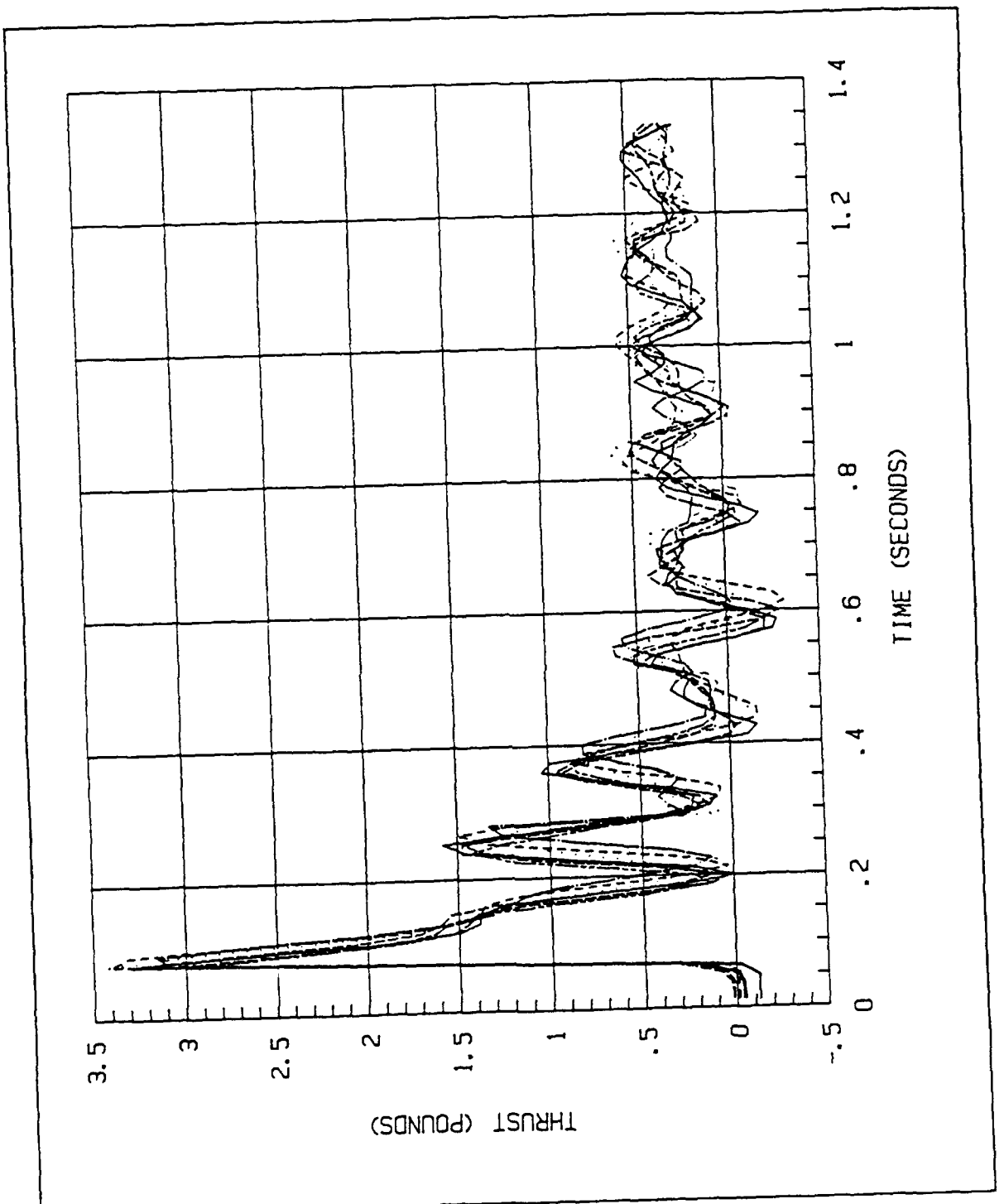

Figure 40 16 Volt Step Response

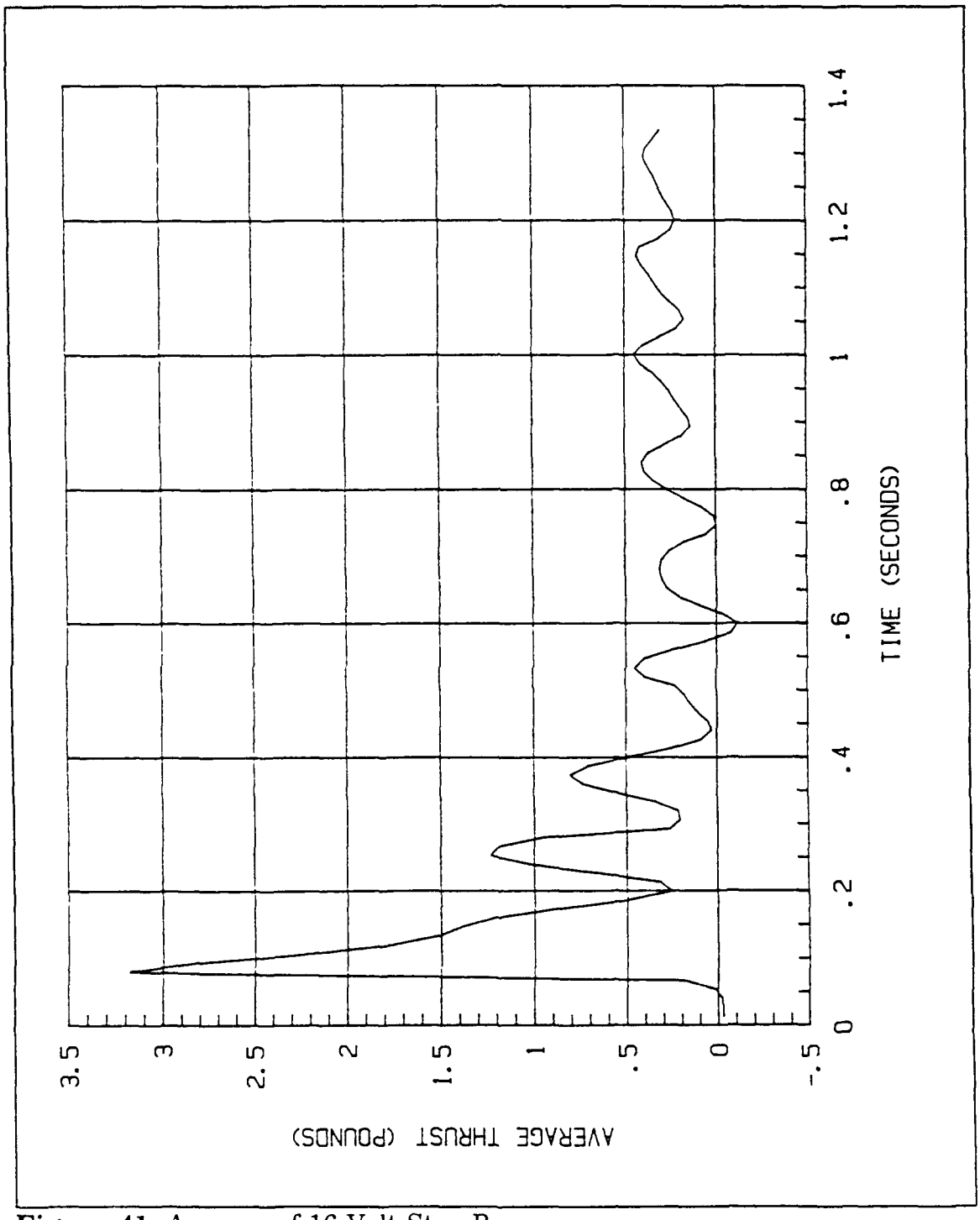

Figure 41 Average of 16 Volt Step Response

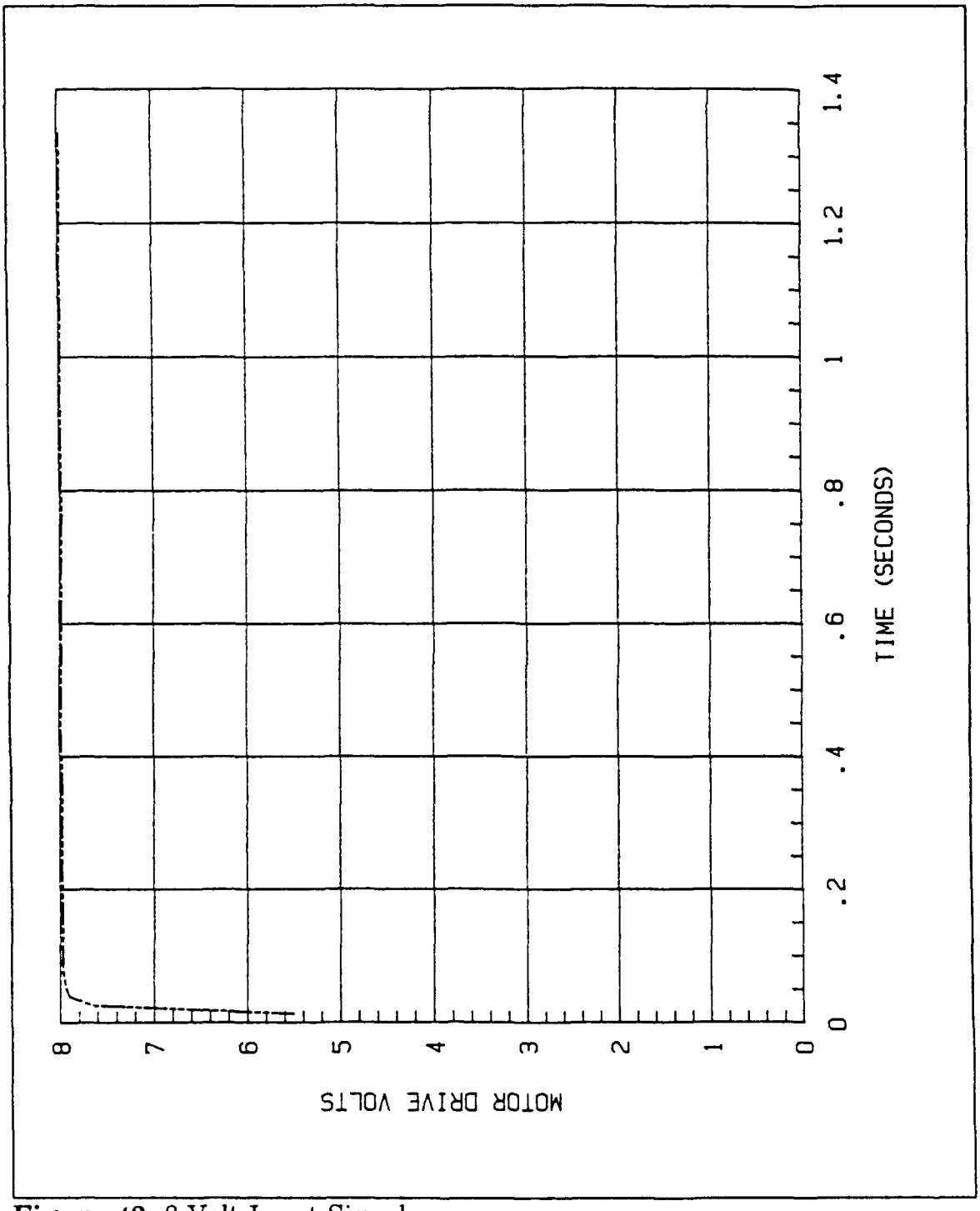

Figure 42 8 Volt Input Signal

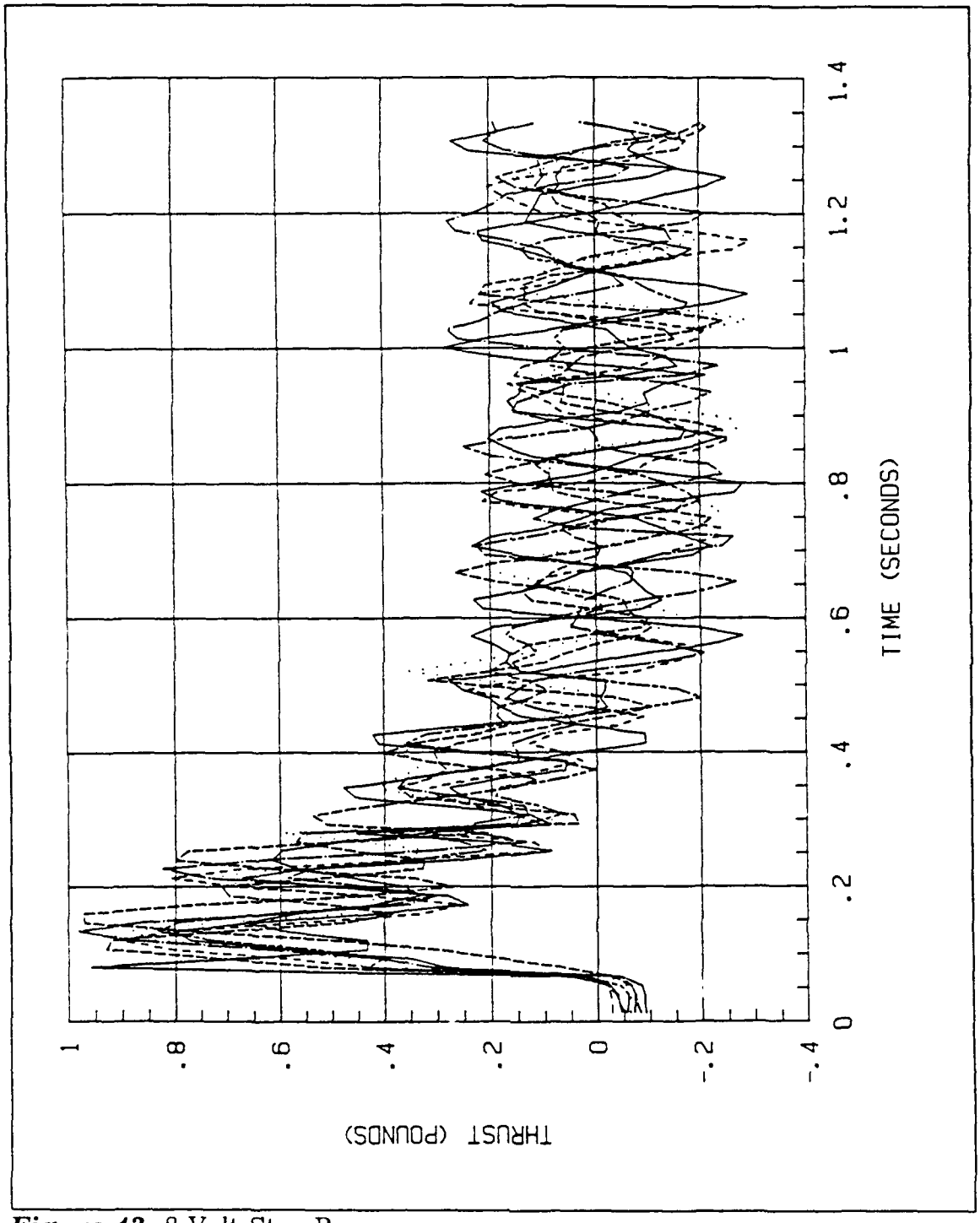

Figure 43 8 Volt Step Response

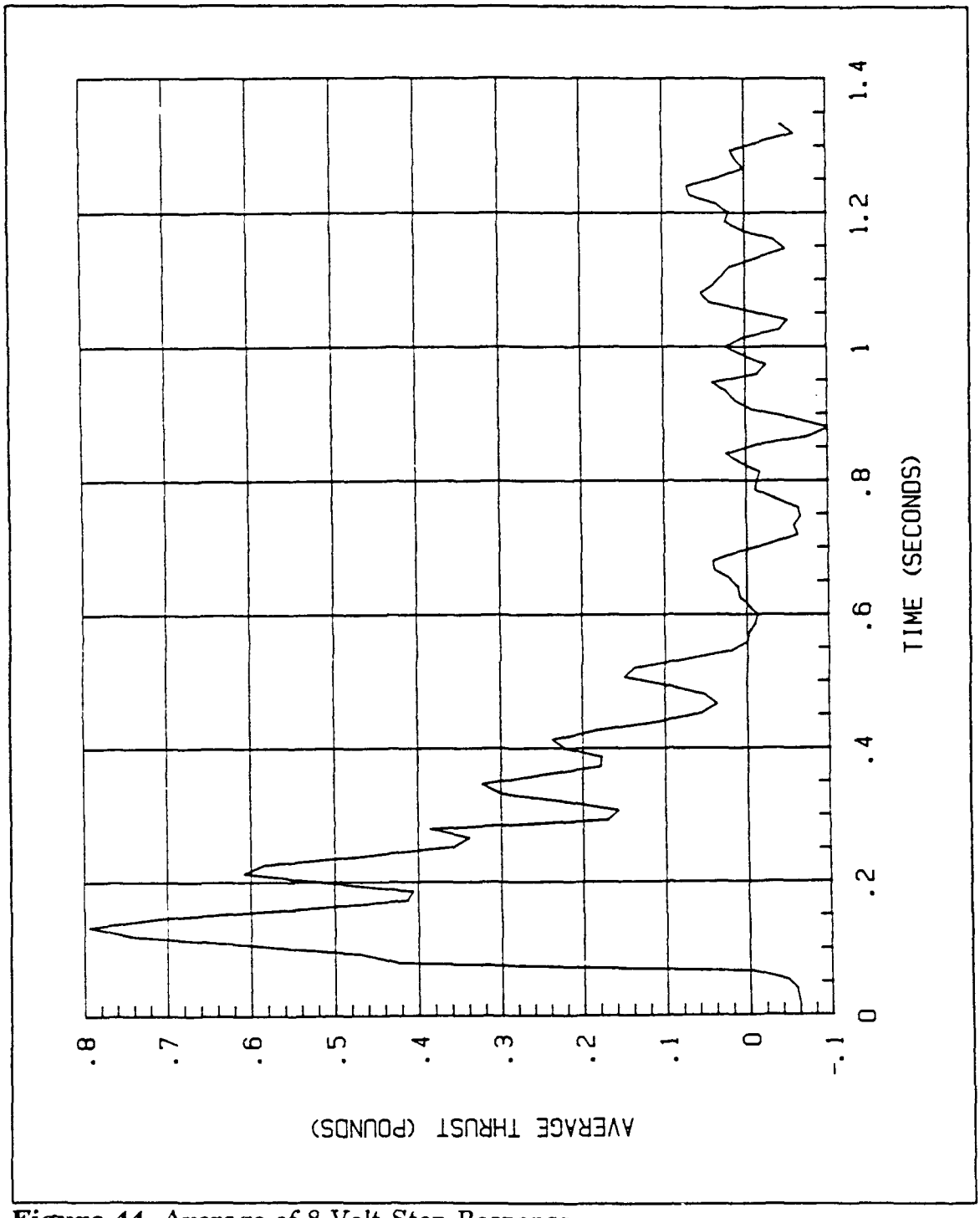

Figure 44 Average of 8 Volt Step Response

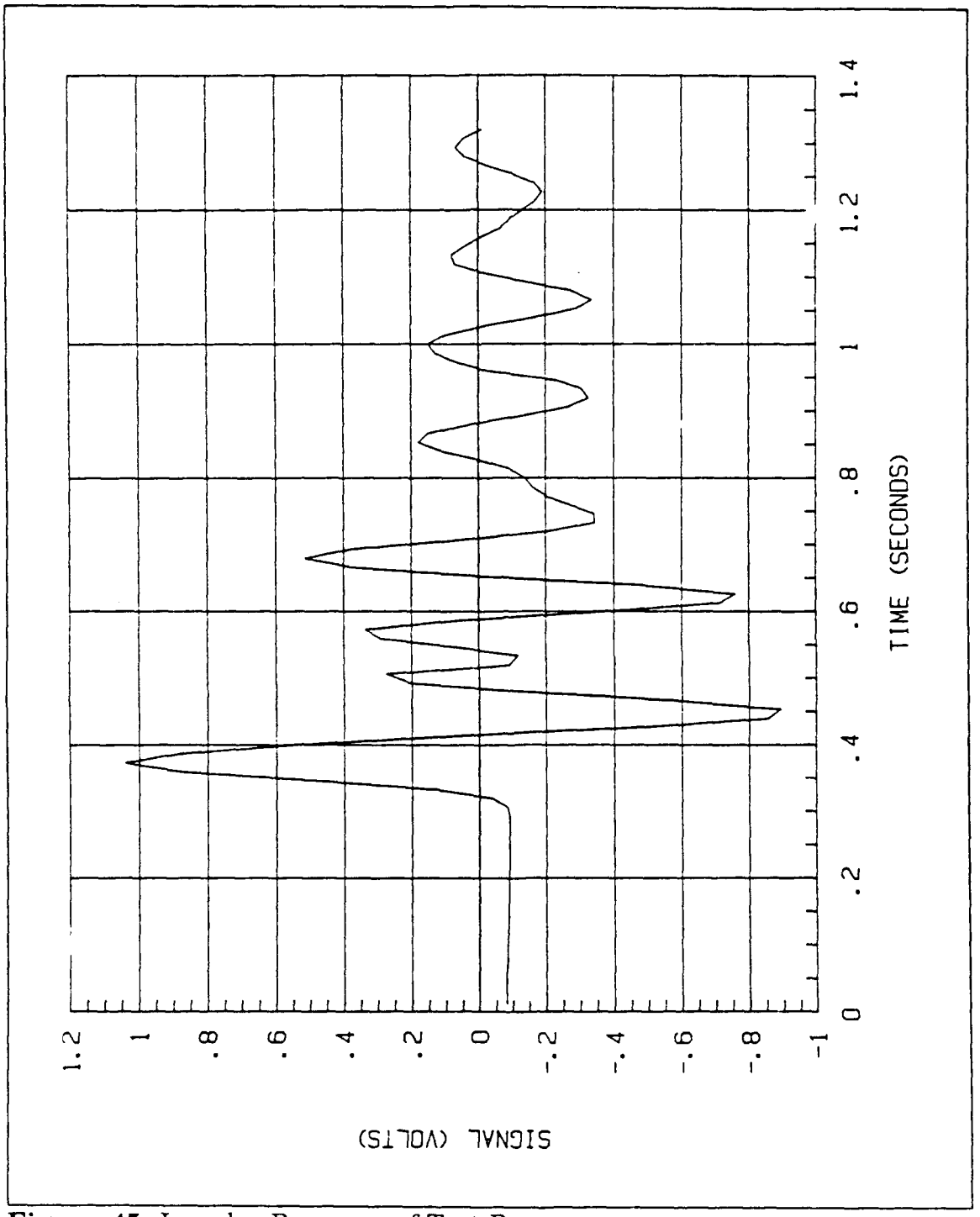

Figure 45 Impulse Response of Test Box

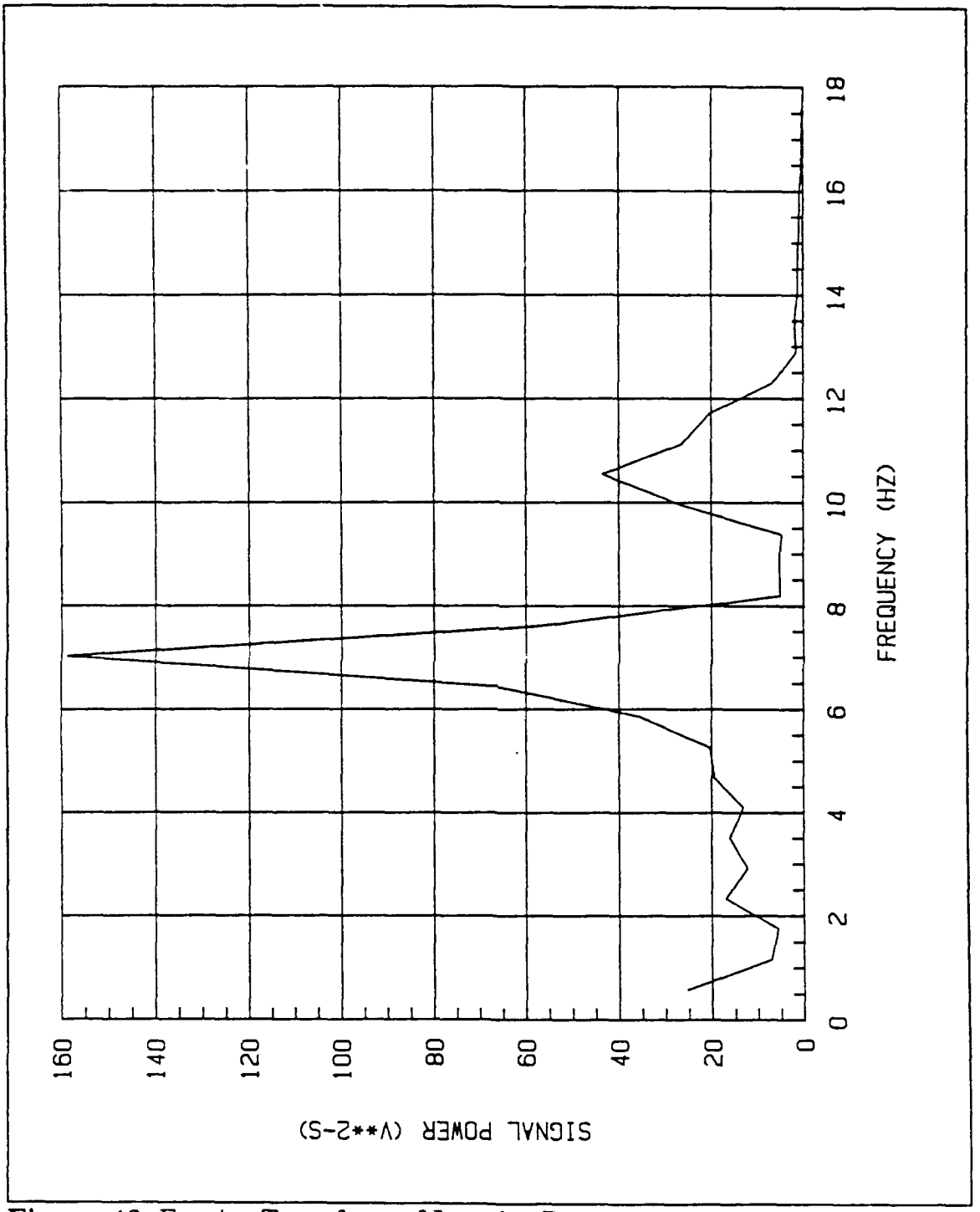

Figure 46 Fourier Transform of Impulse Response

2. Analysis of Output

a. Input Signals

The step input signals for all three cases were similar in shape, which are very close to becoming a true step input; note that the first sample is not taken until the input is approximately 50% or more of full voltage. This is a result of the ADC software, since the trigger required a voltage greater than zero to be sensed before sampling would begin, and the small delay caused by the 75 Hz sample rate.

b. Steady State Thrust

The steady state thrust obtained using this test rig was approximately half of that documented in the previous thesis regarding the AUV II thrusters [Ref. 15]. The pitch angle of the blades for the previous tests is not known, but it was estimated from inspection of the propeller to be 35 degrees. The pitch angle of the blades for this thesis were set to roughly 30 degrees. The 5 degrees difference in pitch angle is not believed to be significant regarding the thrust produced. The only possible explanation that the author can surmise is that corrosion products and foreign particles have increased the friction in the bearings and shafts, resulting in lower steady state speeds. This problem was noted by Saunders [Ref. 15] in his thesis. Although propeller speed was not continuously monitored, it was, however,

observed on several occasions using a hand--held tachometer and appeared consistent with the earlier thesis.

c. Structural Response

The frequency domain analysis of the impulse response for the test box showed a strong resonance at 7 Hz, and this frequency could also be seen clearly in the time response. The initial damping ratio that was chosen was 0.2, realizing that the damping was low from the time response plot; after several simulations of the model while varying ς, a value of 0.16 was retained as the most similar to the experimental results.

d. 24 Volt Runs

The individual runs had a peak output thrust that varied from 5.3 pounds down to 4.8 pounds, with a time to peak between 0.1 and 0.125 seconds. The thrust reached steady state values in about 0.5 seconds, which appeared to be around 0.5 pounds. The slosh mode can be seen in the output, which has a frequency of about 0.5 Hz.

The average thrust graph had a peak thrust of 3.5 pounds that lasted from 0.06 to 0.10 seconds. The large reduction in the average thrust was due to the range of times that the peak occurred at in the individual runs. Note that the impulse from the average thrust is substantial due to the "wide" peak that is exhibited. The same comments for slosh mode and steady state thrust as above apply here also.

e. 16 Volt Runs

The individual runs this time had a peak output thrust that varied between 3.45 and 3.2 pounds, with a time to peak around 0.085 seconds. The thrust reached steady state (0.3 pounds) in 0.5 seconds. These individual runs were very close to each other, with little phase difference between them, resulting in an average thrust plot that looked identical to the individual plots. The slosh mode here again was visible at approximately 0.5 Hz.

The average thrust graph had a peak thrust of 3.2 pounds that occurred at 0.08 seconds. The slosh mode and steady state thrust are very distinguishable. As mentioned above, this group of data resulted in the best repeatability between runs.

f. 8 Volt Runs

The individual runs had a peak output thrust that varied from 0.95 pounds to 0.8 pounds, where the peak occurred between 0.08 and 0.16 seconds. Several of the runs had double peaks of equal magnitude (0.8 pounds) that occurred 0.1 seconds apart. The thrust reached a steady state value of zero pounds after 0.5 seconds. The slosh mode is not visible, due to the large variation in phase difference between runs and the small amount of thrust produced. The data showed oscillations in thrust at steady state that were approximately 50% of the peak value. During the steady state thrust analysis, the motor frequently required four to five volts of input before the propeller

would start to turn. For these reasons, the graphs regarding the 8 volt runs have a low degree of confidence associated with their usefulness.

The average thrust graph had a peak thrust of 0.8 pounds that occurred at 0.12 seconds. The average steady state thrust also appears to be zero, and this occurs at about 0.6 seconds.

In the following chapter, Section A will summarize the results from the experimental testing and computer simulation in the form of tables; significant areas of the results will then be discussed. Section B will then provide recommendations for further research in the area of thruster testing and evaluation.

V. SUMMARY AND RECOMMENDATIONS

A. SUMMARY OF RESULTS

The results from the simulations of the computer model and the experimental testing of the tunnel thruster will be summarized in this section. The findings will be tabulated to allow side--by--side comparisons of the different cases for ease of analysis. First, the computer simulations will be compared to each other; secondly, the experimental results will be compared to each other; and lastly, the computer simulations and experimental results will be compared. After each table has been introduced, pertinent areas will be discussed as appropriate.

1. Computer Simulations

The results from the computer simulations are presented in Table I. The PEAK OUTPUT THRUST is the maximum thrust sensed experimentally by the load cell due to the dynamic response of the thruster test box. The MAX TRUE THRUST is the initial thrust produced from the thruster in response to a step input, without the structural response contamination. The TIME CONSTANT is the time that it took for 63% of the transient response to decay.

A comparison of the three baseline simulations shows that the peak, max, and steady state thrust levels are linear with respect to the input step

voltage. The same can not be said for the time constant or steady state speed. The steady state thrust and input voltage has been shown to be a linear function of signed--square speed [Ref. 9]. Notice that the time constant decreases as the magnitude of the input increases, which is a testament to the nonlinearity of the system. This finding agrees with that reported by Yoerger with respect to shrouded thrusters exhibiting a lagging behavior [Ref. 9].

Regarding the variations of key parameters in the 24 volt baseline model, the following conclusions can be drawn from the output presented in the table. With regard to the length of the tunnel, the longer length resulted in a greater peak output thrust with a longer time constant; the opposite was true of the shorter tunnel length. Since AUV II has a pair of tunnels that are longer (16.5") than those used in the baseline model (10.5"), this result means that the longer tunnels will benefit from the longer time constant. Increasing the added mass coefficient, Ka, resulted in raising the peak output thrust and time constant. It can be seen, then, that increasing the tunnel length has the same effect as increasing the added mass coefficient. Of all the information gleaned from the research conducted for this thesis, probably the most interesting was associated with the effect of changing the effective pitch of the propeller. The finding was that increasing the efficiency and/or pitch of the blades will result in a **decrease** in thrust. This result appears to be counter intuitive. The matching of motor to load analysis (App. A) showed that the thrust was a function of speed, but speed and torque were inversely

proportional so that the problem was very nonlinear, and thus required graphical representation to obtain the operating point. A sensitivity analysis of the conservation equations to effective pitch (Pe) was conducted, and it agreed with the result from the computer simulation. This is not to say that this effect will always dominate in other blade shapes and sizes, but for the propellers used in the AUV II tunnel thruster the thrust is very sensitive to these characteristics. In addition, when the effective pitch was set to zero, the response returns to that of the motor driving an inertial load, as we would expect. For the final case of coulomb friction in place of the motor viscous friction, the response was dampened in all categories. By working with the values for energy and momentum correction factors, the use of the coulomb friction term would most likely produce a more accurate model of the actual thruster. This could especially improve on the difficulty experienced in modeling the 8 volt baseline case.

2. Experimental Results

The results from the laboratory testing of the thruster using the test rig are presented in Table II. The PEAK OUTPUT THRUST was the initial thrust transient registered by the load cell. In general, the initial thrust was a factor of two or more greater than the subsequent peaks. This resulted in short TIME CONSTANTs, which can be seen in column five. The time constant was determined from the time it took the initial thrust to decay to 37% of the peak thrust above the steady state thrust level. The PEAK

Table I COMPUTER SIMULATION RESULTS

CASE	PEAK OUTPUT THRUST	MAX TRUE THRUST	STEADY STATE THRUST	TIME CONSTANT	STEADY STATE SPEED
24 VOLTS	POUNDS	POUNDS	POUNDS	SECONDS	RPM
BASELINE	5.40	3.80	0.50	0.125	925
L = 20"	5.80	3.80	0.50	0.230	925
L = 5"	4.40	3.60	0.50	0.060	925
Ka = 1.0	5.80	3.80	0.50	0.195	925
Ka = 0.5	5.60	3.80	0.50	0.140	925
Pe = 0.0270	8.00	7.00	0.50	0.075	2000
Pe = 0.0721	4.30	2.90	0.40	0.145	640
Pe = 0.0	0.00	0.00	0.00	0.025	3000
COULOMB FRCTN	4.30	3.00	0.40	0.130	800
BASELINE-16V	3.60	2.50	0.33	0.150	725
BASELINE-8V	1.85	1.25	0.15	0.200	480

AVERAGE THRUST was the peak level of the average of all eight individual runs. The STEADY STATE THRUST was the value obtained from the steady state thrust analysis presented as Figure 35 in Chapter IV.

Table II EXPERIMENTAL RESULTS

CASE	PEAK OUTPUT THRUST	PEAK AVERAGE THRUST	STEADY STATE THRUST	TIME CONSTANT
	POUNDS	POUNDS	POUNDS	SECONDS
24 VOLT	5.30	3.50	0.44	0.150
16 VOLT	3.40	3.20	0.25	0.150
8 VOLT	0.95	0.80	0.08	0.300

From the experimental results it is apparent that the 8 volt case was comprised of almost purely random vibrations of the test box. The reason for this is the friction torque that must be overcome before propeller acceleration can begin. As previously mentioned, the motor was seen to require up to five volts of input before motion would commence on a routine basis. In this regard, the coulomb friction element would probably produce more desirable results in the computer simulations. The result of the experimental data from the 8 volt case is that input voltages need to be above this threshold in order to respond predictably. Focusing attention on the 24 and 16 volt cases, the peak and steady state thrust was better than linear with the input voltage, but the peak average thrust between the two cases was almost equal. The reason for the low values regarding the 24 volt case was due to the occurrence of several individual runs that were out of phase with the bulk of the testing (Fig. 36). This phase shift resulted in an average peak of lower magnitude and longer persistence.

3. Simulation and Experimental Results

A comparison of the thruster model to the actual performance can be seen in Table III. The three columns of data that are compared were determined using the same procedures as in the earlier tables. Notice that the model overestimates the peak and steady state thrust in each case. This is also true of the time constants, with the exception of the 16 volt case which is in agreement.

Table III COMBINED RESULTS

CASE	PEAK OUTPUT THRUST	STEADY STATE THRUST	TIME CONSTANT
	POUNDS	POUNDS	SECONDS
24 VOLT			
EXPERIMENTAL	5.30	0.44	0.150
SIMULATION	5.40	0.50	0.125
16 VOLT			
EXPERIMENTAL	3.40	0.25	0.150
SIMULATION	3.60	0.33	0.150
8 VOLT			
EXPERIMENTAL	0.95	0.08	0.300
SIMULATION	1.85	0.15	0.200

B. RECOMMENDATIONS

There are several areas involving this research that could be improved upon to obtain more comprehensive and/or additional results. Several additional facets of the dynamic response of thrusters should be addressed as the topic of future work.

1. Improving the Thruster Design

a. The thruster propeller was very crude and should be replaced with a better design and fabrication process. The flow of water across the propeller should be as smooth as possible and proper balancing is crucial to alleviate vibrations. At the time of this writing, a new propeller is being

designed and built in the M.E. Machine Shop which, combined with higher motor power, should increase the thrust level of the thrusters.

b. Baffles should be placed along the sides of the water tank to dampen the slosh mode resulting from the propeller wake. This would reduce the wait time between runs and result in cleaner output.

2. Further Research

a. The simulations of the computer model to various input schemes, for example square or sawtooth waves, could ascertain if this type of control signal to the thruster would result in a larger mean thrust over some designated period as compared to steady state thrust obtained from a constant voltage input. This idea resulted from the rapid pulsing of the thruster in the laboratory, which appeared to maintain an average thrust level above the steady state value.

b. The steady state and dynamic thrust evaluation of the new propeller will require additional verification testing using the test rig in the near future.

c. Incorporate the findings here regarding true and steady state thrust and the time constant into existing computer models describing the vehicle's horizontal and vertical plane dynamics. The need for this data is discussed in Reference 2.

APPENDIX A. LOAD MATCHING FOR THRUSTER PROPELLERS

A. INTRODUCTION

The AUV II thruster was designed with DC servomotors to supply the required torque to the propeller. As previously mentioned in Chapter II, the motor chosen was a Pittman Model 9514 DC servomotor.

During the static performance testing of the thrusters [Ref. 15], it was noticed that the motors became very hot after operating for a short time at full load. This occurrence indicated that the motors may not be running in an efficient region of their operating curves and therefore the load matching characteristics should be examined more closely.

Two areas of the thruster drive train were considered for design modifications; these areas were the following:

- Different gear ratios
- Larger motor

The larger motor analyzed was a Model 14202[9] DC servomotor that is also utilized for the main propulsion. This motor has a stall torque of 106 ounce inches and a no load speed of 3820 RPM. The required voltage is also 24 volts

[9] Manufactured by Pittman Division of Penn Engineering and Manufacturing Corporation, Harleysville, PA.

and the peak power consumption is 333 watts (stall torque). The physical specifications are 2.125 inch outside diameter and 3.2 inches in length, not to include the shaft. A FORTRAN code was written to allow up to three gear ratios at one time to be compared on one set of axes; these axes are presented in both motor and propeller values.

B. THEORY

1. General

The characteristic, or operating curves of a DC motor driving a mechanical load have a general shape that can be found in any textbook on electromechanical energy conversion [Ref. 11]. DC motors can be controlled using several different schemes[10], but all result in a torque versus speed curve that reflects decreasing torque for increasing speed. This means that a DC motor will drive a larger load at a slower steady state speed and vice--versa.

With respect to the load, or system curve, it is generally found that mechanical loads involving viscous friction and inertial effects are represented by a second--order curve. This type of load curve means that as the speed is increased, the torque applied must increase quadratically.

---

[10] Separately excited, shunt field, or series field, for example.

2. Pittman Motor Characteristic Curves

The curves used for the motor were based on **continuous load torque** capability as defined in the *Pittman Servo Motor Application Notes* [Ref. 16]. The use of this motor curve will result in different operating points as compared to the actual conditions. To obtain operating points that resemble the actual results a linear curve may be used based on the stall torque and no load speed, presented in Figure A.1.

The intent in this paper is to use the most conservative approach for determining the required gear ratio and/or motor size. The continuous load torque approach takes into account the temperature considerations that can affect the motor's performance after operating for an extended length of time or with a large load. The continuous load torque equation is [Ref. 16]:

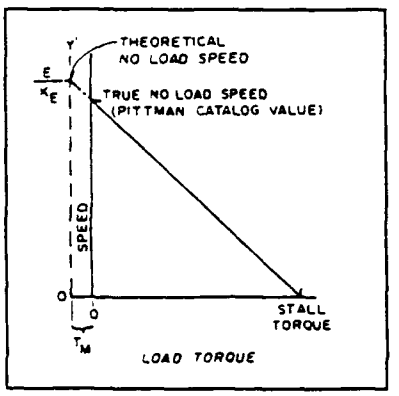

Figure A.1 Typical Speed vs. Torque Curve [Ref. 16]

$$TCONT = \sqrt{\frac{(155 - TAMB)}{TPR} - \frac{TM * S}{C}} * K * PKO - T_F \qquad (A.1)$$

where:

TCONT = continuous load torque capability

155 = maximum winding temperature (°C)

TAMB = ambient temperature (25°C)

TPR = motor thermal impedance

S = motor speed (RPM)

T_F = motor friction torque [the product of no load current (INL) and the torque constant (K_T) for a given winding]

C = conversion factor for motor friction torque in units of ounce--inches (1352)

PKO = motor constant

K = constant equal to 0.71 for brush commutated, ferrite magnet motors

Appendix B contains the values for the necessary motor constants in Equation A.1.

3. Load Curves For AUV II Thruster

The load curve for the thrusters was determined from steady state thrust curves determined in the laboratory by Saunders [Ref. 15]. From graphs of thrust versus propeller speed and thrust versus motor current, motor torque and speed were obtained using the motor law (EQ. 2.1) and gear train principles. The graph for the starboard thrust direction was used for obtaining the following values shown in Table A-I. To obtain the results in column five the motor law was used with column three; for column six the gear train principle was used with column four.

Table A-I EXPERIMENTAL VALUES FOR DETERMINING LOAD TORQUE [Ref. 15]

POINT	THRUST	CURRENT	PROP SPEED	TORQUE	MOTOR SPEED
	POUNDS	AMPS	RPM	OUNCE INCHES	RPM
1	1.125	3.20	775	13.2	1940
2	1.000	2.80	700	11.6	1750
3	0.750	2.00	550	8.26	1380
4	0.500	1.20	360	4.96	900
5	0.375	0.80	245	3.30	613
6	0.250	0.45	100	1.86	250

C. RESULTS

1. General

The following FORTRAN codes were written to graphically illustrate the operating characteristics of various motor/reduction gear/propeller combinations. The general approach was the same in each code. The continuous load torque equation and the experimentally determined points from Table A-I were plotted on the same coordinate system with the gear ratio filling the role as a parameter. The gear ratio's effect on torque and speed across a reduction gear set was discussed in Chapter II.

The first graph (Fig. A.3) presents the curves plotted in motor side values and the following two curves use propeller side values (Figs. A.4,A.5). The propeller coordinates allow the addition of thrust to the graphs, since previously data had been recorded for thrust versus propeller speed [Ref. 15].

The thrust versus speed curve was approximated by a linear relationship after attempts to obtain a second order equation for the data was unsuccessful. The use of the thruster data from this earlier thesis represents a "best case" scenario for the thrust that can be obtained from the tunnel thrusters at steady state, since less extensive testing conducted for this thesis could only obtain approximately 50% of the advertised thrust.

2. Graphs

The graphs that were obtained using CA--DISSPLA[11] subroutines begin on the following pages. The gear ratios chosen for display on the graphs are described below:

- 2.50:1 - the existing gear ratio employed at the time this thesis was written
- 3.67:1 - the largest gear ratio that can be incorporated into the existing design; it has been purchased, and is available for use
- 5.00:1 - a doubling of the existing gear ratio, presented with the Model 14202 graph; this gear ratio was considered to be sufficient with the use of the larger motor
- 10.0:1 - a quadrupling of the existing gear ratio, presented with the Model 9514 graph when a 5.00:1 ratio resulted in very little improvement over the existing 2.50:1 arrangement

---

[11] Registered Trademark, Computer Associates International, Garden City, NY.

3. Discussion

The statement made in the previous subsection regarding the thrust values used in the construction of the propeller coordinate graphs emphasize that when interpreting the plots, the reader must remember that these curves represent the upper bound on the expected thrust. Therefore, they show that the Model 9514 motor coupled with a 2.5:1 reduction gear will not provide the desired design thrust of one pound for an extended period of time. In fact, based on the curves for the Model 9514 motor, the continuous thrust for a 10:1 gear ratio will only reach approximately 0.9 pounds. The last set of curves for the Model 14202 motor show that for a 2.5:1 gear ratio the continuous thrust will be approximately 1.1 pounds, which is a large improvement over the Model 9514. This graph also shows that the 3.67:1 reduction gear set could be used, since the improvement due to a doubling in the gear ratio accounts for only 27% increase in thrust, and would require the thruster housing to be enlarged.

The larger the gear ratio, the faster the motor can be driven for approximately the same amount of continuous torque. Therefore, the larger gear ratio is desired, to allow the motor to run in a more efficient area of its operating region. The efficiency of the motor is a maximum at about 25% of stall torque and then drops linearly to zero at stall torque (Fig. A.2). Of course, size is also a concern in the design process, and the larger the gear ratio, the more room the thruster unit will need inside the AUV II's hull.

These design areas must be analyzed such that trade--offs can be made to optimize the thruster design.

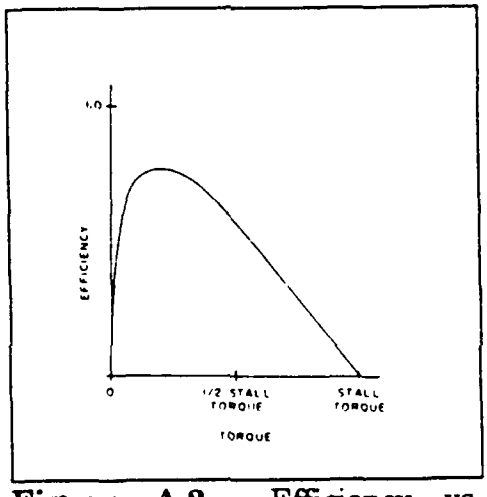

Figure A.2 Efficiency vs. Torque Curve [Ref. 16]

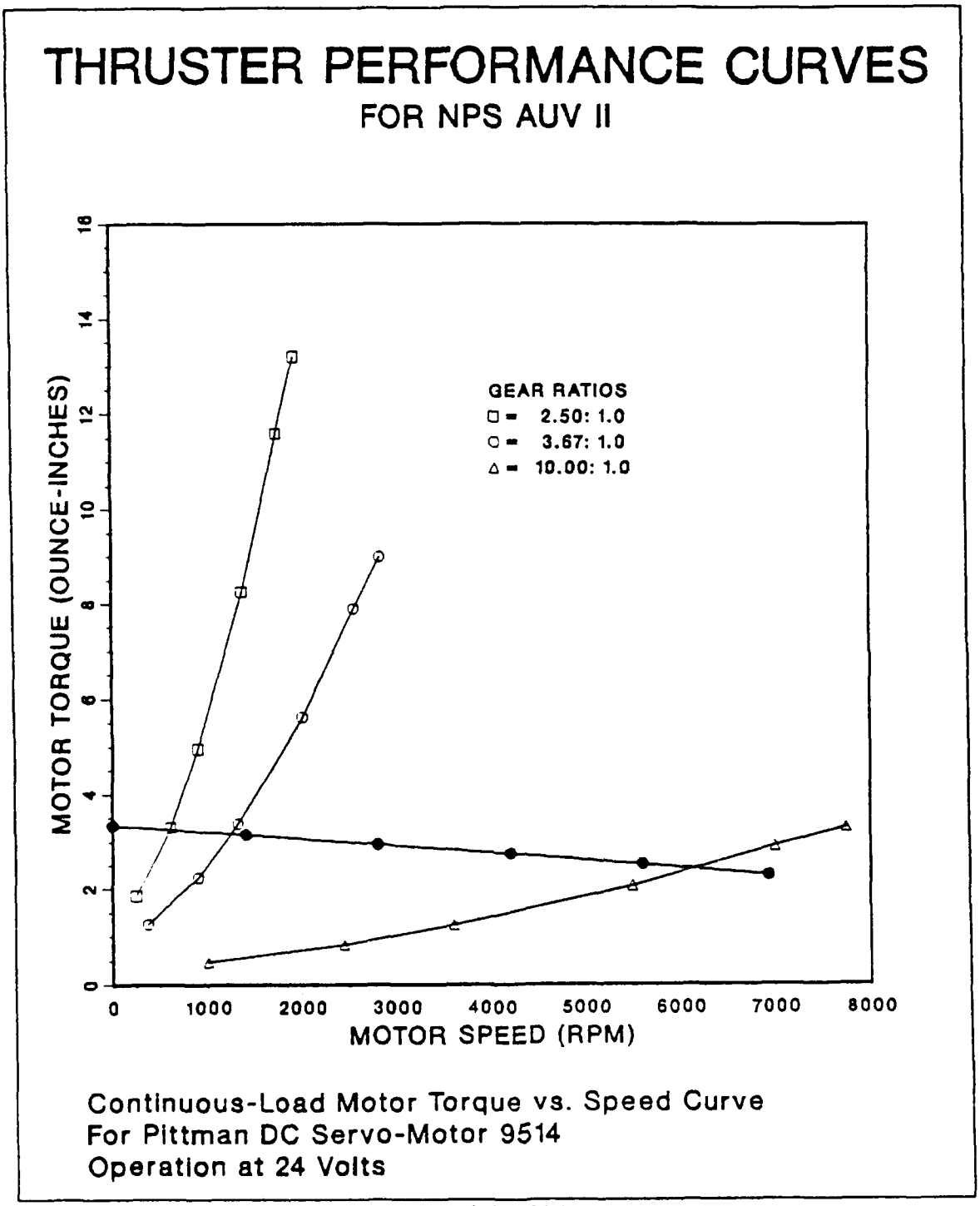

Figure A.3 Load Matching #1 Model 9514

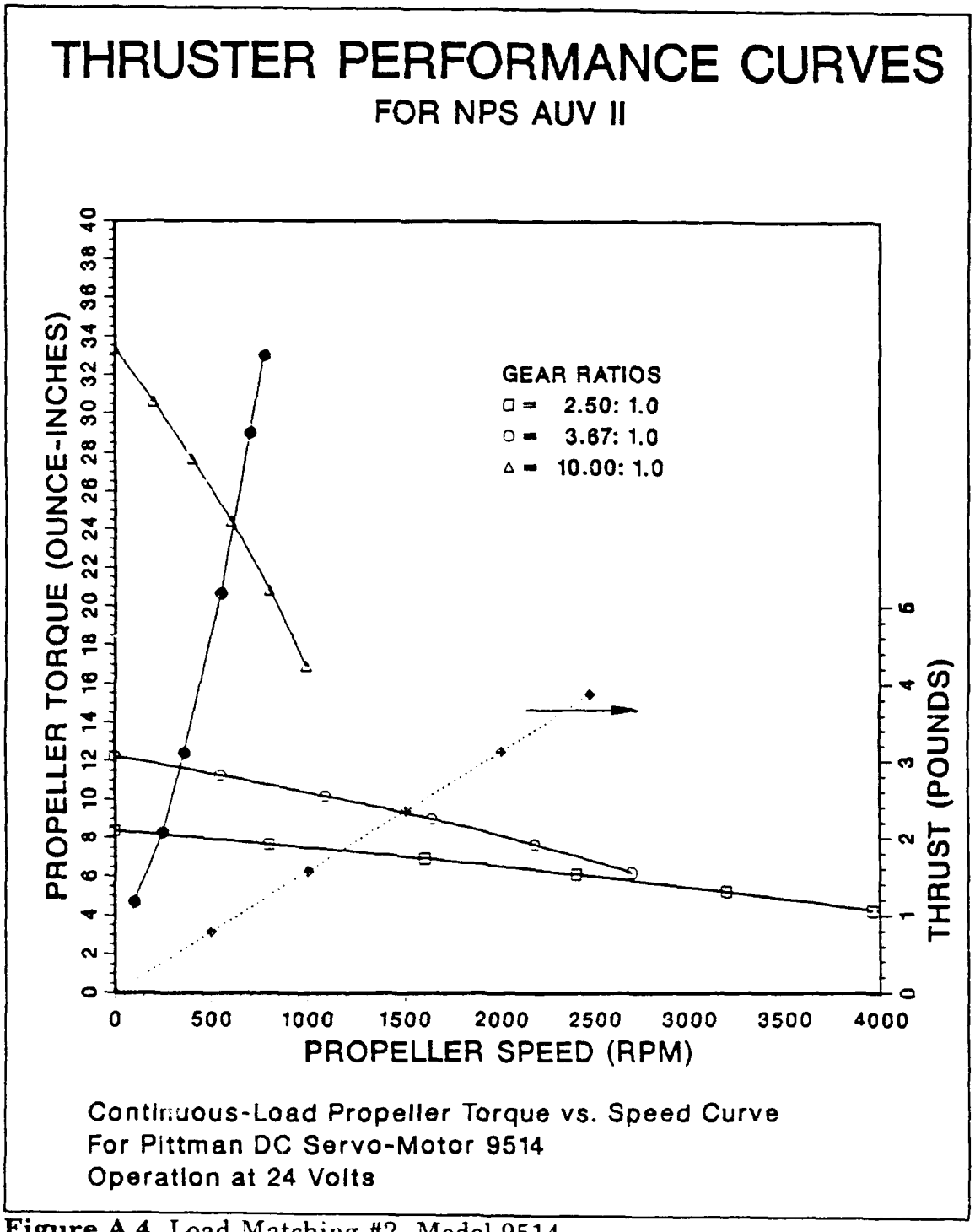

Figure A.4 Load Matching #2 Model 9514

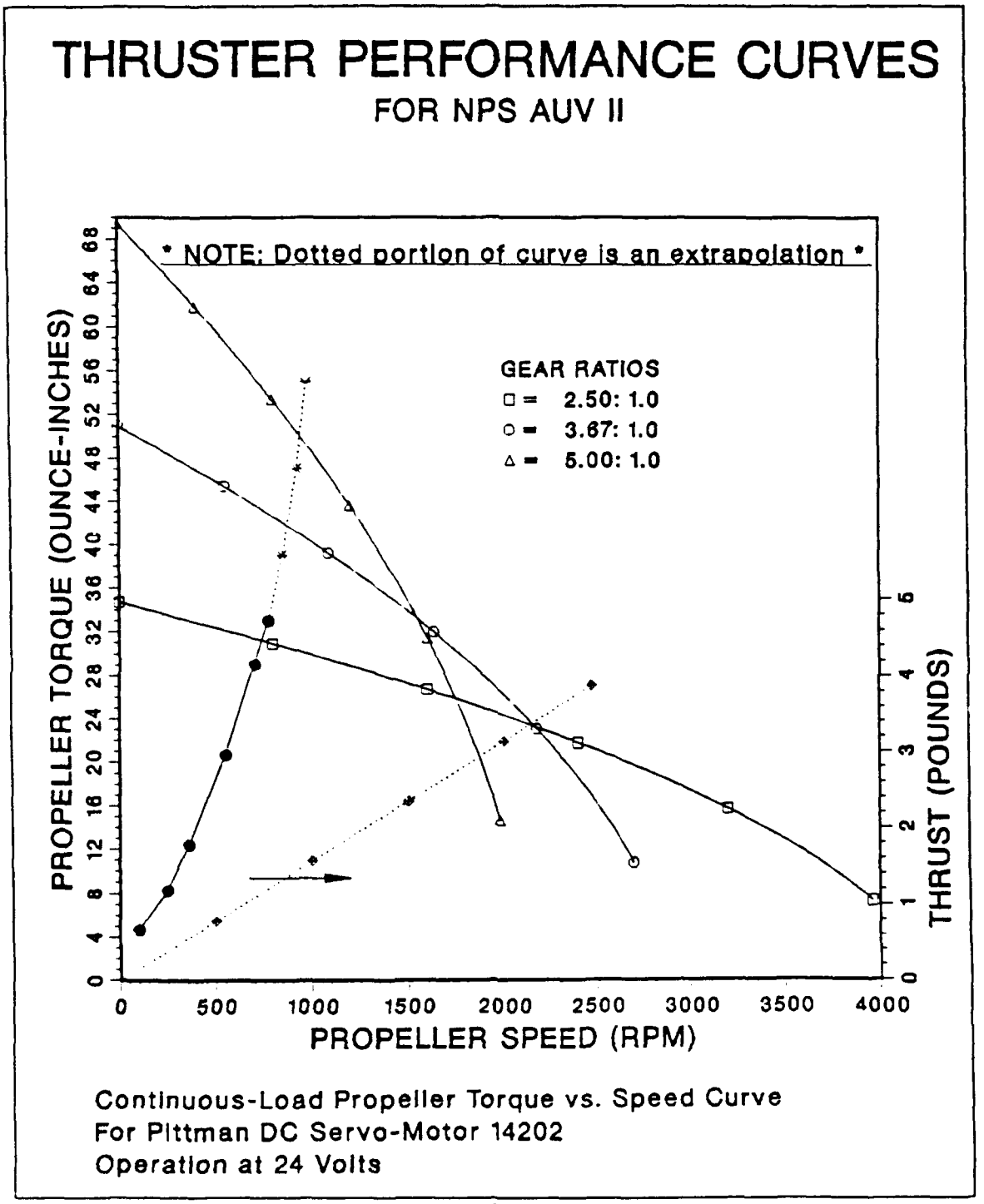

Figure A.5 Load Matching #3 Model 14202

4. Codes

a. Listing of Variables and Constants Used in Codes

ANSWER	real variable for choosing to analyze another gear ratio
C	constant used in continuous torque equation
CHOICE	real variable for choosing device for output
CR	character variable used in legend for gear ratio
FOOTNT	character variable for footnotes
FTNOTE	another character variable for footnotes
K	constant used in continuous torque equation
PKO	motor constant
R	desired gear ratio
RR	desired gear ratio vector
S	motor speed
SL	speed of motor that pertains to a given load torque (TL)
SLA	extrapolation of load speed based on previous trend
SM	motor or propeller speed depending on individual code
SS	propeller speed
SUBTITLE	character variable for graph's subtitle
T	motor or propeller torque depending on individual code
TAMB	ambient temperature
TCONT	continuous torque that motor can provide

THRUST	thrust variable
TITLE	character variable for graph's main title
TL	load torque associated with load speed (SL)
TLA	extrapolation of load torque based on previous trend
TM	motor friction torque
TPR	motor thermal impedance
V	counter for each gear ratio
XAXIS	character variable to name graph's horizontal axis
YAXIS	character variable to name graph's vertical axis

b. Hard Copies

The printouts of the computer codes begin on the following page.

```
*************************************************************************
*  THIS PROGRAM PLOTS THE MOTOR AND LOAD TORQUE VS. SPEED CURVES       *
*  FOR THE AUV II CROSS-BODY THRUSTER UNITS USING DISSPLA SUBROUTINES.*
*  UP TO 3 GEAR RATIOS FOR MODEL 9514 MAY BE PLOTTED AT ONE TIME.      *
*  MAXIMUM GEAR RATIO WITHOUT MODIFYING CODE IS 10:1.                  *
*  CURVES ARE PLOTTED ON MOTOR COORDINATES.                            *
*                                                                      *
*                                                                      *
*                                                                      *
*  MICHAEL B. MCLEAN      NAVAL POSTGRADUATE SCHOOL       JAN 1991     *
*************************************************************************
      PARAMETER (NO=100)
      DIMENSION T(NO),SM(NO),SL(NO),TL(NO),RR(NO)
      CHARACTER XAXIS*75,YAXIS*75,TITLE*75,SUBTITLE*75,FTNOTE(3)*75
      CHARACTER CR*6,FOOTNT(3)*75
      REAL K
      INTEGER CHOICE,V
      WRITE(*,*)'ENTER THE DESIRED GEAR RATIO.'
      READ(5,*)R
      RR(1)=R
      PKO=2.05
      V=0
      K=0.71
      C=1352.0
      TAMB=25.0
      TPR=17.1
      TM=0.677
C
C     CALCULATE THE MOTOR CURVE
C
      DO 100 I=1,NO
      S=(I-1)*70
      TCONT=SQRT(((155.0-TAMB)/TPR)-TM*S/C)*K*PKO-TM
      T(I)=TCONT
      SM(I)=S
 100  CONTINUE
      OPEN(UNIT=35,FILE='MC.DAT',STATUS='NEW')
      DO 200 J=1,NO
      WRITE(35,36) T(J),SM(J)
  36  FORMAT(1X,F7.3,1X,F7.1)
 200  CONTINUE
      CLOSE(UNIT=35)
 201  V=V+1
      R=RR(V)
C
C     DEFINE THE LOAD CURVE
C
      TL(1)=4.65/R
      TL(2)=8.25/R
      TL(3)=12.4/R
      TL(4)=20.65/R
      TL(5)=29.0/R
      TL(6)=33.0/R
      SL(1)=100.0*R
      SL(2)=245.0*R
      SL(3)=360.0*R
      SL(4)=550.0*R
      SL(5)=700.0*R
      SL(6)=775.0*R
      OPEN(UNIT=31,FILE='AUVINFO.DAT',STATUS='NEW')
```

Code for Load Matching #1

```
      WRITE(31,52) RR(V)
   52 FORMAT(1X,F5.2)
      CLOSE(UNIT=31)
C
C   NAME THE GRAPH USING A TITLE AND SUBTITLE
C
        TITLE='THRUSTER PERFORMANCE CURVES '
        SUBTITLE='FOR NPS AUV II '
C
C   INCLUDE FOOTNOTES
C
C **** USE THE OPEN STATEMENT IF THIS SUBPROGRAM IS CALLED BY A MAIN PROGRAM****
C **** IF THIS PLOTTING SUBPROGRAM IS PASTED TO THE END OF A MAIN PROGRAM   ****
C **** VARIABLES SHOULD ALREADY HAVE BEEN DEFINED                          ****
        OPEN(UNIT=31,FILE='AUVINFO.DAT',STATUS='OLD')
        READ(31,13) CR
  13    FORMAT(6A)
        CLOSE(UNIT=31)
        FTNOTE(V)=CR//': 1.0'
        FOOTNT(1)='Continuous-Load Motor Torque vs. Speed Curve'
        FOOTNT(2)='For Pittman DC Servo-Motor 9514'
        FOOTNT(3)='Operation at 24 Volts'
        IF(V.GT.1) GO TO 150
C
C  X-AXIS TITLE
C
        XAXIS='MOTOR SPEED (RPM)'
C
C  Y-AXIS TITLE
C
        YAXIS='MOTOR TORQUE (OUNCE-INCHES)'
C
C  DESCRIBE THE X-AXIS
C
        XMIN=0.0
        XMAX=8000.0
        XSTEP=1000.0
        ITCX=4
C
C  DESCRIBE THE Y-AXIS
C
        YMIN=0.0
        YMAX=16.0
        YSTEP=2.0
        ITCY=4
C
C  OPEN THE DATA FILE AND READ IN THE DATA TO AN ARRAY
C
        OPEN(UNIT=24,FILE='MC.DAT',STATUS='OLD')
        DO 101 M=1,NO
        READ(24,*) T(M),SM(M)
  101   CONTINUE
        CLOSE(UNIT=24)
C
C  DECIDE WHERE TO SEND THE PLOT
C
        PRINT*
        PRINT*,'TO SEE PLOT ON SCREEN, ENTER A 1'
        PRINT*,'TO GO STRAIGHT TO LASER, ENTER A 2'
        PRINT*
```

```
      READ (*,*) CHOICE
      IF(CHOICE.EQ.1) THEN
      CALL PGPX
      ELSEIF(CHOICE.EQ.2)THEN
      CALL LN03I
      ENDIF
C
C  GRAPHING SUBROUTINE CALLS
C
      CALL INTAXS
      CALL HWROT('COMIC')
      CALL CHRPAT(16)
      CALL SWISSM
      CALL AREA2D(6.0,6.0)
      CALL XTICKS(ITCX)
      CALL YTICKS(ITCY)
      CALL HEIGHT(0.2)
      CALL XNAME(XAXIS,100)
      CALL YNAME(YAXIS,100)
      CALL HEIGHT(.15)
      CALL MESSAG(FOOTNT(1),100,-0.20,-1.00)
      CALL MESSAG(FOOTNT(2),100,-0.20,-1.25)
      CALL MESSAG(FOOTNT(3),100,-0.20,-1.50)
      CALL RESET('HEIGHT')
      CALL GRAF(XMIN,XSTEP,XMAX,YMIN,YSTEP,YMAX)
      CALL RESET('HEIGHT')
      CALL THKCRV(0.01)
      CALL THKFRM(0.02)
      CALL FRAME
      CALL LINESP(2.0)
      CALL HEADIN(TITLE,100,2.0,2)
      CALL HEADIN(SUBTITLE,100,1.25,2)
      CALL HEIGHT(0.10)
C
C  PLOT THE CURVES
C
  150 CALL CURVE(SL,TL,6,1)
      PRINT*,'TWO ADDITIONAL GEAR RATIOS MAY BE SHOWN....'
      PRINT*,'DO YOU WANT TO RUN ANOTHER ?'
      PRINT*,'ENTER A 1 FOR YES, A 2 FOR NO.'
      READ(5,*)ANSWER
      IF(ANSWER.EQ.2)GO TO 1
      WRITE(*,*)'ENTER THE DESIRED GEAR RATIO.'
      READ(5,*)RR(V+1)
      GO TO 201
    1 CALL LINES(FTNOTE(1),IPAK,1)
      CALL LINES(FTNOTE(2),IPAK,2)
      CALL LINES(FTNOTE(3),IPAK,3)
      CALL LEGNAM('GEAR RATIOS',11)
      CALL LEGEND(IPAK,3,3,4)
      CALL MARKER(15)
      CALL CURVE(SM,T,NO,20)
      CALL ENDPL(-1)
      CALL DONEPL
      STOP
      END
```

```
*************************************************************************
*  THIS PROGRAM PLOTS THE MOTOR AND LOAD TORQUE VS. SPEED CURVES       *
*  FOR THE AUV II CROSS-BODY THRUSTER UNITS USING DISSPLA SUBROUTINES. *
*  UP TO 3 GEAR RATIOS FOR MODEL 9514 MAY BE PLOTTED AT ONE TIME.      *
*  MAXIMUM GEAR RATIO WITHOUT MODIFYING CODE IS 10:1.                  *
*  MINIMUM GEAR RATIO WITHOUT MODIFYING CODE IS 2.5:1.                 *
*  CURVES ARE PLOTTED ON PROPELLER COORDINATES.                        *
*                                                                      *
*                                                                      *
*                                                                      *
*  MICHAEL B. MCLEAN      NAVAL POSTGRADUATE SCHOOL       JAN 1991     *
*************************************************************************
      PARAMETER (NO=100)
      DIMENSION T(NO),SM(NO),SL(NO),TL(NO)
      DIMENSION RR(NO),THRUST(NO),SS(NO)
      CHARACTER XAXIS*75,YAXIS*75,TITLE*75,SUBTITLE*75,FTNOTE(3)*75
      CHARACTER CR*6,FOOTNT(3)*75
      REAL K
      INTEGER CHOICE,V
      WRITE(*,*)'ENTER THE DESIRED GEAR RATIO.'
      READ(5,*)R
      RR(1)=R
      PKO=2.05
      V=0
      K=0.71
      C=1352.0
      TAMB=25.0
      TPR=17.1
      TM=0.677
C
C   DEFINE THE THRUST ALGORITHM
C
      DO 79 L=1,NO
      SS(L)=(L-1)*25
      THRUST(L)=.0015625*SS(L)
 79   CONTINUE
201   V=V+1
C
C   CALCULATE THE MOTOR CURVE
C
      DO 100 I=1,NO
      S=(I-1)*100
      TCONT=SQRT(((155.0-TAMB)/TPR)-TM*S/C)*K*PKO-TM
      T(I)=TCONT*RR(V)
      SM(I)=S/RR(V)
100   CONTINUE
      OPEN(UNIT=35,FILE='MC.DAT',STATUS='NEW')
      DO 200 J=1,NO
      WRITE(35,36) T(J),SM(J)
 36   FORMAT(1X,F7.3,1X,F7.1)
200   CONTINUE
      CLOSE(UNIT=35)
C
C   DEFINE THE LOAD CURVE
C
      TL(1)=4.65
      TL(2)=8.25
      TL(3)=12.4
      TL(4)=20.65
      TL(5)=29.0
```

Code for Load Matching #2

```
      TL(6)=33.0
      SL(1)=100.0
      SL(2)=245.0
      SL(3)=360.0
      SL(4)=550.0
      SL(5)=700.0
      SL(6)=775.0
      OPEN(UNIT=31,FILE='AUVINFO.DAT',STATUS='NEW')
      WRITE(31,52) RR(V)
   52 FORMAT(1X,F5.2)
      CLOSE(UNIT=31)
C
C   NAME THE GRAPH USING A TITLE AND SUBTITLE
C
        TITLE='THRUSTER PERFORMANCE CURVES '
        SUBTITLE='FOR NPS AUV II '
C
C   INCLUDE FOOTNOTES
C
C **** USE THE OPEN STATEMENT IF THIS SUBPROGRAM IS CALLED BY A MAIN PROGRAM****
C **** IF THIS PLOTTING SUBPROGRAM IS PASTED TO THE END OF A MAIN PROGRAM    ****
C **** VARIABLES SHOULD ALREADY HAVE BEEN DEFINED                           ****
        OPEN(UNIT=31,FILE='AUVINFO.DAT',STATUS='OLD')
        READ(31,13) CR
  13    FORMAT(6A)
        CLOSE(UNIT=31)
        FTNOTE(V)=CR//': 1.0'
        FOOTNT(1)='Continuous-Load Propeller Torque vs. Speed Curve'
        FOOTNT(2)='For Pittman DC Servo-Motor 9514'
        FOOTNT(3)='Operation at 24 Volts'
        IF(V.GT.1) GO TO 150
C
C  X-AXIS TITLE
C
        XAXIS='PROPELLER SPEED (RPM)'
C
C  Y-AXIS TITLE
C
        YAXIS='PROPELLER TORQUE (OUNCE-INCHES)'
C
C  DESCRIBE THE X-AXIS
C
        XMIN=0.0
        XMAX=4000.0
        XSTEP=500.0
        ITCX=10
C
C  DESCRIBE THE Y-AXIS
C
        YMIN=0.0
        YMAX=40.0
        YSTEP=2.0
        ITCY=4
C
C  OPEN THE DATA FILE AND READ IN THE DATA TO AN ARRAY
C
        OPEN(UNIT=24,FILE='MC.DAT',STATUS='OLD')
        DO 101 M=1,NO
        READ(24,*) T(M),SM(M)
  101   CONTINUE
```

```
      CLOSE(UNIT=24)
C
C  DECIDE WHERE TO SEND THE PLOT
C
      PRINT*
      PRINT*,'TO SEE PLOT ON SCREEN, ENTER A 1'
      PRINT*,'TO GO STRAIGHT TO LASER, ENTER A 2'
      PRINT*
      READ (*,*) CHOICE
      IF(CHOICE.EQ.1) THEN
      CALL PGPX
      ELSEIF(CHOICE.EQ.2)THEN
      CALL LN03I
      ENDIF
C
C  GRAPHING SUBROUTINE CALLS
C
      CALL HWROT('COMIC')
      CALL CHRPAT(16)
      CALL SWISSM
      CALL AREA2D(6.0,6.0)
      CALL INTAXS
      CALL XTICKS(ITCX)
      CALL YTICKS(ITCY)
      CALL HEIGHT(.16)
      CALL XNAME(XAXIS,100)
      CALL YNAME(YAXIS,100)
      CALL GRAF(XMIN,XSTEP,XMAX,YMIN,YSTEP,YMAX)
      CALL RESET('HEIGHT')
      CALL MESSAG(FOOTNT(1),100,-0.20,-1.00)
      CALL MESSAG(FOOTNT(2),100,-0.20,-1.25)
      CALL MESSAG(FOOTNT(3),100,-0.20,-1.50)
      CALL THKCRV(0.01)
      CALL THKFRM(0.02)
      CALL FRAME
      CALL LINESP(2.0)
      CALL HEADIN(TITLE,100,2.0,2)
      CALL HEADIN(SUBTITLE,100,1.25,2)
C
C  PLOT THE CURVES
C
  150 CALL CURVE(SM,T,NO,20)
      PRINT*,'TWO ADDITIONAL GEAR RATIOS MAY BE SHOWN....'
      PRINT*,'DO YOU WANT TO RUN ANOTHER ?'
      PRINT*,'ENTER A 1 FOR YES, A 2 FOR NO.'
      READ(5,*)ANSWER
      IF(ANSWER.EQ.2)GO TO 1
      WRITE(*,*)'ENTER THE DESIRED GEAR RATIO.'
      READ(5,*)RR(V+1)
      GO TO 201
    1 CALL HEIGHT(.12)
      CALL LINES(FTNOTE(1),IPAK,1)
      CALL LINES(FTNOTE(2),IPAK,2)
      CALL LINES(FTNOTE(3),IPAK,3)
      CALL LEGNAM('GEAR RATIOS',11)
      CALL LEGEND(IPAK,3,3,4)
      CALL MARKER(15)
      CALL CURVE(SL,TL,6,1)
      CALL VECTOR(3.2,2.2,4.1,2.2,0301)
      CALL YINTAX
```

```
      CALL YTICKS(5)
      CALL HEIGHT(.16)
      CALL YGRAXS(0.0,1,5,3,'THRUST (POUNDS)',-15,6,0)
      CALL DOT
      CALL MARKER(9)
      CALL CURVE(SS,THRUST,NO,20)
      CALL ENDPL(-1)
      CALL DONEPL
      STOP
      END
```

```
************************************************************************
*  THIS PROGRAM PLOTS THE MOTOR AND LOAD TORQUE VS. SPEED CURVES       *
*  FOR THE AUV II CROSS-BODY THRUSTER UNITS USING DISSPLA SUBROUTINES.*
*  UP TO 3 GEAR RATIOS FOR MODEL 14202 MAY BE PLOTTED AT ONE TIME.     *
*  MAXIMUM GEAR RATIO WITHOUT MODIFYING CODE IS 5.0:1.                 *
*  MINIMUM GEAR RATIO WITHOUT MODIFYING CODE IS 2.5:1.                 *
*  A LINEAR APPROXIMATION OF THRUST IS PLOTTED AGAINST PROPELLER RPM.  *
*  AN EXTRAPOLATION OF THE LOAD CURVE IS INCLUDED TO ALLOW THE         *
*  ESTIMATION OF OPERATING POINTS.                                     *
*  CURVES ARE PLOTTED ON PROPELLER COORDINATES.                        *
*                                                                      *
*                                                                      *
*                                                                      *
*  MICHAEL B. MCLEAN       NAVAL POSTGRADUATE SCHOOL       JAN 1991    *
************************************************************************
      PARAMETER NO(100)
      DIMENSION T(NO),SM(NO),SL(NO),TL(NO)
      DIMENSION RR(NO),THRUST(NO),SS(NO)
      DIMENSION SLA(NO),TLA(NO)
      CHARACTER XAXIS*75,YAXIS*75,TITLE*75,SUBTITLE*75,FTNOTE(3)*75
      CHARACTER CR*6,FOOTNT(4)*75
      REAL K
      INTEGER CHOICE,V
      WRITE(*,*)'ENTER THE DESIRED GEAR RATIO.'
      READ(5,*)R
      RR(1)=R
      PKO=5.81
      V=0
      K=0.71
      C=1352.0
      TAMB=25.0
      TPR=9.0
      TM=1.794
C
C     DEFINE THE THRUST ALGORITHM
C
      DO 79 L=1,NO
      SS(L)=(L-1)*25
      THRUST(L)=.0015625*SS(L)
   79 CONTINUE
  201 V=V+1
C
C     CALCULATE THE MOTOR CURVE
C
      DO 100 I=1,NO
      S=(I-1)*100
      TCONT=SQRT(((155.0-TAMB)/TPR)-TM*S/C)*K*PKO-TM
      T(I)=TCONT*RR(V)
      SM(I)=S/RR(V)
  100 CONTINUE
      OPEN(UNIT=35,FILE='MC.DAT',STATUS='NEW')
      DO 200 J=1,NO
      WRITE(35,36) T(J),SM(J)
   36 FORMAT(1X,F7.3,1X,F7.1)
  200 CONTINUE
      CLOSE(UNIT=35)
C
C     DEFINE THE LOAD CURVE (SUFFIX 'A' MEANS IT IS EXTRAPOLATED)
C
      TL(1)=4.65
```

Code for Load Matching #3

```
C  DESCRIBE THE Y-AXIS
C
      YMIN=0.0
      YMAX=70.0
      YSTEP=4.0
      ITCY=4
C
C  OPEN THE DATA FILE AND READ IN THE DATA TO AN ARRAY
C
      OPEN(UNIT=24,FILE='MC.DAT',STATUS='OLD')
      DO 101 M=1,NO
      READ(24,*) T(M),SM(M)
 101  CONTINUE
      CLOSE(UNIT=24)
C
C  DECIDE WHERE TO SEND THE PLOT
C
      PRINT*
      PRINT*,'TO SEE PLOT ON SCREEN, ENTER A 1'
      PRINT*,'TO GO STRAIGHT TO LASER, ENTER A 2'
      PRINT*
      READ (*,*) CHOICE
      IF(CHOICE.EQ.1) THEN
      CALL PGPX
      ELSEIF(CHOICE.EQ.2)THEN
      CALL LN03I
      ENDIF
C
C  GRAPHING SUBROUTINE CALLS
C
      CALL HWROT('COMIC')
      CALL CHRPAT(16)
      CALL SWISSM
      CALL AREA2D(6.0,6.0)
      CALL INTAXS
      CALL XTICKS(ITCX)
      CALL YTICKS(ITCY)
      CALL HEIGHT(.16)
      CALL XNAME(XAXIS,100)
      CALL YNAME(YAXIS,100)
      CALL GRAF(XMIN,XSTEP,XMAX,YMIN,YSTEP,YMAX)
      CALL RESET('HEIGHT')
      CALL MESSAG(FOOTNT(1),100,-0.20,-1.00)
      CALL MESSAG(FOOTNT(2),100,-0.20,-1.25)
      CALL MESSAG(FOOTNT(3),100,-0.20,-1.50)
      CALL MESSAG(FOOTNT(4),100,-0.20,-2.00)
      CALL THKCRV(0.01)
      CALL THKFRM(0.02)
      CALL FRAME
      CALL LINESP(2.0)
      CALL HEADIN(TITLE,100,2.0,2)
      CALL HEADIN(SUBTITLE,100,1.25,2)
C
C  PLOT THE CURVES
C
 150  CALL CURVE(SM,T,NO,20)
      PRINT*,'TWO ADDITIONAL GEAR RATIOS MAY BE SHOWN....'
      PRINT*,'DO YOU WANT TO RUN ANOTHER ?'
      PRINT*,'ENTER A 1 FOR YES, A 2 FOR NO.'
      READ(5,*)ANSWER
```

```
      TL(2)=8.25
      TL(3)=12.4
      TL(4)=20.65
      TL(5)=29.0
      TL(6)=33.0
      TLA(1)=33.0
      TLA(2)=39.0
      TLA(3)=47.0
      TLA(4)=55.0
      SL(1)=100.0
      SL(2)=245.0
      SL(3)=360.0
      SL(4)=550.0
      SL(5)=700.0
      SL(6)=775.0
      SLA(1)=775.0
      SLA(2)=850.0
      SLA(3)=925.0
      SLA(4)=975.0
      OPEN(UNIT=31,FILE='AUVINFO.DAT',STATUS='NEW')
      WRITE(31,52) RR(V)
   52 FORMAT(1X,F5.2)
      CLOSE(UNIT=31)
C
C    NAME THE GRAPH USING A TITLE AND SUBTITLE
C
       TITLE='THRUSTER PERFORMANCE CURVES '
       SUBTITLE='FOR NPS AUV II '
C
C    INCLUDE FOOTNOTES
C
C **** USE THE OPEN STATEMENT IF THIS SUBPROGRAM IS CALLED BY A MAIN PROGRAM****
C **** IF THIS PLOTTING SUBPROGRAM IS PASTED TO THE END OF A MAIN PROGRAM   ****
C **** VARIABLES SHOULD ALREADY HAVE BEEN DEFINED                          ****
      OPEN(UNIT=31,FILE='AUVINFO.DAT',STATUS='OLD')
      READ(31,13) CR
  13  FORMAT(6A)
      CLOSE(UNIT=31)
      FTNOTE(V)=CR//': 1.0'
      FOOTNT(1)='Continuous-Load Propeller Torque vs. Speed Curve'
      FOOTNT(2)='For Pittman DC Servo-Motor 14202'
      FOOTNT(3)='Operation at 24 Volts'
      FOOTNT(4)='* NOTE: Dotted portion of curve is an extrapolation *'
      IF(V.GT.1) GO TO 150
C
C  X-AXIS TITLE
C
       XAXIS='PROPELLER SPEED (RPM)'
C
C  Y-AXIS TITLE
C
       YAXIS='PROPELLER TORQUE (OUNCE-INCHES)'
C
C  DESCRIBE THE X-AXIS
C
       XMIN=0.0
       XMAX=4000.0
       XSTEP=500.0
       ITCX=10
C
```

```
      IF(ANSWER.EQ.2)GO TO 1
      WRITE(*,*)'ENTER THE DESIRED GEAR RATIO.'
      READ(5,*)RR(V+1)
      GO TO 201
1     CALL HEIGHT(.12)
      CALL LINES(FTNOTE(1),IPAK,1)
      CALL LINES(FTNOTE(2),IPAK,2)
      CALL LINES(FTNOTE(3),IPAK,3)
      CALL LEGNAM('GEAR RATIOS',11)
      CALL LEGEND(IPAK,3,3,4)
      CALL MARKER(8)
      CALL DOT
      CALL CURVE(SLA,TLA,4,1)
      CALL RESET('DOT')
      CALL MARKER(15)
      CALL CURVE(SL,TL,6,1)
      CALL VECTOR(1.0,.8,1.8,.8,0301)
      CALL YINTAX
      CALL YTICKS(5)
      CALL HEIGHT(.16)
      CALL YGRAXS(0.0,1,5,3,'THRUST (POUNDS)',-15,6,0)
      CALL MARKER(9)
      CALL DOT
      CALL CURVE(SS,THRUST,NO,20)
      CALL ENDPL(-1)
      CALL DONEPL
      STOP
      END
```

APPENDIX B. PITTMAN CATALOG VALUES

Table B-I MOTOR CONSTANTS [Refs. 17,18]

MOTOR SERIES		9514	14202
ELECTRICAL TIME CONSTANT milliseconds	TCE	0.80	1.47
MECHANICAL TIME CONSTANT milliseconds	TCM	18.1	8.5
FRICTION TORQUE ounce-inches	T_F	0.677	1.79
ARMATURE INERTIA ounce-inches-seconds^2	I_M	5.37×10^{-4}	2.3×10^{-5}
MOTOR WEIGHT ounces	WGT	10.1	26.0
MOTOR CONSTANT ounce-inches/watt$^{0.5}$	PKO	2.05	5.81
MOTOR THERMAL IMPEDANCE degrees celsius/watt	TPR	17.1	9.0

Table B-II WINDING CONSTANTS [Refs. 17,18]

MOTOR SERIES WINDING NUMBER		9514 3	14202 3
VOLTAGE volts	V	24.0	24.0
TORQUE CONSTANT ounce-inches/amp	K_T	4.13	8.67
TERMINAL RESISTANCE ohms	R	4.06	1.01
BACK EMF volt-seconds/radian	K_G	0.0292	0.061
NO LOAD CURRENT amps	INL	0.164	0.210
STALL CURRENT amps	IST	5.91	23.8

LIST OF REFERENCES

1. Papoulias, F.A., et. al., "Modeling, Sliding Mode Control Design, and Visual Simulation of AUV Dive Plane Dynamics Response," *Proceedings, 6TH International Symposium on Unmanned, Untethered Submersible Technology*, pp.536-547, June 1989.

2. Hawkinson, T., *Multiple Input Sliding Mode Control For Autonomous Diving and Steering of Underwater Vehicles*, Master's Thesis, Naval Postgraduate School, Monterey, California, December 1990.

3. Norrby, R.A., and Ridley, D.E., "Notes on Thrusters for Ship Maneuvering and Dynamic Positioning," *SNAME Transactions*, Volume 88, pp.377-402, 1980.

4. Marine Systems Engineering Laboratory, *Technology Development For Unmanned Untethered Submersible Vehicle Systems*, prepared for Office of Naval Research, University of New Hampshire, Durham, New Hampshire, June 1984.

5. Baker, D.W., and Patterson, C.L.,Jr., "Some Recent Developments in Representing Propeller Characteristics," *Naval Engineers Journal*, Volume 84, pp.35-44, February 1972.

6. Naval Ship Research and Development Center Report 3611, *Design and Performance of Bow Thrusters*, by J.L. Beveridge, September 1971.

7. Thompson, D.E., *Measurement of Time--Dependent Propeller Thrust and Correlation with Theory*, TM 72-116, prepared for Naval Ordnance Systems Command, Pennsylvania State University, Ordnance Research Laboratory, University Park, Pennsylvania, July 1972.

8. Naval Ship Research and Development Center Report 3901, *Deep Submergence Rescue Vehicle Four--Quadrant Propulsion Dynamics*, by C.J. Rubis, A.J. Moken, and R.D. Johnson, September 1972.

9. Yoerger, D.R., Cooke, J.G., and Slotine, J.-J.E., "The Influence of Thruster Dynamics on Underwater Vehicle Behavior and Their Incorporation into

Control System Design," *IEEE Journal of Oceanic Engineering*, Volume 15, Number 3, pp.167-177, July 1990.

10. Cook, J.G., *Incorporating Thruster Dynamics in the Control of an Underwater Vehicle*, Master's Thesis, Massachusetts Institute of Technology, Cambridge, Massachusetts, September 1989.

11. Zorbas, D., *Electric Machines*, West Publishing Company, St. Paul, Minnesota, pp.479-487, 1989.

12. Sarpkaya, T., "Unsteady Flow of Fluids in Closed Systems," *ASCE Journal of the Engineering Mechanics Division*, Volume 88, pp.1-15, June 1962.

13. *Principles of Naval Architecture*, E.V. Lewis, editor, 2ND Rev., Vol. 2, pp.137-138, Society of Naval Architects and Marine Engineers, 1988.

14. White, F.M., *Fluid Mechanics*, McGraw--Hill, Inc., New York, New York, pp.162-173,132-142, 1986.

15. Saunders, T.E., *Performance of Small Thrusters and Propulsion Systems*, Master's Thesis, Naval Postgraduate School, Monterey, California, March 1990.

16. Saner, F.E., *PITTMAN Servo Motor Application Notes*, Pittman Division of Penn Engineering and Manufacturing Corporation, Harleysville, Pennsylvania, October 1988.

17. Pittman Division of Penn Engineering and Manufacturing Corporation Bulletin 9000, *LO--COG DC Servo Motors (Series 9000)*, November 1987.

18. Pittman Division of Penn Engineering and Manufacturing Corporation Bulletin 14000, *LO--COG DC Servo Motors (Series 14000)*, June 1987.